MASTER THESIS

Extreme response estimation of umbilical on very deep water

Torfinn Ottesen

Department of Marine Technology - NTNU 2010

Abstract

The scope of study is an umbilical arranged in a lazy wave configuration at 1300 m depth in Brazilian waters. The surface vessel is a ship, about 300 m long and 55 m wide. The wave environment is given by a wave scatter diagram and a 100-year contour curve and is acting in the beam sea direction of the ship. The long term extremes of important top end excitation parameters have been determined using frequency domain methods. This includes the wave elevation, the top end umbilical axial motion and velocity as well as the vessel roll angle. Long term extremes of important umbilical response parameters as bend stiffener angle and tension have been estimated in addition to the sag tension through time domain simulations considering the entire wave scatter diagram. The long term extremes have been compared to results from simulations of sea states on the 100-year wave contour curve. A selected 100-year sea state have been investigated using full non-linear time domain analysis. Extreme value estimates from ten three hour realizations have been established for top and sag tension including top angle. The relation between the top end axial velocity and the sag tension have been investigated. The results demonstrates that the extreme top axial velocity is well correlated to the sag tension and show that the the axial velocity extreme occurs practically at the same time as the sag tension extreme.

Acknowledgements

I would like to thank my supervisor, Carl M. Larsen, for guidance during this work. I would also thank Nexans Norway AS for the opportunity of this study and Håkon Ward, SeaFlex AS, for providing the vessel transfer function.

Torfinn Ottesen
Orkanger, June 2010

Contents

List of Tables

List of Figures

Nomenclature

$\dot{X}$	Axial velocity in static direction of umbilical at the upper end (m/s).
γ	Euler's constant, $\gamma = 0.5772156649015328606065...$
γ	Wave spectrum peakedness factor
ω_p	Spectral peak frequency, $\omega_p = 2\pi/T_p$
ρ	Material density kg/m^3.
σ	Shape parameter, standard deviation, scale parameter
θ'_y	Component of angle vector in Y-direction, associated with Euler's theorem on rotation.
θ_y	Component of angle vector in Y-direction, associated with Euler's theorem on rotation.
ζ	Wave elevation.
k	In relation to buoyancy, buoyancy key factor is the relative weight of the buoyancy section per meter.
N	Number of cycles, periods or events
S_{hh}	Hoop stress due to pressure
S_{hr}	Shear stress in r-direction on surface with normal in h-direction
S_{rr}	Radial stress due to pressure
S_{wB}	Buoyancy section averaged submerged weight per meter.
S_w	Umbilical/cable submerged weight per meter.
S_{xh}	Shear stress in h-direction on surface with normal in x-direction
S_{xr}	Shear stress in r-direction on surface with normal in x-direction
S_{xxc}	Axial stress due to global curvature
S_{xxp}	Axial stress due to pressure, end-cap effect
S_{xxt}	Axial stress due to effective tension
t_x	Tube wall thickness relevant for a particular stress calculation
X_e	Expected largest value, average value of the largest (of N)
X_N	Characteristic largest value, exceeded on the average once in N periods
D	Tube nominal outer diameter
Hmax	Maximum height of regular wave

Hs Significant wave height

ID Tube nominal inner diameter

OD Tube nominal outer diameter

Rm Material tensile strength, SMTS or measure values

Rp0.2 Material yield strenght, SMYS or measured value

SMTS Specified minimum tensile strength, see Rm

SMYS Specified minimum yield strenght, see Rp0.2

T Time span, e.g. some period or duration of sea state

THmax Period of regular wave with height Hmax

Tp Spectral peak period

Tz Zero up-crossing period

WT Tube nominal wall thickness

X Axial motion in static direction of umbilical at the upper end (m).

Xh Hang-off coordinate, vessel coordinate system

Yh Hang-off coordinate, vessel coordinate system

Zh Hang-off coordinate, vessel coordinate system

1 Introduction

The main objective of this work is to investigate extreme value estimation procedures that are suitable for simulations that give results in the form of long time series.

The investigated umbilical system is arranged in a lazy wave configuration connected to a ship. There is significant tension dynamics and compression in the sag region of the umbilical. This system was chosen for the desire to see if the main cause for this could be determined.

Further motivation for this work is related to the practical task of bend stiffener design in irregular wave analysis. The interesting parameters are the simultaneous combinations of umbilical tension and angle – in the statistical sense.

Simplified methods are of general interest, partly because long non-linear simulations of useful length are still associated with hours of computer time compared to minutes if applying deterministic regular waves for design checks – but also because of the large amounts of data produced. Hence, simplifications that may more easily lead towards a solution in practical engineering cases are always valuable. Particularly those simplified method whose accuracy can be made explicit and tested.

The Master thesis assignment can be found in appendix A.

2 Summary

This report starts with a brief description of the purpose of an umbilical in the oil and gas industry. The umbilical carry in most cases electric, hydraulic or light signals for operation of subsea equipment such as valves or pumps.

Next, the umbilical cross section and the geometry of the applied global lazy wave configuration is presented. This is followed by a description of the environmental conditions typical for deep waters east of east of Brazil. The water depth at the field is 1300 m.

Then there are some chapters presenting some theory for bend stiffener design, methods for dynamic analysis and a simplified method for determining the long term 100-year extreme. This is followed by a chapter regarding the use of the Poisson distribution for estimating short term and long term extreme values by use of empirically obtained level up-crossing frequencies from simulated time series.

The simplified method evaluated in this document is based on using the top axial velocity for predicting interesting time instants for sag tension extremes. The investigation of this issue is mainly performed using the concept of rank order, e.g. the largest value gets rank 1, the second largest value gets rank 2 and so on. Hence, our object of study is lists as [1,2,3,...] and [2,1,4,...] for axial velocity and sag tension respectively. The correlation coefficient between such rank order lists is Spearman's rho. Therefore, Spearman's rho is reviewed and

some investigations are done to see if we can learn something about what rank order correlation to expect for a non-perfect approximation method – with an explicit success rate.

The top axial velocity is caused by the floating vessel, whose motions are given by transfer functions, RAOs. The chapter on RAOs give some background on their meaning and also some information regarding checking of RAO-values when using the Riflex computer program. Also, part of this chapter is a section on transformation of RAOs and a brief summary on how to calculate the response from transfer functions and wave spectrum based on the Gaussian assumption.

The Gaussian response calculations are then used to estimate the long term 100-year extreme for wave and vessel motions at the umbilical hang-off point. Also, the long term 100-year extreme of selected umbilical responses are calculated by time domain analysis. These results are also used to investigate which of the top end parameters that are better correlated with the umbilical response. As expected, instead of the wave elevation – top axial velocity is a better indicator for the important sea states considering umbilical tension. Likewise, the vessel angle is a better indicator for the most important sea states considering umbilical top angle.

These long term 100-year extreme estimates are then compared to the results obtained from the 100-year contour curve sea states. The non-exceedance quantile α needed to realize the long term 100-year extreme by the contour curve approach has also been determined. It appears that $\alpha = 0.90$ is an overall suitable value for the response quantities studied.

The final chapter deals with non-linear analysis of a selected sea state. In this section the two main issues are extreme value estimation for selected response parameters and rank order investigation of the relation between the top axial velocity and sag tension. Empirical level up-crossing frequencies are also presented for two response quantities.

3 Umbilical technology

Within the oil and gas industry, the purpose of an umbilical is to carry electric, hydraulic or light signals to operate equipment as valves or pumps. An umbilical may therefore also called an Electric, Optical and Hydraulic (EOH) cable. Some tubes may also be included for the purpose of injecting fluids, chemicals or gas, into other system pipe lines for flow assurance. Larger electrical conductors for power transmission may also be included.

3.1 Electric signal and power cables

The typical voltage of signal cables is about 1 kV whereas power cables typically operate at voltage level 6 kV. Four conductors are usually assembled in a quad, this is a circular bundle with typical outer diameter in the range 15-20 mm.

The electric signals are carried through small area copper conductors. The conductor size is small, typically 7.5 mm^2 corresponding to a outer diameter (outside the copper) of about 3 mm. Power cables are more varied in size, a typical diameter over the copper may be about 20 mm.

The conductors are made of almost pure copper for high electrical conductivity. Each conductor typically consists of a small center strand surrounded by minimum 6 equal strands – the latter are wound helically around the first. For a signal cable, the strand diameter is about 1 mm. The strands are drawn by the manufacturer from annealed circular copper wire with initial dimension about 10 mm.

Parameter	Unit	Value
Yield strength, Rp0.2	MPa	70
Tensile strength, Rm	MPa	210
Elongation at break	%	45
E-modulus, E	MPa	115000
Density, ρ	kg/m^3	8920

Table 1: Typical mechanical properties for annealed copper.

3.2 Tubes and hoses

The hydraulic control signals are transmitted through steel tubes or hoses filled with hydraulic fluid. The density of the hydraulic fluid is typically around 1050 kg/m3. The internal pressure is typically between 69-103 Mpa (10000-15000 psi). The internal pressure of these hydraulic lines keeps spring loaded valves opened. The valves are made so that they close if the hydraulic pressure is lost due to some event, this is the fail-safe principle.

The tube material is high strength steel, Super Duplex. The yield strength is typically in excess of 650 MPa and the E-modulus is around 200000 MPa. This material is more corrosion resistant than most other materials for most fluids and temperatures as used in umbilicals. Since high strength steel has a different cathodic potential than ordinary steel, the tubes are therefore usually plastic coated, mainly to avoid corrosion of the Super Duplex steel tubes.

3.3 Design criteria

The steel tubes are usually designed checking two load cases separately. The load case with internal pressure only – and a load case with combined pressure load, static and dynamic loads.

The design criteria is associated with the von Mises stress and the allowable value is usually limited to some fraction of the yield stress. This is the approach used in the standard “ISO 13628-5:2009, part 5: Subsea umbilicals”. However,

there are other standards under which the calculated stress shall be compared to the ultimate tensile stress.

Fatigue is conventionally checked for dynamic umbilicals. The allowed fatigue damage is usually 0.10 over the entire service life. The conventional Miner-Palmgren method using a SN-curve is applied in the fatigue calculations.

3.4 Equations for tube stress calculations

The total tube stress is calculated based on the principle of linearity. This means that the effect of the various loads are simply added. A cylindrical coordinate system will be adopted in the following. Indices, x, h and r will be adopted to designate the stress components in the axial direction (S_{xx}), hoop direction (S_{hh}) and radial direction (S_{rr}) respectively. To the extent that shear stresses are needed, they will be labeled in the conventional fashion, example S_{rh}, reference Mase (1970) [15].

Assuming that the stress check is to be performed by calculating the maximum von Mises stress and comparing this to the allowable stress. The allowable stress is a fraction of the material yield strength (SMYS), ηS_{yield}.

The pressure induced stresses, the end-cap pressure, S_{xxp}, the hoop stress S_{hh} and the radial stress S_{rr} are calculated by Lames' equation, see equations 1, 2 and 3. Note regarding axial stress, the concept of effective tension is applied.

$$S_{xxp} = \frac{P_i r_i^2 - P_o r_o^2}{r_o^2 - r_i^2} \tag{1}$$

$$S_{hh} = \frac{P_i r_i^2 - P_o r_o^2}{r_o^2 - r_i^2} - \frac{r_i^2 r_o^2 (P_o - P_i)}{r^2 (r_o^2 - r_i^2)} \tag{2}$$

$$S_{rr} = \frac{P_i r_i^2 - P_o r_o^2}{r_o^2 - r_i^2} + \frac{r_i^2 r_o^2 (P_o - P_i)}{r^2 (r_o^2 - r_i^2)} \tag{3}$$

The axial stress does also get contributions from the effective tension T (S_{xxt}) and bending curvature C (S_{xxc}). These components are calculated as follows:

$$S_{xxt} = \frac{T}{\pi (r_o^2 - r_i^2)} = aT \tag{4}$$

$$S_{xxc} = CrE = bC \tag{5}$$

The total axial stress, S_{xx} is obtained as the sum of the axial contributions since the problem is linear, se equation 6:

$$S_{xx} = S_{xxt} + S_{xxc} + S_{xxp} \tag{6}$$

Having determined these stresses and for generality assuming also that the shear stress components S_{xh}, S_{xr} and S_{hr} exist – the von Mises stress is calculated from equation 7.

$$S_{vm} = \sqrt{\frac{(S_{xx} - S_{hh})^2 + (S_{hh} - S_{rr})^2 + (S_{rr} - S_{xx})^2}{2} + 3\left(S_{xh}^2 + S_{xr}^2 + S_{hr}^2\right)} \tag{7}$$

Assuming that there is only pressure acting on the tube, the shear stresses are zero.

The von Mises stress equation can be used to determined the capacity curve for a simple tube. This is done by neglecting the shear stresses and introducing $S_{xx} = Y + S_{xxp}$ where $Y = S_{xxt} + S_{xxc}$ is the combined effect of the tension and bending. This give 8.

$$\begin{aligned} S_{vm}^2 &= \frac{1}{2}\left((Y + S_{xxp} - S_{hh})^2 + (S_{hh} - S_{rr})^2 + (Y + S_{xxp} - S_{rr})^2\right) \\ &= \frac{1}{2}\left[2Y^2 + 2Y\left(S_{xxp} - S_{hh} + S_{xxp} - S_{rr}\right) + \left((S_{xxp} - S_{hh})^2 + (S_{hh} - S_{rr})^2 + (S_{xxp} - S_{rr})^2\right)\right] \\ &= Y^2 + Y\beta + S_{vm0}^2 \end{aligned} \tag{8}$$

Here we see that the square of the von Mises stress is a quadratic polynomial in $Y = S_{xxt} + S_{xxc}$, the axial stress resulting from the external loads, the effective tension T and the bending curvature C. Furthermore we see that the square of Mises stress from pressure alone takes the role of a constant. The constant $B = 2S_{xxp} - S_{hh} - S_{rr}$ is interesting – because this tells us that for $B \neq 0$, the minimum von Mises stress happens for $Y = -\beta/2$, that is – for external load greater than zero.

Likewise, it is of considerable interest to learn that the von Mises stress is constant for any constant value of $Y = S_{xxt} + S_{xxc}$. Since $Y = S_{xxt} + S_{xxc} = aT + bC$ where T and C are the effective tension and curvature respectively. This tells us the that isocline curves for von Mises stress are parallell when plotted on a $T/|C|$-diagram.

It may be also shown that for any chosen radius between the inner and the outer of the tube, there will be two lines in a $T/|C|$-diagram that delimits the allowable tension/curvature combinations for the single pressurised tube. One line for each of the solutions of Y in equation 8.

Note: The dependancy on the radius occurs since the radius affects the radial and hoop stress. Of the two lines mentioned, one will have a positive slope and the other will have a negative slope.

4 Umbilical description

The umbilical consist of 16 tubes in total, 2 tubes with inner diameter of 1 inch (25.4 mm) tubes and 14 with inner diameter of 1/2 inch (12.7 mm). In addition to this, we find two electric signal cables, see figure 1.

The two largest tubes are arranged as helicals in the first layer together with two of the smallest tubes. In the second layer, we find the remaining smaller tubes and the signal cables, also arranged in helicals. Outside of this we find the inner polyethylene (PE) sheet, two layer of round armouring wires with diameter close to 5 mm and finally – the outer polyethylene sheath.

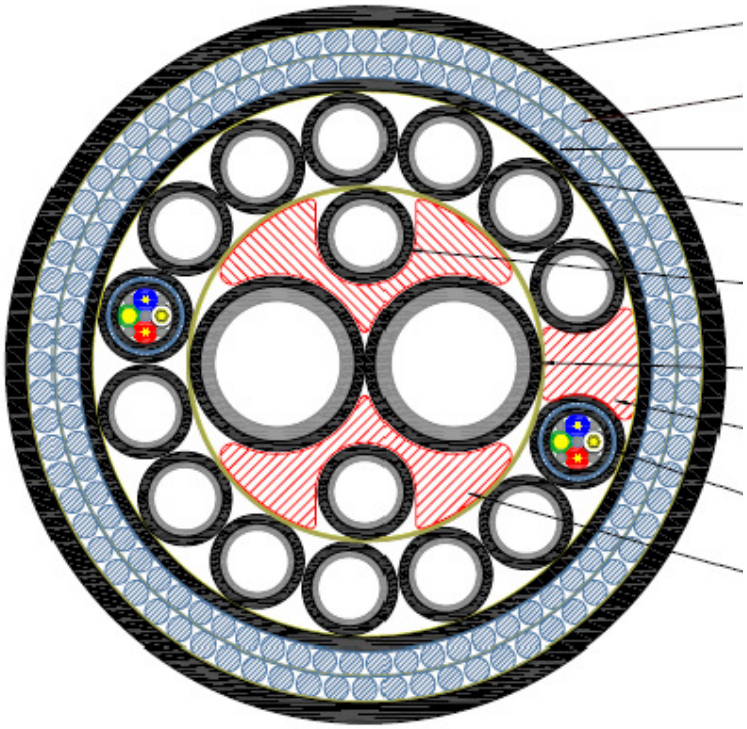

Figure 1: Umbilical cross-section.

4.1 Mechanical properties

Table 2 give geometrical information for the tubes of this umbilical. Cross-section properties including hydrodynamic coefficients are given in table 3.

4.2 Capacity curves

The design pressure is 69 MPa (10 000 psi) for all tubes. Table 4 contains stress isoclines for simultaneous effective tension and global curvature acting on the umbilical. The capacity curves are illustrated on figure 2. The curves have been prepared numerically by Nexans using the computer program Uflex2d version

Item	No. off (-)	ID (mm)	OD (mm)	WT (mm)	Material (-)	SMYS (MPa)	SMTS (MPa)	E-modulus (MPa)
1 inch tubes	2	25.40	31.10	2.85	SD steel	600	850	200 000
1/2 inch tubes	14	15.70	15.22	1.26	SD steel	670	850	200 000
Armouring wires	142	-	5	-	Steel	400	650	210 000

Table 2: Main elements of the umbilical.

Parameter	Symbol	Value	Unit
Mass (filled and flooded)	m	43.1	(kg/m)
Submerged weight (filled and flooded)	Sw	0.259	(kN/m)
Outer diameter	OD	0.144	(m)
Axial stiffness	EA	659	(MN)
Bending stiffness	EI	18.5	(kNm^2)
Torsion stiffness	GJ	96.1	(kNm^2)
Drag-coefficient, longitudinal	CDt	0.01	(-)
Drag-coefficient, normal (upper 300 m)	CDn	1.1	(-)
Added mass coefficient, longitudinal	Cat	0	(-)
Added mass coefficient, normal	Can	1	(-)

Table 3: Cross-section mechanical properties and hydrodynamic coefficients.

2.2.2 (2010) [25]. Issues such as non-linearities because of contact and friction are included in these analysis.

It should be mentioned that the stress isoclines used in this study are defined under Petrobras specific requirement for umbilicals. Under this regime, the stress levels shall be measured relative to the ultimate strength of the material, the relevant stress isoclines are for stress levels $0.60 \times SMTS$ and $0.77 \times SMTS$. These stress levels shall not be exceeded for normal and abnormal extreme conditions respectively.

With reference to the capacity curve figure, 2 and table 4. The upper part of the $0.60 \times SMTS$-curve defined by the 1/2 inch tube appears to be non-straight.

The reason for the non-straight deviation is mainly the friction that acts between the elements. Once a negligible and small curvature has been established, so that there is full slip between elements – there is an element friction stress amplitude due to the contact pressures. This friction stress amplitude is determined by the tension level in the umbilical. The tension level is determined from the umbilical effective tension, the internal tube pressures and the potential external static pressure. (Note that the internal voids of the umbilical, those between umbilical elements is sea water filled and that the pressure in these voids is equal to the external hydrostatic pressure, $P_o = \rho g h$.)

The friction stress amplitude is to a first approximation independent of the curvature level provided that the curvature is greater than the so called slip-level.

Because the friction stress amplitude is linearly increasing with the effective tension, we would expect to see slightly greater effects for larger tension levels. For this reason, the departure from linearity for the 1/2 inch tube is as expected.

The part of the curve defined by the larger 1 inch tube is found to be straight. after inspection of the results between data points 1 to 7. The only notable finding is that there is a slight slope reduction from the $0.60 \times SMTS$-curve to the $0.77 \times SMTS$-curve. This is mentioned since stress isoclines for an single tube would be parallel.

The slope reduction is small, only 3%. The reason is partially the friction stress amplitude, but the more significant cause is that stress components as S_{rr} and S_{hh} would obviously depend on the tension level – because of the direct connection with the contact pressure. The dependency on the curvature level would be comparatively less.

The construction elements that defines these capacity curves are: the large 1 inch tube, the smaller 1/2 inch tube and the copper within the electrical signal cables. The copper requirement is manufacturer specific.

It is worth noting that the largest 1 inch tube determine the part of the capacity curve for the very low tension levels. For close to the highest tension level, the 1/2 inch tube becomes critical. For the highest tension level the copper is critical since the manufacturer considers it unwise to allow material yield in an extreme condition. Stress analysis have been performed to determine the marked points on the capacity curves. Regarding the straight lines connecting any two adjacent points. The finding from section 3.4, that the capacity curves for individual tubes (or rods) are indeed straight lines in a $T/|C|$-diagram supports this practice.

	Normal extreme conditions $S_{vm} = 0.60$ SMTS		Abnormal extreme conditions $S_{vm} = 0.77$ SMTS	
Point	Tension (kN)	Curvature (1/m)	Tension (kN)	Curvature (1/m)
1	0.0	0.130	0.0	0.189
2	84.0	0.123	108.9	0.179
3	168.0	0.116	217.7	0.169
4	252.0	0.108	326.6	0.160
5	336.0	0.101	435.5	0.150
6	420.0	0.094	544.4	0.140
7	504.0	0.086	653.2	0.130
8	588.0	0.079	762.1	0.120
9	672.0	0.060	871.0	0.110
10	756.0	0.034	979.9	0.100
11	840.0	0	1089.	0

Table 4: Umbilical capacity curves, internal tube pressure is 69 MPa.

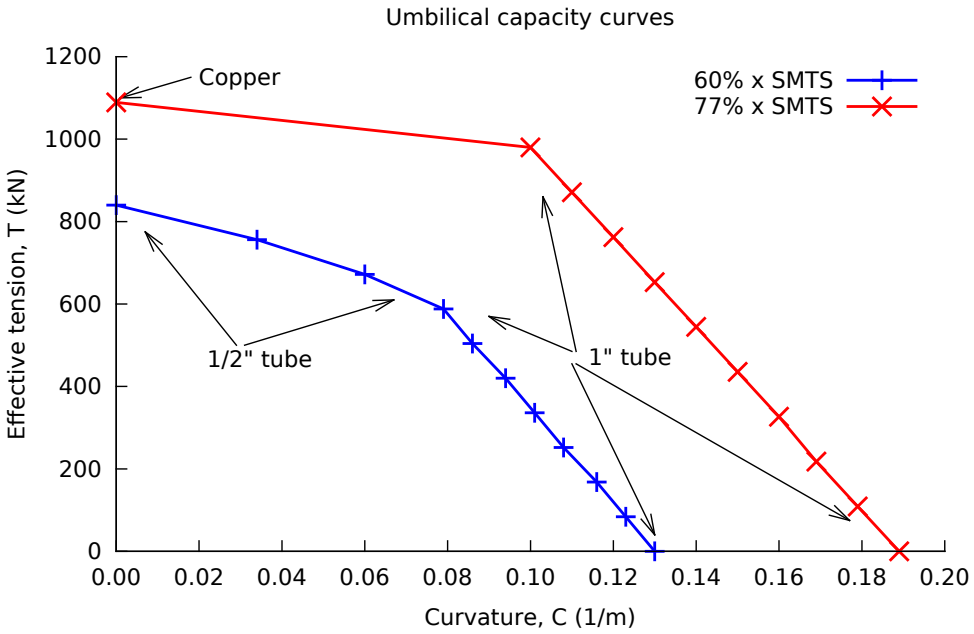

Figure 2: Umbilical capacity curves with identification of the defining element.

5 Global configuration

The umbilical is arranged in a lazy wave type of global configuration. At the top end there is a bend stiffener, this is attached to the I-tube of the vessel by a steel flange. Near the seabed there is a buoyancy section of distributed buoyancy modules.

The nominal top angle is 7 degree with the vertical. This angle matches that of the vessel I-tube. This contributes to reduce the overall length of the bend stiffener. The length of the buoyancy section is 125 m, the length averaged submerged weight of the buoyancy section is -3 times that of the umbilical itself, i.e. $k = S_{wB}/S_w = -3$.

The umbilical hang-off location of the umbilical is at the vessel port side. However, the umbilical goes under the vessel keel and lands on the seabed at the vessel starboard side. The umbilical direction is -90° relative to the vessel longitudinal axis. The vessel is oriented such that the vessel X-axis points in the south-east direction. This means that waves from south-west propagate in the vessel Y-direction. Hence, creating the maximum roll motion. See table 6 and figure 3.

Note that the global coordinate system as applied in the analysis model coincides with the vessel coordinate system as shown on figure 3.

Parameter	Value	Unit
Water depth	1300.0	(m)
Bend stiffener flange location, depth below water line	6.0	(m)
Top departure angle with vertical	7.0	(°)
Vertical distance from bend stiffener flange to seabed	1294.0	(m)
Horizontal distance from bend stiffener flange to model end at seabed	1100.0	(m)
Length from bend stiffener flange to buoyancy section, L_1	1520.0	(m)
Length of buoyancy section (k=-3), L_2	125.0	(m)
Length from buoyancy to model end at seabed	430.0	(m)
Total umbilical length in model	2075.0	(m)

Table 5: Description of lazy wave configuration, see figure .

	Xh (m)	Yh (m)	Zh (m)	Heading rel. vessel X (°)
Umbilical hang-off and heading	10.00	29.00	2.00	-90°

Table 6: Umbilical hang-off coordinates in vessel coordinate system, origin in vessel center and at keel. See figure 3.

	Effective tension		Curvature		
Vessel position	Top (kN)	Bottom (kN)	Sag/Touchdown (1/m)	Hog (1/m)	Top angle (°)
Nominal configuration	358.3	43.67	0.00593	-0.01780	7.00
Far offset, 150.5 m	373.2	69.90	0.00371	-0.01112	10.80
Near offset, 150.5 m	351.4	27.95	0.00927	-0.02780	4.56

Table 7: Key results, tension and curvature, for lazy wave configuration with nominal top angle equal to 7°, see figures 4, 5 and 6.

	Horizontal distance	Vertical distance	
Vessel position	Top to touch-down point (m)	Sag bottom to seabed (m)	Hog top seabed (m)
Nominal configuration	898	79.5	153.1
Far offset, 150.5 m	940	123.2	149.4
Near offset, 150.5 m	877	45.4	167.6

Table 8: Key results, distances, for lazy wave configuration with nominal top angle equal to 7°, see figures 4, 5 and 6.

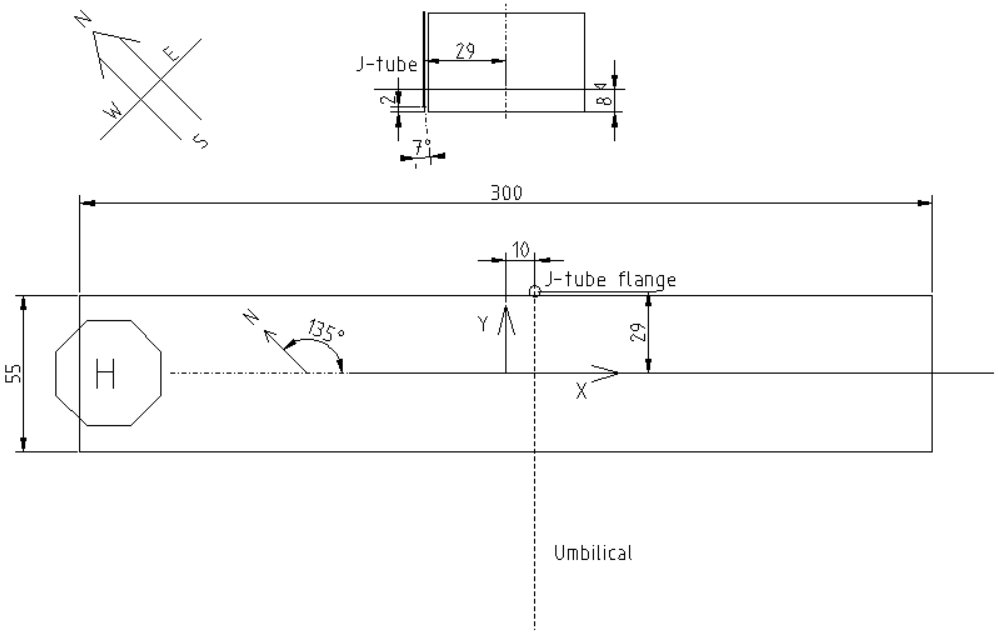

Figure 3: Vessel orientation and umbilical hang-off locations, see table 6. Note that the coordinate system used in the analysis coincides with the X- and Y-directions shown for the vessel.

5.1 Computer model and analysis details

The time domain analysis are performed using the computer program Riflex version 3.6.5 (2008), developed by Marintek, reference [13] and [14].

The simulation length is either 11000 seconds or 3660 seconds. The initial 60 seconds are discarded from post-processing. The pre-generated time series of wave kinematics and vessel motion are sampled every half second. The time step used in the integration algorithm is 0.125 s and the analysis results are sampled every 0.25 s.

The applied integration algorithm is of Newmark type, the parameter values are $\beta = 1/4$ and $\gamma = 1/2$. Hence, constant average acceleration is assumed in the integration.

The simulations are performed using a constant Rayleigh damping matrix which is defined at analysis start. The assumed level of Rayleigh damping is such that the relative damping is about 14% for a loading period of 10 seconds and 7% for a loading period of 20 seconds. The cause of the damping is internal friction, mainly associated with bending and occuring in the armouring layer of the construction.

See tables 9 and 10 for modelleing details as beam element discretization, mass and stiffness.

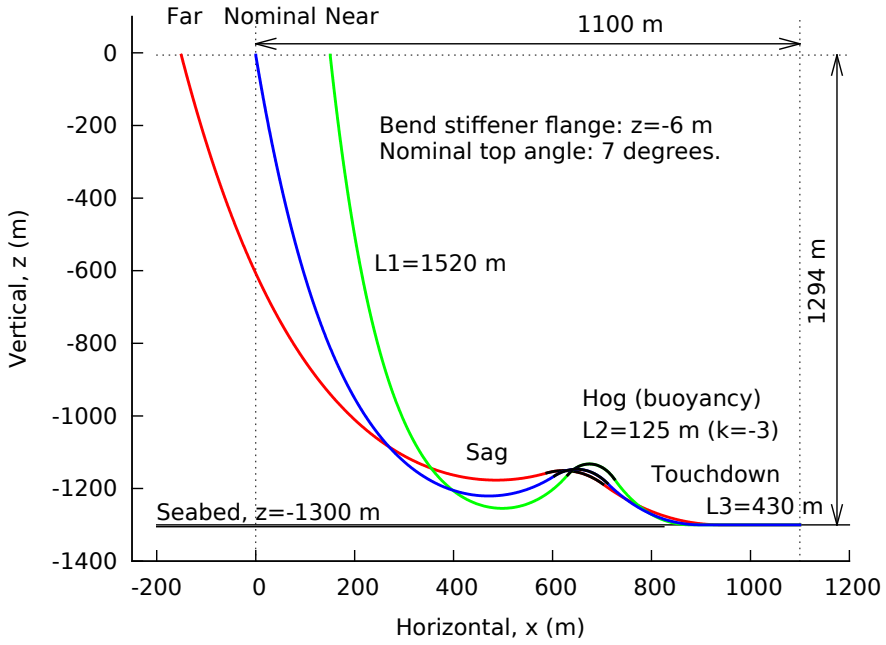

Figure 4: Geometry of the lazy wave configuration, see tables 7 and 8.

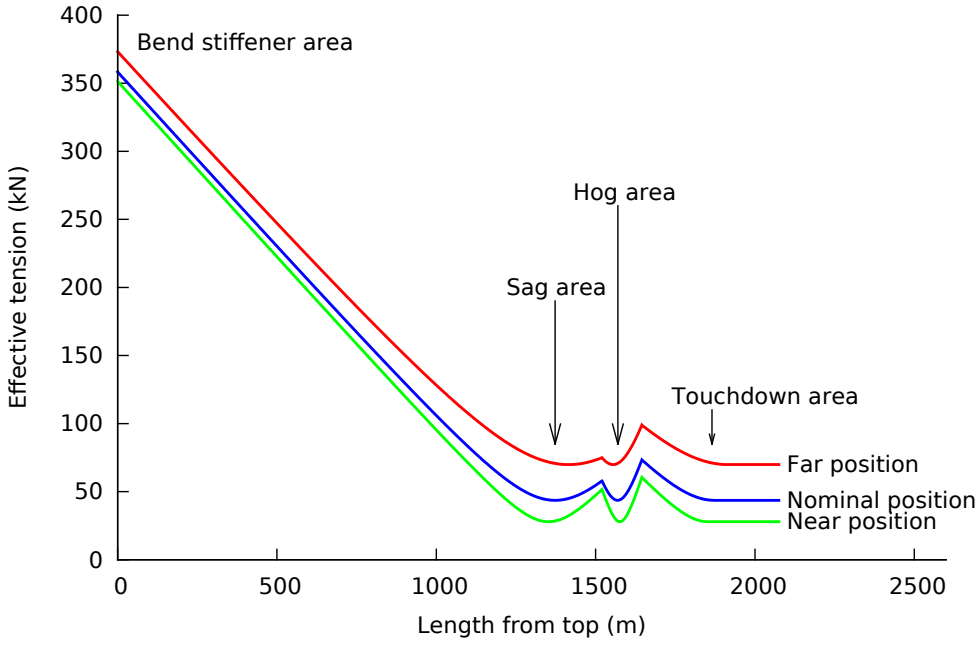

Figure 5: Effective tension along the length of the umbilical, see also tables 7 and 8.

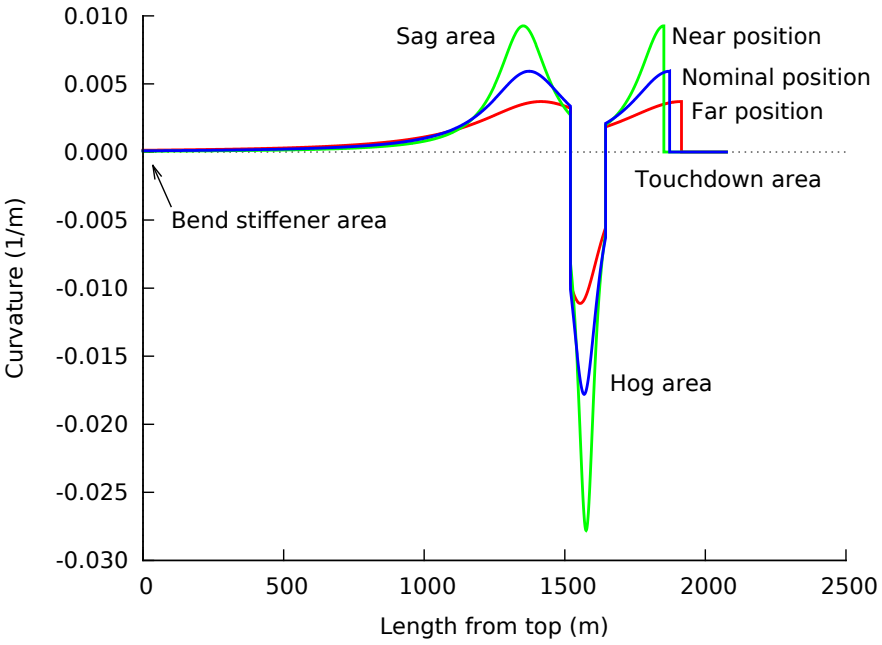

Figure 6: Curvature along of the length of the umbilical, see also tables 7 and 8.

Segment	Length (m)	No. elements (-)	El. length (m)	Mass (kg/m)	Dia. (m)	EI (kNm^2)	Sum length (m)
1	0.300	5	0.060	43.1	0.144	120000	0.3
2	0.350	4	0.087	43.1	0.144	120000	0.6
3	0.204	2	0.102	43.1	0.144	5725.6	0.9
4	0.204	2	0.102	43.1	0.144	5083.8	1.1
5	0.204	2	0.102	43.1	0.144	4497.7	1.3
6	0.204	2	0.102	43.1	0.144	3963.9	1.5
7	0.204	2	0.102	43.1	0.144	3479.3	1.7
8	0.204	2	0.102	43.1	0.144	3040.7	1.9
9	0.204	2	0.102	43.1	0.144	2645.2	2.1
10	0.204	2	0.102	43.1	0.144	2289.7	2.3
11	0.204	2	0.102	43.1	0.144	1971.6	2.5
12	0.204	2	0.102	43.1	0.144	1688	2.7
13	0.204	2	0.102	43.1	0.144	1436.4	2.9
14	0.204	2	0.102	43.1	0.144	1214.3	3.1
15	0.204	2	0.102	43.1	0.144	1019.3	3.3
16	0.204	2	0.102	43.1	0.144	849.1	3.5
17	0.204	2	0.102	43.1	0.144	701.4	3.7
18	0.204	2	0.102	43.1	0.144	574.3	3.9
19	0.204	2	0.102	43.1	0.144	465.6	4.1
20	0.204	2	0.102	43.1	0.144	373.6	4.3
21	0.204	2	0.102	43.1	0.144	296.4	4.5
22	0.204	2	0.102	43.1	0.144	232.4	4.7
23	0.204	2	0.102	43.1	0.144	179.9	4.9
24	0.204	2	0.102	43.1	0.144	137.4	5.1
25	0.204	2	0.102	43.1	0.144	103.7	5.3
26	0.204	2	0.102	43.1	0.144	77.4	5.5
27	0.204	2	0.102	43.1	0.144	57.3	5.7
28	0.200	2	0.100	43.1	0.144	48.7	5.9
29	0.300	2	0.150	43.1	0.144	18.5	6.2
30	0.500	2	0.250	43.1	0.144	18.5	6.7
31	0.750	2	0.375	43.1	0.144	18.5	7.5
32	1.250	2	0.625	43.1	0.144	18.5	8.8
33	7.000	10	0.700	43.1	0.144	18.5	15.8
34	20.000	15	1.333	43.1	0.144	18.5	35.8
35	25.000	14	1.786	43.1	0.144	18.5	60.8
36	25.000	10	2.500	43.1	0.144	18.5	85.8
37	110.000	29	3.793	43.1	0.144	18.5	195.8
38	110.000	19	5.789	43.1	0.144	18.5	305.8
39	20.000	2	10.000	43.1	0.144	18.5	325.8
40	864.250	44	19.642	43.1	0.144	18.5	1190.0
41	20.000	2	10.000	43.1	0.144	18.5	1210.0
42	10.000	3	3.333	43.1	0.144	18.5	1220.0
43	300.000	150	2.000	43.1	0.144	18.5	1520.0
44 (buoyancy)	125.000	62	2.016	192.41	0.580871	18.5	1645.0
45	320.000	150	2.133	43.1	0.144	18.5	1965.0
46	100.000	50	2.000	43.1	0.144	18.5	2065.0
47	10.000	3	3.333	43.1	0.144	18.5	2075.0

Table 9: Model details, mass, length, diameter and bending stiffness. The model starts at the top with segments 1 and 2 representing the stiff (steel) part of the bend stiffener, segments 3-28 being the soft (polymer) part of bend stiffener and segment 44 as the buoyancy section. The buoyancy section properties are averaged over the length, see also table 10

	Cd_t	Cd_n	Ca_t	Ca_n
Umbilical	0.01	1.1	0	1
Buoyancy section	0.16	0.65	0.46	0.85

Table 10: Hydrodynamic coefficients for analysis model. Axial and normal drag: Cd_t and Cd_n. Axial and normal added mass: Ca_t and Ca_n. The buoyancy section properties are averaged over the length, see also table 9.

6 Environmental conditions

6.1 Wind and vessel induced offset

The direct effect of wind speed, the potential wind induced drag load is usually neglected in conventional riser analysis. This simplification is done, even when the riser hangs freely from the deck of the floater. However, the effect of the wind on the floater horizontal offset is accounted for.

The floater offsets applied in the riser analysis are the extremes as determined from mooring analysis. These extreme offsets should not include the first order wave induced floater motions because these are added separately in the the dynamic umbilical analysis.

It is usual to consider both a maximum and minimum offset associated with specified wave, current and offset directions. In this study, all analysis are performed with no vessel offset.

6.2 Waves

The wave conditions described here are typical for the deep waters east of Brazil. The data are for the Jubarte Field which is 70 km offshore the Brazilian state of Espirito Santo, see figure 7. The state capital Vitoria is about 500 km north of the city Rio de Janeiro. The Jubarte offshore field is part of the Campos Basin area, the area of the latter is about 100 000 km^2. The water depth at the Jubarte field is 1300 m.

Figure 7: Jubarte field location east of Brazil.

Only wave data for direction south-west, from south-west, are given here. The wave data have been obtained from reference [3]. The so-called contour curves are illustrated on figure 8 for different return periods, the numerical data are given in tables 11 and 12. The observed wave scatter diagram consistent with the contour curves is given in table 13. Section 6.3 defines the applicable wave spectrum which is of Jonswap type - and adapted for the location.

Regarding table 11, it should be mentioned that the parameters Hmax and THmax are the extreme regular wave height and period associated with the irregular sea state as described by the Hs- and Tp-values.

	RETURN PERIOD (YEARS)				
Parameter	1 year	10 year	30 year	50 year	100 year
Hs (m)	6.37	7.16	7.49	7.64	7.84
Tp (s)	13.93	14.78	15.15	15.32	15.55
Tz (s)	10.18	10.78	11.05	11.17	11.33
Hmax (m)	11.89	13.30	13.90	14.17	14.53
THmax (s)	13.72	14.40	14.69	14.82	14.99

Table 11: Extreme waves from south-west, irregular and regular wave data.

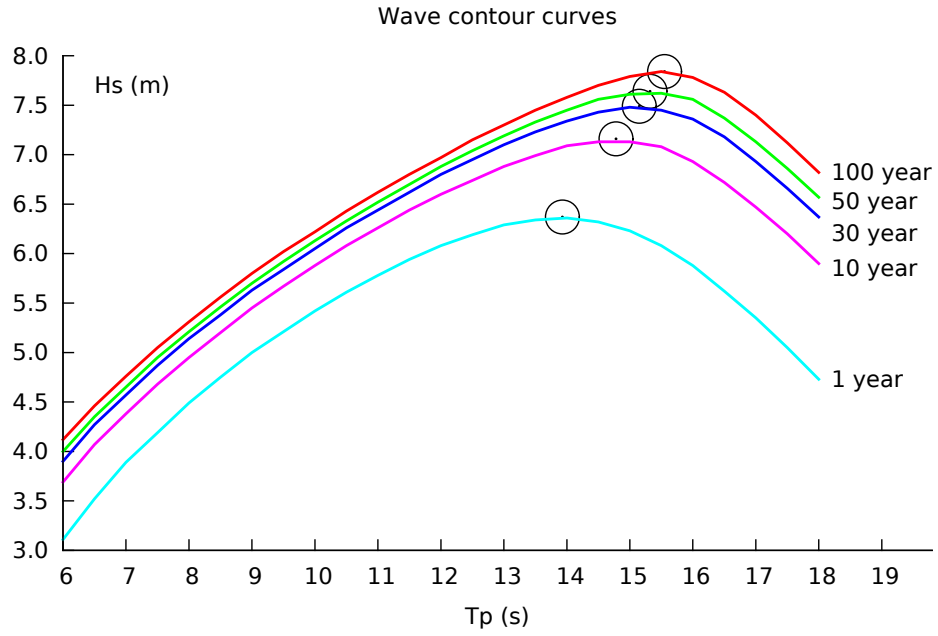

Figure 8: Contour curves for extreme waves from south-west, data from tables 12 and 11.

	RETURN PERIOD (YEARS)				
Period Tp(s)	1 year Hs(m)	10 year Hs(m)	30 year Hs(m)	50 year Hs(m)	100 year Hs(m)
6.0	3.11	3.69	3.90	4.00	4.12
6.5	3.52	4.07	4.27	4.35	4.46
7.0	3.89	4.38	4.57	4.65	4.76
7.5	4.19	4.68	4.87	4.95	5.05
8.0	4.49	4.95	5.14	5.21	5.31
8.5	4.75	5.20	5.38	5.46	5.56
9.0	5.00	5.45	5.63	5.70	5.80
9.5	5.21	5.67	5.84	5.92	6.02
10.0	5.42	5.88	6.05	6.13	6.22
10.5	5.61	6.08	6.26	6.33	6.43
11.0	5.78	6.26	6.44	6.52	6.62
11.5	5.94	6.44	6.62	6.70	6.80
12.0	6.08	6.60	6.80	6.88	6.97
12.5	6.19	6.74	6.95	7.04	7.15
13.0	6.29	6.88	7.10	7.19	7.30
13.5	6.34	6.99	7.23	7.33	7.45
14.0	6.36	7.09	7.34	7.45	7.58
14.5	6.32	7.13	7.43	7.56	7.70
15.0	6.23	7.13	7.48	7.61	7.79
15.5	6.08	7.08	7.45	7.62	7.84
16.0	5.88	6.93	7.36	7.56	7.78
16.5	5.62	6.72	7.18	7.37	7.63
17.0	5.35	6.47	6.93	7.13	7.40
17.5	5.05	6.20	6.66	6.86	7.12
18.0	4.73	5.90	6.37	6.57	6.82

Table 12: Contour curves for extreme waves from south-west, see figure 8.

6.3 Wave spectrum definition

The Jonswap wave spectrum has been adapted for the Jubarte field location, see the Metocean specification (2005) [3].

The Jonswap wave spectrum is formulated as follows:

Tp(low)	(s)	5	6	7	8	9	10	11	12	13	14	15	16	17			
Tp(high)	(s)	6	7	8	9	10	11	12	13	14	15	16	17	18			
Hs(low) (m)	Hs(high) (m)														Sum	Pr(h≤Hs)	Mean Tp (s)
0.0	0.5														0	0.00%	0
0.5	1.0		2				1								3	0.34%	7.78
1.0	1.5	3		4	10	16	9	14	3	1		1			61	6.94%	9.89
1.5	2.0		6	13	21	28	37	21	5	2					133	15.13%	9.78
2.0	2.5		6	12	24	39	56	40	22	8					207	23.55%	10.30
2.5	3.0		1	2	13	31	49	43	33	8	1				181	20.59%	10.84
3.0	3.5			4	14	18	23	37	22	12	4	5			139	15.81%	11.22
3.5	4.0			1		13	15	13	19	15	2	1		1	80	9.10%	11.70
4.0	4.5					7	4	5	11	11	6	1			45	5.12%	12.26
4.5	5.0					1	4	2	6	3	3	1			20	2.28%	12.48
5.0	5.5						1	1	1	3	1				7	0.80%	12.77
5.5	6.0							1							1	0.11%	11.13
6.0	6.5									2					2	0.23%	13.48
6.5	7.0														0	0.00%	0
	Sum	3	15	36	82	153	199	177	122	65	17	9	0	1	879		
Pr(t≤Tp)		0.34%	1.71%	4.10%	9.33%	17.41%	22.64%	20.14%	13.88%	7.39%	1.93%	1.02%	0.00%	0.11%			
Mean Hs (m)		1.35	1.89	2.13	2.27	2.53	2.56	2.67	3.10	3.53	4.01	3.40	0.00	3.78			

Table 13: Wave scatter diagram for waves from south-west.

$$S(\omega) = \frac{5}{16}\frac{H_s^2 T_p}{2\pi}\left(\frac{\omega_p}{\omega}\right)^5 (1 - 0.287\ln\gamma)\exp\left[-\frac{5}{4}\left(\frac{\omega_p}{\omega}\right)^4\right]\gamma^{\exp\left[-\frac{1}{2}\left(\frac{\omega-\omega_p}{\sigma\omega_p}\right)^2\right]}$$

Where:

$$\begin{aligned}\sigma &= \begin{cases} 0.07\ ,\ \omega \leq \omega_p \\ 0.09\ ,\ \omega > \omega_p \end{cases} \\ \gamma &= 6.4/T_p^{0.491} \\ \omega_p &= 2\pi/T_p \end{aligned} \tag{9}$$

The relation between T_z and T_p for the adapted Jonswap wave spectrum is given by:

$$T_z = T_p\sqrt{\frac{5+\gamma}{10.89+\gamma}} \tag{10}$$

7 Bend stiffener basics

The task of the bend stiffener is to protect the umbilical from being over bent when subjected to a specified combination of tension (T) and angle (θ), see figure 9. Over bending is defined to occur if the resulting maximum curvature (C) within the bend stiffener exceed that defined by the capacity curve for the associated tension level. Normally, there are several defined load combinations that must be checked as indicated on figure 10.

The bend stiffener supplier is responsible for designing a suitable bend stiffener meeting the requirements associated with purchaser specified load cases. The load cases that must be considered are those associated with extremes, see figure 10 but also fatigue loads must be given. The fatigue loads are usually given as histograms where the number of cycles and associated tension and angle variations are given for several bins. This histogram description is deceptively simple since it is not obvious that the true vector nature of the bend stiffener angle is properly accounted for. With reference to the next section and figure 11, the length of the angle vector $|\mathbf{V}(t)| = \theta$ may be constant even if the direction of the angle vector $\mathbf{V}(t)$ is changing. Hence, loads and material strains could be varying even if the bend stiffener angle θ is constant.

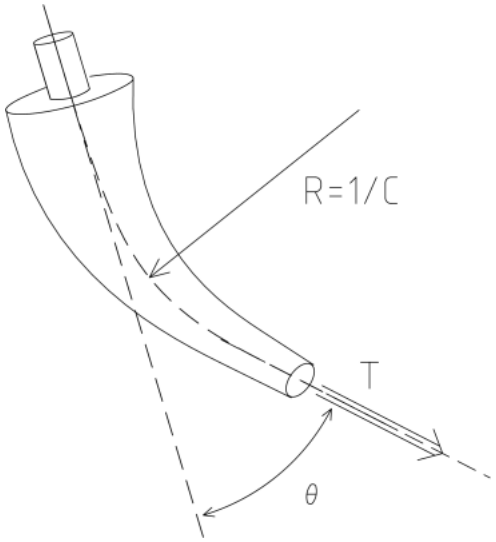

Figure 9: A bend stiffener subjected to a tension/angle-load and resulting curvature.

Figure 9 clarifies the application of the simultaneous tension/angle-load on the bend stiffener. The figure does also show the resulting curvature within the bending stiffener.

7.1 The bend stiffener angle is a vector

For calculation of the bend stiffener angle, see figure 11. The procedure is to calculate the angle between two vectors, $\mathbf{A}(t)$ which follows the vessel and the

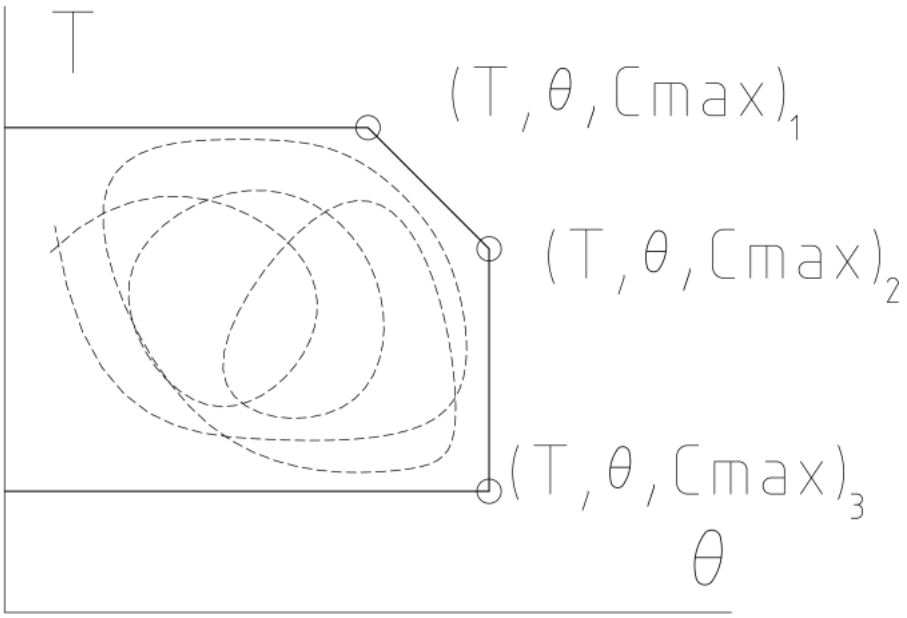

Figure 10: Tension, angle and curvature requirements for bend stiffener design.

vector $\mathbf{B}(t)$ below the tip of the bend stiffener. The position of the vector $\mathbf{B}$(t) should be sufficiently below the bend stiffener tip so that there is negligible bending at that location, see Sødahl [26]. A ball joint model may be applied in the first iteration if the bend stiffener is not known in advance.

The bend stiffener angle is a vector determined from the cross-product between a vector at the top end (fat end) $\mathbf{A}$ of the bend stiffener, from a beam element at the vessel fixation side, and a vector from a beam element just below the bend stiffener tip $\mathbf{B}$. Their cross product is normalized and assigned a length equal to the angle between the vectors $\mathbf{A}$ and $\mathbf{B}$, this is the rotation vector $\mathbf{V}$.

The bend stiffener angle vector is calculated as follows:

$$\mathbf{V} = \mathbf{e}_v\theta = \frac{\mathbf{A}(t) \times \mathbf{B}(t)}{|\mathbf{A}(t) \times \mathbf{B}(t)|}\theta \tag{11}$$

where θ is determined from $|\mathbf{A}(t)||\mathbf{B}(t)| \sin(\theta) = |\mathbf{A}(t) \times \mathbf{B}(t)|$.

This angle vector $\mathbf{V}$ contains all the information that is needed to accurately rotate the vector $\mathbf{A}(t)$ onto the vector $\mathbf{B}(t)$. Note that this vector is always laying the plane of the bend stiffener flange and that it therefore may be arbitrarily decomposed into a suitable coordinate system that follows the bend stiffener flange (vessel) motion.

This is an application of the Euler's rotation theorem for a solid body. Observe that the use of the three Euler angles to rotate a solid body is a different representation for exactly the same, see Arfken and Weber, Mathematical methods for physicist, pp. 188 [5].

Note that a convenient approximation may be obtained by decomposing the $\mathbf{B}(t)$ vector into its static and time variant part, $\mathbf{B}(t) = \mathbf{B_0} + \Delta\mathbf{B}(t)$. If the time variant part $\Delta\mathbf{B}(t)$ is negligible, $\mathbf{V}(t) \approx \mathbf{V}'(t) = \frac{\mathbf{A}(t)\times\mathbf{B_0}}{|\mathbf{A}(t)\times\mathbf{B_0}|}\theta'$, where $\sin(\theta') = |\mathbf{A}(t) \times \mathbf{B_0}|/(|\mathbf{A}(t)||\mathbf{B_0}|)$.

Conceptually we may therefore consider the bend stiffener angle as the sum of two parts, $\theta = \theta' + \theta''$:

θ'**:** The angle between the moving vessel versus the static top end direction of the umbilical.

θ''**:** The deviation in the umbilical direction from the static direction due to the dynamic loads and the forced top end motion of the umbilical.

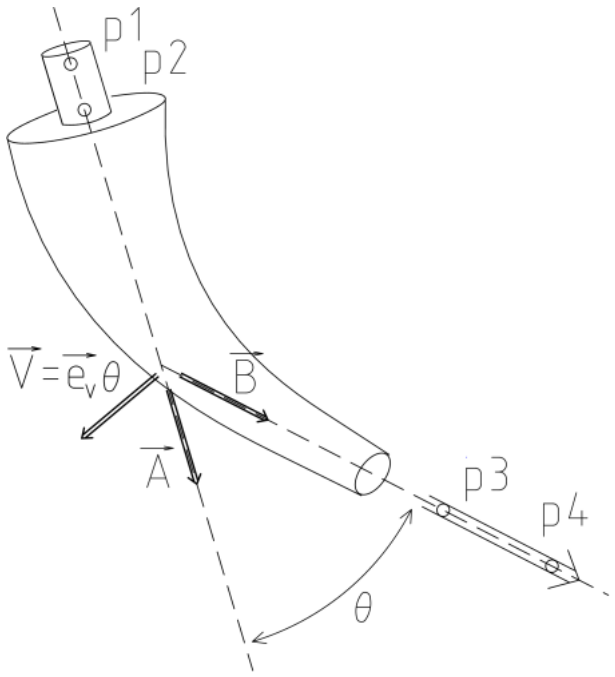

Figure 11: Parameters for the bend stiffener angle calculation.

7.2 A convenient approximation for bend stiffener curvature

The bend stiffener curvature vector $\mathbf{C}$ may be assumed parallel to the angle vector $\mathbf{V}$ discussed in the previous section if there is no bending moment or torque acting at the lower end of the beam element defining the vector $\mathbf{B}(t)$ and the loads directly acting on the bend stiffener are neglected.

Under this assumption, the value of the curvature at a particular length location can be assumed a function of the tension, T, and the bend stiffener angle θ. A planar problem will be assumed in the following. We expect: $C = f(T, \theta)$. Studying the Taylor expansion around $\theta = 0$ considering the angle θ we obtain

the approximation $C \approx a(T)\theta + b(T)\theta^3 + \ldots$ since the curvature is obviously an odd function of the angle (from the planar assumption). For small angles, the θ^3 term is negligible compared to the leading term. Hence, if also the tension is constant, we may write $C \approx k\theta$ where k is a number that characterizes this bend stiffener and umbilical assembly.

The above approximation is particularly useful when the driving design criteria is fatigue. Such fatigue driven design situations are often claimed to be iterative and may be experienced as confusing. Here it is claimed that the k-factor offers much desired control in exactly this kind of situation since the dominating fatigue conditions are usually associated with a near constant tension and small angles. For such a situation, the fatigue damage would be proportional to typically k^m where m is a characteristic slope of the SN-curve, typically m is around 4. It is here assumed that the bending stresses are proportional to curvature (therefore also proportional to k) and that the fatigue damage is calculated using SN-curves and the Miner-Palmgren approach. It is also assumed that the fatigue loading is dominated by bending which is the only case where an improved bend stiffener design could help.

The relation that should dictate the iteration procedure when the bend stiffener design is governed by fatigue requirements is described by the following: Given a known fatigue damage result D_1 for a particular bend stiffener identified by k_1, the result for a different k_2-value would be about $D_2 = D_1(k_2/k_1)^m$. Since D_2 is known as the requirement, the required k_2 can be determined and converted to a bend stiffener requirement. Note that the unit of k is curvature per angle, e.g. $1/\mathrm{m}^\circ$.

7.3 Bend stiffener coordinate system

The bend stiffener angle vector $\mathbf{V}$ is as described in the previous section 7.1 is always laying in the plane of the bend stiffener flange at the top end, see figure 11. It is convenient to define a local coordinate system for the bend stiffener flange. This is a right-handed Cartesian coordinate system as follows:

- The X-axis is in the umbilical tangent direction and is positive upwards.
- The Y-axis is in the plane of the bend stiffener flange, it is also perpendicular to the nominal umbilical configuration plane.
- The Z-axis is also in the plane of the bend stiffener flange, the nominal umbilical configuration is in the XZ-plane.

Practically, this coordinate system is established using two beam elements both attached to the vessel at the same point and spanning out a part of the XZ-plane. The first of these is indicated by the $\mathbf{A}$-vector of figure 11, the second has no structural purpose and is not illustrated.

This bend stiffener coordinate system will move as a function of the time since the bend stiffener is fixed to the vessel. However, since the nodal coordinate

positions are known for every point in time, the coordinate system is also known. Velocities and accelerations in the different directions, such as the axial direction are obtained by numerical differention using the central difference scheme as described by Bergan et al [6] pp. 210. The time series ends are treated specially, using the forward and backward scheme.

8 Dynamic analysis methods

The purpose of all dynamic analysis methods is to determine the combined load on the system as the sum of the static plus dynamic loads. The dynamic loads arise from the time varying loads or boundary conditions for the system. The system equation that must be solved is the following according to Bergan et al, "Svingning av konstruksjoner" (1981) pp. 223 [6].

$$\mathbf{M}\ddot{\mathbf{r}}(t) + \mathbf{C}\dot{\mathbf{r}}(t) + \mathbf{K}\mathbf{r}(t) = \mathbf{R}(t) \tag{12}$$

where $\mathbf{M}$, $\mathbf{C}$ and $\mathbf{K}$ are the mass, damping and stiffness matrices of the system. The nodal displacements and its time derivatives are given by $\mathbf{r}(t)$, $\dot{\mathbf{r}}(t)$ and $\ddot{\mathbf{r}}(t)$. The load is given by $\mathbf{R}(t)$

The damping matrix usually given as Rayleigh damping, which is a linear combination of the mass and stiffness matrices, [6] pp. 201:

$$\mathbf{C} = \alpha_1\mathbf{M} + \alpha_2\mathbf{K} \tag{13}$$

The coefficients α_1 and α_2 can be determined from the known relative damping λ at two frequencies since for any circular frequency ω_i.

$$\lambda_i = \frac{1}{2}\left(\frac{\alpha_1}{\omega_i} + \alpha_2\omega_2\right) \tag{14}$$

8.1 Frequency domain analysis

If the system matrices $\mathbf{M}$, $\mathbf{C}$ and $\mathbf{K}$ are constant, or frequency dependent – and the load is linear, the total response from a sum of harmonic loads at different frequencies (including zero, the static load) is obtained by super-positioning.

The calculation of the load effect is then most conveniently done in the frequency domain, considering the harmonic response caused by a harmonic load. This yields the following where the load and the response are complex numbers to account for their phase difference, Passano (1994) [24] pp. 11:

$$(-\omega^2\mathbf{M} + \mathrm{i}\omega\mathbf{C} + \mathbf{K})\mathbf{r}(\omega) = \mathbf{R}(\omega) \tag{15}$$

For a slender marine structure as an umbilical, a prominent load is the drag load which is quadratic in the relative velocity between the umbilical and the water particles. If such a structure is to be analyzed in the frequency domain, the

drag load must be linearized. It should be noted that a frequency domain does not yield information about the response distribution. However, the consistent choice associated with the assumption of a linear Gaussian narrow banded response is Rayleigh distributed maxima- and minima-values. This assumption is usually made in practical work when using the frequency domain method.

The transfer function, generally $\mathbf{H}(\omega)$ is an important concept in frequency domain analysis. Here, $\mathbf{H}(\omega)^{-1} = -\omega^2\mathbf{M} + \mathrm{i}\omega\mathbf{C} + \mathbf{K}$.

Application of the transfer function $\mathbf{H}(\omega)$s and the procedure for calculating the response caused by a Gaussian sea state is described in section which deals with the vessel motions transfer function, RAOs. The method for calculating the response spectrum, standard deviation and zero up-crossing frequency is described in section 12.4.

8.2 Time domain analysis

Time domain analysis is capable of handling non-linearities in both the system matrices and in the load term. This is therefore the natural choice for riser analysis in which the non-linear drag load is a significant.

The system matrices may then be updated in each time step accounting for the geometry and tension at each time instant. However, the system matrices may also be practically constant if the deformations or the tension variations are small. This may be the case for some analysis task, like e.g. fatigue evaluation. It should however be noted that proper modelling of seafloor interaction would require a full non-linear analysis where system matrices are updated in each time step.

The equation of motion is then used in the following incremental form [24] pp. 10 and [6] pp. 223:

$$\mathbf{M}\Delta\ddot{\mathbf{r}} + \mathbf{C}\Delta\dot{\mathbf{r}} + \mathbf{K}\Delta\mathbf{r} = \Delta\mathbf{R}(t) \tag{16}$$

The load on the right hand side may depend on unknown incremental values on the left hand side. In such a case iteration must be used to solve the equation. Typical integration methods for solving such problems are the Newmark and the Wilson θ methods.

8.3 Damping

According to Bergan et al (1981) pp. 192-194 [6], the energy dissipation in a harmonic deformation cycle is given by:

$$W_d = \oint F \,\mathrm{d}u \tag{17}$$

The unit of the product Fu must energy conjugated dimensions, meaning that the unit of the product must be that of energy, kNm. Examples are *force-deflection*, *moment-curvature* and also *stress-strain* where integration over a material volume is implied for the latter.

The loss coefficient is the energy loss per radian $Wd/(2\pi)$ divided by the peak potential or strain energy $U = 1/2ku_0^2$ for a linear material. Here, $k = \mathrm{d}F/\mathrm{d}u$ and u_0 is the maximum deflection amplitude for the cycle.

No matter the type of damping, the *loss coefficient* η, or the specific damping capacity per radian is given by:

$$\eta = \frac{1}{2\pi}\frac{W_d}{U} \tag{18}$$

The damping level relative to the critical, ξ can be determined from the *loss coefficient* η. This damping level ratio is exact if the source of the damping is viscous and a reasonable approximation for a harmonic motion sequence [6].

$$\xi = \frac{1}{2}\eta \tag{19}$$

9 Method for determining the long term extreme

A simplified methodology to determine the 100-year response maxima (or minima) has been described by Larsen and Olufsen (1992) [10]. This method is based on the initial assumption of Gaussian distribution of response quantities – and is described as follows:

- Step 1: Obtain the wave scatter diagram. This wave scatter diagram is then divided into a suitable number of bins for numerical work. Establish for each bin a representative sea state $(\mathrm{Hs},\mathrm{Tp},\gamma)_i$ and the associated sea state probability (fraction of time with this sea state), P_i. Note: that the full scatter diagram may be used since frequency domain methods are fast.

- Step 2: Establish the wave standard deviation (σ_i) and the zero up-crossing frequency (ν_{0i}) for each defined bin per the previous step. Use this to establish the long term distribution of wave maxima. This is done by assuming that the wave response is Gaussian distributed within each sea state. This assumption means that the maxima/minima distribution is known for all sea states. The maxima/minima distribution may be taken as the Rayleigh distribution if narrow bandedness is assumed. Alternatively, the level up-crossing frequency relation for a Gaussian stochastic process can be used directly. (Note that if an exact long term result is wanted, the exact level up-crossing frequency relation can be used – if available.)

- Step 3: Calculate the wave level that is exceeded on the average once in 100-year. This is done by summation over all sea states in 100-years, either by weighed summation over the Rayleigh distributed peaks or by the Poisson approach where weighed summation of up-crossing level frequencies is performed. Note that the Poisson approach is used in this

report, this give exactly the same result as assuming Rayleigh distributed maxima/minima as shown below. This happens since the equation for the Poisson approach can be converted to the equation associated with the Rayleigh approach. Also, the importance (contribution) of the sea states with respect to the long term extreme is calculated.

- Step 4: Perform response calculations by approximate frequency domain method (Gaussian assumption) using the most important sea states found in step 3.
- Step 5: Establish the long term response extreme based on the Gaussian assumption which is exceeded on the average once in 100-year. As in step 3, also the importance (contribution) of the sea states with respect to the long term extreme is calculated. For each of this sea states (and others if desired) determine the duration of the sea state under the condition that the long term extreme shall be the most probable extreme (under the Gaussian assumption) for this particular sea state and that storm duration
- Step 6: Use refined time domain calculation method for one (or more) selected sea state found in step 5 with storm duration as also found in step 5 for this sea state. Estimate the most probable extreme based on this simulation result.

This procedure is a staged procedure where sea states that are not considered significant contributors to the long term maximum are discarded early. The wave height is used in this first stage for this purpose – assuming Rayleigh distribution of the wave maxima within each sea state (consistent with a Gaussian narrow banded wave spectrum). Only the most contributing sea states to the long term wave maximum are kept for the response calculations. In effect, detailed analysis effort is not wasted on sea states with suspected negligible effect on the end result – this being the main objective of the procedure.

The fourth step according to Larsen and Olufsen is to perform simplified response analysis (using e.g. frequency domain method) for the remaining sea states. Only those with significant contribution to the long term wave elevation maxima are used in this step. The results from these calculations are again used to determine the most contributing sea states, this time considering the contribution to the long term response maxima (not the wave elevation). Furthermore, for each of these most contributing stationary sea states – the storm duration needed to establish the determined long term response maxima as the characteristic largest is calculated. Note that the method applied to calculate this storm duration must be consistent with that applied in the previous step.

Now, the crucial sixth step comes – Larsen and Olufsen suggest that this storm duration (for a specific sea state) provides the link to the more accurate long term response maxima. In brief, the maximum response that is exceeded on the average once for this storm duration is claimed to be a proper estimate for the long term response. Note that *once per storm duration* is a specified up-crossing frequency.

Hence, the final step is to perform a most detailed analysis in order to determine the response level that is indeed exceeded only once for the specified storm duration and associated sea state.

Equation 29 is basis for determining the long term response x_D, it is the x-value that solves the following equation,

$$\text{Prob}(M(T) \leq x) = \exp(-1) = \exp\left[-T\sum_{i=1}^{n}\nu^{+}(x, W_i)P_{W_i}\right]$$

Here the left hand side equals $\text{Prob}(M(T) \leq x) = \exp(-1)$ since we are determining the characteristic largest of x for the duration T which is 100-years expressed in seconds, see table 14. For a Gaussian response, the up-crossing frequency is given by equation 30, $\nu^{+}(x, W_i) = \nu_{0i}^{+}\exp(-1/2(x/\sigma_i)^2)$. Here σ_i and ν_{0i}^{+} are the response standard deviation and the zero up-crossing frequency respectively, the sea state probability is P_{W_i}.

The above equation is obviously most easily solved in the following form,

$$1 = T\sum_{i=1}^{n}\nu_{0i}^{+}\exp\left[-\frac{1}{2}\left(\frac{x}{\sigma_i}\right)^2\right]P_{Wi}$$

This is readily transformed to the one suggested by Larsen and Olufsen, their equation 4, note that they do not write out the equation in full. The first step is to divide by the average number of cycles in the period T (100 years), $N = T\bar{\nu}$. The equation as given by Larsen and Olufsen under the Gaussian (Rayleigh) assumption is obtained after rearrangement. Note that the final term $(\nu_{0i}^{+}/\bar{\nu} = \bar{T}_z/T_{zi})$ is the weight factor associated with going from a time based probability to a cycle based probability,

$$\begin{aligned}\frac{1}{N} &= T\sum_{i=1}^{n}\nu_{0i}^{+}\exp\left[-\frac{1}{2}\left(\frac{x}{\sigma_i}\right)^2\right]P_{Wi}\frac{1}{N}\\ &= T\sum_{i=1}^{n}\nu_{0i}^{+}\exp\left[-\frac{1}{2}\left(\frac{x}{\sigma_i}\right)^2\right]P_{Wi}\frac{1}{T\bar{\nu}}\\ &= \sum_{i=1}^{n}\exp\left[-\frac{1}{2}\left(\frac{x}{\sigma_i}\right)^2\right]P_{Wi}\left(\frac{\nu_{0i}^{+}}{\bar{\nu}}\right)\end{aligned}$$

Once the specified long term maximum x_D is determined, the contribution for each sea state to this maximum can be calculated. The contribution c_i from sea state number i is given by: $c_i = T\nu_{0i}^{+}\exp(-1/2(x_D/\sigma_i)^2)P_{Wi}$, note that T is the number of seconds in 100-years here.

To prepare for the final step we need to determine the duration D_i for sea state i, such that the characteristic largest value for this sea state with unknown

duration D_i equals the found long term value x_D. The desired storm duration D_i solves the following equation, $1 = D_i \nu_{0i}^+ \exp(-1/2\,(x_D/\sigma_i)^2) P_{Wi}$ where everything except D_i is known.

Finally, when doing the detailed analysis – the characteristic maximum, the value that is exceeded on the average once per storm duration D_i is needed. This translates to solving $\exp(-1) = \exp[-D_i \nu_i^+(x)]$ when using the Poisson approach, see section 10.2.3. Here the function $\nu_i^+(x)$ is determined to fit the simulation results. It has been shown in section 10.2.3 that this is equivalent to the response value which is exceeded once in $N_i = D_i \nu_{0i}^+$ cycles.

Verification of this simplified method is possible if determining for each sea state the exact distribution of cycles, or perhaps simpler – the level up-crossing frequencies. The exact long term extreme may then be calculated. This is however a major task which is rarely performed in routine design work.

10 Poisson distribution, use of up-crossing frequency

Naess have in a series of papers advocated the use of the level up-crossing frequency and the assumption of the Poisson distribution for estimating extreme values of a response parameter ξ, see Naess (1984) [19] and [20], Naess et al (2007) [2] and [18], (2008) [16] and [17]. The derivation of the Poisson distribution is described by Newland (2005) pp. 194-195 [21].

This section summarize some of the information referred to above. The main objective of this section is to present the equations needed for using the Poisson approach in a ready-to-use form. This material is used when calculating the long term extreme mainly, see section 9 – but is also used in section 15 considering extreme value estimation.

The use of the Poisson distribution in extreme estimation implies that the up-crossing events for large response values are assumed independent.This is the so-called Poisson assumption. This assumption is normally acceptable. Exceptions are very short time durations or very narrow band processes.

The Poisson assumption means that there is a direct link between the extreme value, the up-crossing rate and the cumulative probability distribution (*cdf*), Naess (1984) [19]. Let $M(T) = \max\{X(t), 0 \le t \le T\}$ be the extreme value of the response process $X(t)$. The *cdf* for the largest response value $M(T)$ in a stationary short-term sea-state with duration T is then:

$$\begin{aligned} F_{M(T)}(\xi) &= \text{Prob}(M(T) \le \xi) \\ &= \exp\left[-\int_0^T \nu^+(\xi,t)\,\mathrm{d}t\right] \\ &= \exp\left[-\left\{\frac{1}{T}\int_0^T \nu^+(\xi,t)\,\mathrm{d}t\right\} T\right] \\ &= \exp\left[-\bar{\nu}^+(\xi) T\right] \end{aligned} \tag{20}$$

The basic idea is to estimate $\bar{\nu}^+(\xi)$, the average mean up-crossing rate of the level ξ from the short term time series:

$$\bar{\nu}^+(\xi) = \frac{1}{T}\int_0^T \nu^+(\xi, t)\,\mathrm{d}t \tag{21}$$

Only a minor modification is required to establish the *cdf* for the long term extreme value. The instantaneous ξ-level up-crossing rates must be summed over the full long term period T. This summation is in practice performed by considering the long term period built-up by a series of stationary short-term sea-states characterized by $W = (Hs, Tp)$. For each such sea-state we know the probability density (*pdf*) $f_W(W)$ and the level up-crossing rate $\bar{\nu}^+(\xi, W)$. The long term *cdf* for the largest response value $M(T)$ in the long term period T:

$$\begin{aligned} F_{M(T)}(\xi) &= \mathrm{Prob}(M(T) \le \xi) \\ &= \exp\left[-\int_0^T \nu^+(\xi, t)\,\mathrm{d}t\right] \\ &= \exp\left[-T\int_W \nu^+(\xi, W) f_W\,\mathrm{d}W\right] \end{aligned} \tag{22}$$

In practice, the integral is usually evaluated numerically over a discrete selection of sea states $W_1, W_2, \ldots, W_n$ where each sea state has an associated probability equal to $P_{W_1}, P_{W_2}, \ldots, P_{W_n}$,

$$\begin{aligned} F_{M(T)}(\xi) &= \mathrm{Prob}(M(T) \le \xi) \\ &= \exp\left[-T\sum_{i=1}^{n} \nu^+(\xi, W_i) P_{w_i}\right] \end{aligned} \tag{23}$$

10.1 Empirical estimation of the mean up-crossing rate

From an ergodic time series with total duration kT seconds, both the sample mean up-crossing rate $\hat{\bar{\nu}}^+(\xi)$ and the associated sample standard deviation $\hat{s}(\xi)$ can be estimated in addition to the 95% confidence interval $\mathrm{CI}_{0.95} = [\mathrm{CI}^-_{0.95}(\xi), \mathrm{CI}^+_{0.95}(\xi)]$ of $\bar{\nu}^+(\xi)$.

The procedure is to divide the longer time series into e.g. $k \ge 30$ pieces with equal length T. The confidence interval is based on the standard deviation, $\hat{s}(\xi)$, assuming a normal distribution. The latter is the reason for the required large k. Let $n_j^+(\xi, [0, T])$ be the number of level ξ-up-crossing events during the time interval $[0, T]$ from piece j of the total time series.

$$\begin{aligned}\hat{\bar{\nu}}^{+}(\xi) &= \frac{1}{k}\sum_{j=1}^{k}\frac{n_j^{+}(\xi,[0,T])}{T} \\ &= \frac{1}{k}\sum_{j=1}^{k}\hat{\nu}_j^{+}(\xi) \\ &= \frac{1}{T}\frac{1}{k}\sum_{j=1}^{k}n_j^{+}(\xi,[0,T]) \\ &= \frac{\hat{n}^{+}(\xi,[0,T])}{T}\end{aligned} \tag{24}$$

$$\begin{aligned}\hat{s}(\xi)^2 &= \frac{1}{k-1}\sum_{j=1}^{k}\left[\frac{n_j^{+}(\xi,[0,T])}{T}-\hat{\bar{\nu}}^{+}(\xi)\right]^2 \\ &= \frac{1}{k-1}\sum_{j=1}^{k}\left[\hat{\nu}_j^{+}(\xi)-\hat{\bar{\nu}}^{+}(\xi)\right]^2 \\ &= \frac{1}{k-1}\sum_{j=1}^{k}\left[\frac{n_j^{+}(\xi,[0,T])}{T}-\frac{\hat{\bar{n}}^{+}(\xi,[0,T])}{T}\right]^2 \\ &= \frac{1}{T^2}\frac{1}{k-1}\sum_{j=1}^{k}\left[n_j^{+}(\xi,[0,T])-\hat{\bar{n}}^{+}(\xi,[0,T])\right]^2 \\ &= \left(\frac{\mathrm{std}(n_j^{+}(\xi,[0,T])}{T}\right)^2\end{aligned} \tag{25}$$

Note that if the number of level up-crossings $n_j^{+}(\xi,0,T])$ is a Poisson variable as assumed, the standard deviation can be estimated without sub-dividing the longer time series into k shorter time intervals. The standard deviation is then determined by the equation:

$$\begin{aligned}\hat{s}(\xi)^2 &= \frac{\hat{\bar{\nu}}^{+}(\xi)}{T} \\ &= \frac{1}{kT}\sum_{j=1}^{k}\hat{\nu}_j^{+}(\xi)\end{aligned} \tag{26}$$

The confidence interval for the mean up-crossing rate of the level ξ is calculated as:

$$\mathrm{CI}_{0.95}^{\pm}(\xi) = \hat{\bar{\nu}}^{+}(\xi) \ \pm 1.96\ \frac{\hat{s}(\xi)}{\sqrt{k}} \tag{27}$$

10.2 Use of empirical up crossing rates

10.2.1 Calculating the extreme value for a short term condition

The interesting extreme value is the maximum of X for a short time span T. The time span T is typically 0.5 hour in Gulf of Mexico and 3 hours for the North Sea. The environmental conditions are expected to be stationary within this time span. The short term extreme value is determined using the assumed known up-crossing rate function $\nu^+(X)$. With reference to the following equation, let $M(T) = \max\{X(t), 0 \leq t \leq T\}$ be the extreme value of the response process $X(t)$.

$$F_P(X) = \text{Prob}(M(T) \leq X) \quad = \exp\left[-\nu^+(X)T\right] \tag{28}$$

To define the maximum X-value for the duration T – a specific definition is required. The following extreme value definitions are in common use:

The value associated with a specified quantile , the quantile is the non-exceedance probability. A quantile value of $\alpha = 0.90$ is suggested by Sverre Haver (2007) [1]. Hence, $\text{Prob}(M(T) \leq X) = \alpha$ is specified.

The characteristic largest value is the peak value which is exceeded on the average only once during the time span T. The characteristic largest value X_N is usually obtained from $F(X_N) = 1 - 1/N$ where $N = T\nu_{\bar{X}}$ is the number of peaks and $F(X_N)$ is the individual peak distribution, counting one peak between each mean level upcrossing.

The probability that all peaks are less than X_N is given by: $\text{Prob}(M(T) < X_N) = (1 - 1/N)^N$ – since the entire time span (all N peak values) is considered. This is the relevant non-exceedance probability when using the Poisson approach to determine the characteristic largest value. When N is large, say $N > 100$, it is more convenient to use the asymptotic limit: $\text{Prob}(M(T) \leq X_N) = 1/e = 0.3679$.

The most probable largest can be obtained by investigating the extremal point of the *pdf* of $F_p(X)$, $f = \mathrm{d}F_P/\mathrm{d}X$. The sought extreme value of X is determined from solving $\mathrm{d}f/\mathrm{d}X = 0$. In practice, the characteristic largest is often taken as the most probable largest. This approximation is very good if the asymptotic extreme value distribution is indeed Gumbel, which is correct when the underlying peak distributions are Rayleigh or Weibull type, Bury (1975) [7].

The expected largest is particularly useful because this statistical estimate is readily compared with the obtained sample extremes, especially when the sample size is large. The exact expected extreme value can be estimated from: $X_e = \int X f_P(X)\,\mathrm{d}X$ where $f_P(X) = \mathrm{d}F_p(x)/\mathrm{d}X$. However, a useful approximation is readily available if the Gumbel extreme value distribution is the asymptotic limit for large duration T (or large number

of peaks N). Since the expected extreme value (X_e) for the Gumbel distribution, $F_G(X) = \exp(-\exp(-(X-X_N)/\sigma))$ is known to be $X_e = X_N + \gamma\sigma$ where $\gamma \approx 0.57722$ (Euler's constant). The asymptotic non-exceedance probability is readily determined as: $\text{Prob}(M(T) \leq X_e) = F_G(X_e) = \exp(-\exp(-\gamma)) = 0.5704$.

It is seen that the most direct method for obtaining the extreme value of X is by specifying the non-exceedance probability $\text{Prob}(M(T) < X_N)$ of the equation: $\text{Prob}(M(T) \leq X) = \exp[-\nu^+(X)T]$. Here, both $\nu^+(X)$ and T are known.

Table 14 provides a convenient summary, assuming that T (or N is large) and that the Gumbel distribution is the asymptotic extreme value distribution.

Definition	$\text{Prob}(M(T) \leq X)$	
Characteristic largest	$F_P(X_N) = \exp(-1)$	≈ 0.3679
Expected largest	$F_P(X_e) = \exp(-\exp(-\gamma))$	≈ 0.5704
Typical quantile,	$F_P(X_\alpha) = \alpha$	$= 0.90$

Table 14: Values for $\text{Prob}(M(T) \leq X)$ when determining the extreme value X for duration T. Solve $\text{Prob}(M(T) \leq X) = \exp[-\nu^+(X)T]$ for the short term extreme. For the long term extreme, solve $\text{Prob}(M(T) \leq \xi) = \exp[-T\sum_{i=1}^{n} \nu^+(\xi, W_i)P_{w_i}]$.

10.2.2 Calculating the extreme value for a long term condition

The procedure of the previous section applies. Table 14 give the left hand side value for $\text{Prob}(M(T) \leq \xi)$. The difference is found on the right hand side considering the up-crossing frequency. For the long term extreme, the weighed sum of (the average) up-crossing frequency over all sea states W_i is used. The weight factor is the sea state probability P_{W_i}.

$$\begin{aligned} F_{M(T)}(\xi) &= \text{Prob}(M(T) \leq \xi) \\ &= \exp\left[-T\sum_{i=1}^{n} \nu^+(\xi, W_i)P_{w_i}\right] \end{aligned} \tag{29}$$

10.2.3 Application example, comparison with results from Rayleigh distribution

The extreme value results obtained from the Poisson distribution will be compared to conceptually similar results from the Rayleigh distribution.

The Rayleigh distribution is the correct distribution of peaks when a stationary and ergodic Gaussian process is narrow banded, Newland (2005) [21]. When the process is broadbanded, it is well known that the peaks are Rice-distributed if broadbanded. In both cases the Rayleigh distribution is suitable to predict

extreme values, Leira et al "Stochastic theory of sealoads" (2005) [12]. The Rayleigh distribution is exact in the narrow banded case and a conservative approximation otherwise.

According to Newland, the level up-crossing frequency for a general stationary Gaussian process with zero mean is given by equation 30.

$$\nu^+(X) = \nu_0^+ \exp\left[-\frac{1}{2}\left(\frac{x}{\sigma}\right)^2\right] \tag{30}$$

The required extreme value is obtained simply by replacing the left hand side value of $\text{Prob}(M(T) \leq X) = F_P(X) = \exp\left[-\nu^+(X)T\right]$ with a fixed value taken from table 14. The equation is thereafter solved for X.

$$\begin{aligned}
F_P(X) &= \exp\left[-T\nu_0^+ \exp\left[-\frac{1}{2}\left(\frac{X}{\sigma}\right)^2\right]\right] \\
\ln[F_P(X)] &= -N \exp\left[-\frac{1}{2}\left(\frac{X}{\sigma}\right)^2\right] \\
-\frac{\ln[F_P(X)]}{N} &= \exp\left[-\frac{1}{2}\left(\frac{X}{\sigma}\right)^2\right] \\
\ln\left(-\frac{\ln[F_P(X)]}{N}\right) &= -\frac{1}{2}\left(\frac{X}{\sigma}\right)^2 \\
\ln\left(-\ln[F_P(X)]\right) - \ln(N) &= -\frac{1}{2}\left(\frac{X}{\sigma}\right)^2 \\
\sigma\sqrt{2\ln(N) - 2\ln\left(-\ln[F_P(X)]\right)} &= X
\end{aligned} \tag{31}$$

To obtain the characteristic largest, $F_p(X_N) = \exp(-1)$ is substituted according to table 14. A familiar result emerges: $X_N = \sigma\sqrt{2\ln N}$, note that N is the number of zero up-crossings.

Likewise, the expected largest is obtained by substituting $F_P(X_e) = \exp(-\exp(-\gamma))$. This yield $X_e = \sigma\sqrt{2\ln N + 2\gamma}$ – unlike the expected $\sigma\left(\sqrt{2\ln N} + \frac{\gamma}{\sqrt{2\ln N}}\right)$. However, recalling that N must be large for the asymptotic approach, it is clear that the first term under the square root sign is much larger than the second. A Taylor expansion keeping first terms up to first order demonstrates that the Poisson asymptotically give the same result:

$$\begin{aligned}
X_e &= \sigma\sqrt{2\ln N + 2\gamma} \\
&= \sigma\sqrt{2\ln N}\sqrt{1 + \frac{2\gamma}{2\ln N}} \\
&\approx \sigma\sqrt{2\ln N}(1 + \frac{\gamma}{2\ln N}) = \sigma\left(\sqrt{2\ln N} + \frac{\gamma}{\sqrt{2\ln N}}\right)
\end{aligned} \tag{32}$$

It should be noted that the expected extreme from the Rayleigh distribution is also an asymptotic result. Where the exact extreme value distribution, $F_R(X)^N$

is approximated by a Gumbel distribution, also keeping terms to the first order in a Taylor series, Bury (1975) [7].

10.3 Curve-fit

Naess et al suggests to fit a curve to the empirical values $\hat{\hat{\nu}}^+(\xi)$. For improved curve-fit and extrapolation behavior the focus should be on response values larger than a specified lower value, $\xi_L \leq \xi$ where the lower threshold ξ_L is greater than the mean response $\bar{\xi}$.

The suggested model function by Naess can:

- Exactly represent the response up-crossing rate for a Gaussian stochastic process where the response is linear with the load.
- Exactly represent the response up-crossing rate for a Gaussian stochastic process where the response is quadratic with the load.
- Exactly represent the asymptotic behavior of the Gumbel distribution for large response levels.

The suggested model function contain 4 unknown parameters a, b, c and d that must be determined to best fit the empirical up-crossing rates.

$$\begin{aligned} &\nu^+(\xi) = \exp[-f(\xi)] \text{ where } f(x) = a(\xi - b)^c - d \\ &\text{where:} \\ &\qquad \bar{\xi} \leq \xi_L \leq \xi \\ &\qquad b \leq \xi_L \leq \xi \\ &\qquad a, c > 0 \end{aligned} \tag{33}$$

It should be noted that the d-parameter is essentially a slowly varying function that for practical purposes can be represented by a constant for large response levels ξ. This is one of the reasons for introducing a the specified lower value ξ_L.

The curve-fit is done by regression based on the logarithm of the empirical up-crossing frequency, $\ln \hat{\nu}^+_{\xi}$. The model parameters a, b, c and d minimize the weighed squared sum of residuals:

$$S = \sum_{i=1}^{n} \frac{1}{2}\, w_i \,[\, \ln \hat{\nu}^+_{\xi_i} + f(\xi_i) \,]^2 \tag{34}$$

The weight for each data point is suggested as $w_i = [\ln(CI_i^+) - \ln(CI_i^-)]^2$ by Naess. The parameters CI_i^+ and CI_i^- are the upper and lower limits of the 95% confidence interval for the empirical up-crossing frequency.

The applied curve fit procedure by Naess et al is the Marquardt-Levenberg algorithm according to the referred papers.

In this report, only empirically level up-crossing frequencies have been determined. Figures 43 and 45 show some of the more interesting empirical level up-crossing frequency results from the simulations reported in section 15.

11 Spearman's rho

11.1 Motivation

This section deals with the expectation of a rank correlation coefficient $-1 \leq \rho \leq 1$ when we are studying an approximation versus the true result. The puzzle started when the author read section "3.2 Evaluating and comparing time series", pages 17, 18 and table 3.1 of Passano (1994) [24]. In this table the rank correlation coefficient between both maxima and minima of two realizations (two different time series both representative of the same sea state) is reported as high as 0.786. As mentioned by Passano on page 17, this is of course misleading since maxima are restricted to correspond to maxima and minima to minima. However, this led to the question – what do we expect regarding the rank correlation value when studying the performance of an approximation method?

The following is the result of the authors investigation. Section 11.4 contain table 17 which contain critical values, ρ_{critical} based on a claimed quality of the approximation method P_{success} – the author is not aware of similar published information. To qualify the method, some published results according to table 15 have been reproduced.

11.2 Description of Spearman's rho

Charles Spearman's rank correlation coefficient, rho, is a non-parametric measure of order correlation between two associated variables X and Y, see Wikipedia [30]. It is therefore useful to judge how well an arbitrary but not necessarily known monotonic function $f(X)$ is approximating the value of Y. The rank correlation is independent of the frequency distribution of the variables.

Definition of monotonic functions:

- A monotonically increasing function: $a \leq b \iff f(a) \leq f(b)$.
- A monotonically decreasing function: $a \geq b \iff f(a) \geq f(b)$.

Spearman's rho is a number in the range -1 to $+1$. A value of zero (0) means that there is no rank correlation whereas $+1$ means that the order is exactly the same. A value of -1 means that the order is perfectly opposite. Spearman's rho is often designated ρ when calculated for a population and r when calculated using sample data.

The X- and Y-values are lists: $[X_1, X_2, \ldots, X_n]$ and $[Y_1, Y_2, \ldots, Y_n]$ where (X_t,Y_t) are associated values.

11.2.1 How to calculate Spearman's rho

To calculate Spearman's rho, the raw data values X_t and associated Y_t are first converted to rank values x_t and associated y_t. That is: $X_t \rightarrow x_t$ and $Y_t \rightarrow y_t$. The rank value of X_t and Y_t is the sequence number after sorting, maintaining the association between X_t and Y_t. A rank value of one (1) is assigned to the largest value of X (or Y), two (2) to the second largest value, ..., and finally n to the lowest value. Ties are handled differently – the applied rank value for a group of ties is the average of their positions in the sorted list. As an example, if the second (2) largest is exactly equal to the third (3) largest – these two equals would both get a rank value of $(2+3)/2 = 2.5$.

Spearman's rho is calculated as the Pearson product-moment correlation coefficient, Pearson's r. It is obtained by dividing the covariance of the two variables (ranks)) by the product of their standard deviations. For a population:

$$\rho_{x,y} = \frac{\mathrm{cov}(x,y)}{\sigma_x \sigma_y} \tag{35}$$

or – for a sample – where it should be observed that the sample standard deviations s_x and s_y have been normalized by $\sqrt{n-1}$ to be unbiased:

$$r_{x,y} = \frac{1}{n-1} \sum_{i=1}^{n} \frac{(x_i - \bar{x})}{s_x} \frac{(y_i - \bar{y})}{s_y} \tag{36}$$

It should also be observed that for finite n — Spearman's rho would obtain discrete values in the interval -1 to $+1$, ends included. This occurs since the rank values of X and Y are permutations of the integers: $1, 2, \ldots, n$.

11.3 Classical, H_0: There is no relation between X and Y

This is the classical method. The question here is whether the correlation ρ between a fixed rank vector $y = [y_1, y_2, \ldots, y_n]$ and $x = [x_1, x_2, \ldots, x_n]$ is significantly better than what would result if $x = [x_1, x_2, \ldots, x_n]$ is completely random. Here, *better* implies correlation $\rho > 0$.

This can be checked by performing a hypothesis check. The *null*-hypothesis, H_0, is that x is the result of randomness. If this is the case - the most likely ρ-value is zero (0) whereas ρ-values close to -1 and $+1$ are very unlikely. Our alternative hypothesis, H_1, is that $x = [x_1, x_2, \ldots, x_n]$ is not the result of randomness. This may be true and may imply causality if the observed ρ is close to $+1$.

Given randomness,the probability distribution of ρ can be obtained by Monte-Carlo simulation. The probability for exceeding the calculated (observed) ρ-value can then be taken from the simulated cumulative probability distribution. We reject the *null*-hypothesis if the exceedance probability for the observed ρ-value is small, say probability less than 0.01.

If the full probability distribution is not available, we may still perform the hypothesis check by consulting a table of critical ρ-values. The procedure is to

choose the significance level α (the exceedance probability), say $\alpha = 0.01$ – and to determine the associated ρ_{critical} for the relevant sample size n. The observed ρ-value is then compared to ρ_{critical} and the *null*-hypothesis (randomness) is rejected if the observed ρ is greater than the critical value, $\rho_{\text{observed}} \geq \rho_{\text{critical}}$.

Table 15 provides critical values of Spearman's rho for small sample sizes n and different significance levels, α. The leftmost part of the table has been taken from Zar (1972) [4]. The rightmost part is the result of the Monte Carlo simulation performed here, see section 11.4.2. The results compares well for corresponding significance levels α. The results from the Monte Carlo simulation appears correct to two decimals for sample size $n > 10$. The results for the median case, $\alpha = 0.50$ allows for a comparison with the true median value, zero (0).

n	$\alpha = 0.05$	$\alpha = 0.01$	n	$\alpha = 0.50$	$\alpha = 0.10$	$\alpha = 0.05$	$\alpha = 0.01$
5	0.900	-	5	0.000	0.700	0.800	0.900
10	0.564	0.745	10	-0.006	0.442	0.552	0.733
15	0.443	0.604	15	0.000	0.350	0.439	0.596
20	0.380	0.520	20	-0.002	0.296	0.376	0.517
25	0.337	0.466	25	-0.002	0.263	0.335	0.465
30	0.306	0.425	30	0.000	0.241	0.306	0.424
35	0.283	0.394	35	0.001	0.221	0.282	0.395
40	0.264	0.368	40	-0.001	0.205	0.262	0.365
45	0.248	0.347	45	0.001	0.194	0.248	0.348
50	0.235	0.329	50	0.000	0.183	0.234	0.327

Table 15: Critical values of Spearman's rho for hypothesis test against randomness. H_0: x is completely random. H_1: x is not random. The leftmost values are taken from Zar (1972) [4]. The rightmost values are obtained by Monte Carlo simulation as described in section 11.4.2.

The reasons for the minor deviations in table 15 may be found in:

- The number of realizations, 100 000 for each n in the Monte Carlo simulations.
- The random number generator.
- The way the critical ρ-value for at given significance level was obtained. This is mentioned since the ρ-values are discrete values in the interval $[-1, +1]$. Here a single look-up in the empirical *cdf* is used for each significance level α. This disregards the fact that the ρ-value may be constant for a small α-change. It is therefore reasonable to expect that the tabulated critical values obtained from Zar (1972) [4] corresponds to the next higher ρ-value since the purpose of this test is to discriminate between randomness or not – via the calculated correlation coefficient r.

11.4 Alternative, H_0: There is a strong relation between X and Y

The issue is to evaluate the goodness of approximations to the *true* values $Y = [Y_1, Y_2, \ldots, Y_n]$ where the approximations are given by $X = [X_1, X_2, \ldots, X_n]$.

The basic idea is that the Spearman's rank correlation, rho, between the n largest results from an approximate analysis and an advanced analysis can be used to judge if the approximation method is still performing well. This was mentioned by Passano (1994) pp. 17 [24].

The aim here is to describe a hypothesis test by which the quality of an approximative method can be tested routinely by checking the value of Spearman's rho.

The *null*-hypothesis (H_0) is that the approximative method has a specified success rate, P_{success} where P_{success} is the strength of the relation. The alternative hypothesis (H_1) is that the success rate is lower, implying a lower quality approximation.

The success rate measures the quality of the approximation process. It is a number between zero (0) and one (1). For a value of zero (0) the approximation process is similar to random guessing. A value of one (1) would mean that the approximation process always gets it right.

Such a hypothesis test would enable us to: check the performance of the approximation method for each new simulation; identify situations where more simulation is needed - or identify situations where the approximative method fails. The key to suspect a failing approximation is obviously an observed low value of Spearman's rho, the rank correlation coefficient. But how low can the rank correlation coefficient be, given a specified P_{success}?

The probability density distribution of rho for a given P_{success} is the key to the answer.

11.4.1 How to determine P_{success} in time domain analysis

Within the context of time domain analysis of a riser system, the following description is given to obtain $Y = [Y_1, Y_2, \ldots, Y_n]$ and $X = [X_1, X_2, \ldots, X_n]$. The below description identifies the scenario that leads up to the hypothesis test and the Monte Carlo simulation that is needed to establish the critical rho-values including significance levels, α.

1. The values of $Y = [Y_1, Y_2, \ldots, Y_n]$ are the n largest *true* response values (maxima) from a long accurate time domain analysis considering the full length time series, say 3 hours. The index t of Y_t indicates the time window containing the extreme value, $t \in [1, n]$, n is a small number in comparison to all occuring maxima.

2. The purpose of the approximation method is to identify a time window containing the time instant of a *true* extreme value Y_t. The time window

is a centered around the critical time instant as found by the approximate method. The interval length is small, in the order of 2-3 characteristic wave periods.

3. The approximation method is assumed a stochastic process where the probability that the suggested time window contains one of $[Y_1, Y_2, \ldots, Y_n]$ is constant and equal to p_{success}. Either it contains the value or not.

4. This success rate, p_{success}, can be determined as the overlap ratio of the n largest results from several trial analysis. This is full length analysis using both the detailed and the approximative method. The time instant for each of the n largest results found using the approximative method is needed. The time instants are also needed for the n largest results found using the detailed method.

5. For success, the critical time window is identified by the approximation process. The value of the simplified result X_t will then be exactly equal to Y_t because X_t is determined by the most advanced time domain method on this identified small time window. Due care should be given to avoid transients from the start-up in the dynamic simulation.

6. For failure, the critical time window is not identified. The value of X_t would be less than $\min[Y_1, Y_2, \ldots, Y_n]$ since these Y_t are by definition the n largest found after a full simulation. Since this failure occurs at random with probability $1 - p_{\text{success}}$, the consistent choice of X_t is a random value less than $\min[Y_1, Y_2, \ldots, Y_n]$.

7. From X and Y, the ranks x and y are determined and finally the rank correlation coefficient, r is computed. (Note that the possibility of experiencing equal values, $X_i \equiv X_j$ or $Y_i \equiv Y_j$ $(i \neq j)$ may be neglected since we are using floating point numbers in our simulation).

11.4.2 Monte Carlo simulation

The above procedure may be implemented in a Monte Carlo simulation. The simulation is performed considering unique rank values only. Without loss of generality, the n Y-values have been ordered and the associated rank values are $y = [1, 2, \ldots, n]$. The success ratio of the simplified method is input and provided as P_{success}.

The procedure to simulate one realization of the approximation x and calculating Spearman's rho is described below. It is also described how to establish the empirical *cdf* and critical rho-values.

1. Create $y = [1, 2, \ldots, n]$, this needs to be done once only.

2. Create the n-length zero-initiated rank list: $x = [0, 0, \ldots, 0]$.

3. Create a random vector: $u = [u_1, u_2, \ldots, u_n]$, where $u_i \in [0, 1]$ and uniformly distributed.

4. Identify the failure instances, those where $u_i > P_{\text{success}}$. The ranks of the identified failure instances is next put into the x-vector at their corresponding positions. The largest u_{failure} is assigned rank n, the second largest u_{failure} is assigned rank $n-1$ and so on.

5. Assign rank values to all unset positions of x, those with values 0. Start at the leftmost position and assign rank values $1, 2, \ldots$ and so on.

6. Calculate Spearman's rho, ρ, and register the result.

7. Repeat the procedure from step 1 until the sample size of ρ is sufficient.

8. Prepare the empirical cumulative distribution function for Spearman's rho. This is done by sorting the obtained ρ-values and assigning the probability $F_i = i/(n+1)$ to ρ_i where $i \geq 1$ is the sort position.

9. The critical ρ-values are then determined by a simple table look-up for each interesting significance level α. This procedure does not account for the discrete distribution of the ρ-values. The effect of this simplification is considered small, but greater for smaller sample sizes n.

Table 16 illustrates how to assign rank values, steps 1 to 5.

y (rank)	u (random number)	x (rank)
1	0.43	1
2	0.20	2
3	0.69	3
4	*0.93 (failure)*	*10*
5	0.21	4
6	0.51	5
7	*0.87 (failure)*	*9*
8	0.72	6
9	0.27	7
10	0.11	8

Table 16: An example Monte Carlo simulation illustrating the rank assignment procedure, $P_{\text{success}} = 0.80$, Spearman's $\rho = 0.6727$.

It should be observed that the values of x would be fully arbitrary if a zero success rate is specified, $P_{\text{success}} = 0$. This allows for verification of the performed Monte Carlo simulation by comparison with published data, Zar (1972) [4]. The total number of random realizations for each different n is 100 000 here. The comparison is shown in table 15. The differences are small and considered insignificant. The above procedure is therefore concluded correctly implemented in the prepared program.

11.4.3 Critical rho-values for given P_{success}.

The competing hypothesis are:

- H_0: The success rate of the approximation method is equal to or better than $p_{success}$.
- H_1: The success rate of the approximation method is less than $p_{success}$.

Monte Carlo simulations have been performed to establish critical ρ-values for $P_{\text{success}} = 0.80$ and $P_{\text{success}} = 0.90$. The critical ρ-values have been determined for significance levels $\alpha = 0.50$, $\alpha = 0.10$, $\alpha = 0.05$ and $\alpha = 0.01$. The critical rho-values are given in table 17.

The hypothesis test is done as follows:

1. Define a success ratio for the approximate method, P_{success}, see section 11.4.4.
2. Choose a significance level, $\alpha = \text{Prob}(R < \rho_{\text{critical}})$.
3. Determine ρ_{critical} from table 17.
4. Use the results from the simplified method $X = [X_1, X_2, \ldots, X_n]$ and the most advanced method $Y = [Y_1, Y_2, \ldots, Y_n]$. Convert the results to ranks $x = [x_1, x_2, \ldots, x_n]$ and $y = [y_1, y_2, \ldots, y_n]$. Calculate the rank correlation coefficient, $r_{x,y}$, see section 11.2.1.
5. The rule is to reject hypothesis H_0 in favor of H_1 if $r_{x,y} < \rho_{\text{critical}}$.

Figures 12 and 13 illustrates how the critical ρ-values are influenced by the sample size n. These figures considers significance levels $\alpha = 0.10$ and $\alpha = 0.50$ (the median) only.

Figures 14, 15, 16 and 17 show some results from the Monte Carlo simulation for sample size $n = 20$. Figure 14 shows the obtained cumulative distribution functions for success ratios, $P_{success}$: 0.0, 0.80 and 0.90. The associated histograms of the Monte Carlo results are presented on figures 15, 16 and 17.

If the approximation method is perfect, $P_{\text{success}} = 1$, the probability density function will become the *Dirac delta* function: $\delta(\rho - 1)$ (an infinite spike at $\rho = 1$). The corresponding cumulative distribution function is Heaviside's step function, formulated as: $H = 0$ for $\rho < 1$ and $H = 1$ for $\rho = 1$ – since ρ is discrete, see [28] and [29]. The histograms presented on figures 15, 16 and 17 show that the histograms indeed are narrowing as the success ratio is approaching one (1).

11.4.4 On qualifying an approximate method

The rank order of the approximate results versus the ranks of the advanced results should be investigated considering full length time series. The rank results for the n extremes should be compared graphically and quantified numerically using Spearman's rho.

	$\alpha = 0.50$		$\alpha = 0.10$		$\alpha = 0.05$		$\alpha = 0.01$	
P_{success}	0.80	0.90	0.80	0.90	0.80	0.90	0.80	0.90
n=5	0.900	1.000	0.000	0.200	-0.100	0.000	-0.600	-0.300
10	0.661	0.927	0.212	0.455	0.055	0.333	-0.212	0.030
15	0.668	0.868	0.300	0.532	0.182	0.421	-0.032	0.225
20	0.660	0.839	0.349	0.567	0.253	0.486	0.071	0.314
25	0.655	0.828	0.380	0.600	0.296	0.525	0.142	0.378
30	0.653	0.827	0.407	0.622	0.330	0.554	0.184	0.420
35	0.652	0.827	0.424	0.636	0.355	0.575	0.221	0.451
40	0.650	0.824	0.438	0.646	0.373	0.590	0.248	0.480
45	0.650	0.822	0.452	0.657	0.392	0.605	0.279	0.502
50	0.647	0.821	0.460	0.665	0.405	0.616	0.298	0.517

Table 17: Critical values of Spearman's rho, for different success ratios, P_{success}, and significance levels, α. Hypothesis, H_0: The success rate of the method is equal to or better than P_{success}. Alternative hypothesis, H1: The success rate of the method is less than P_{success}. Reject H_0 in favor of H_1 if the calculated rank correlation coefficient r is less than ρ_{critical}.

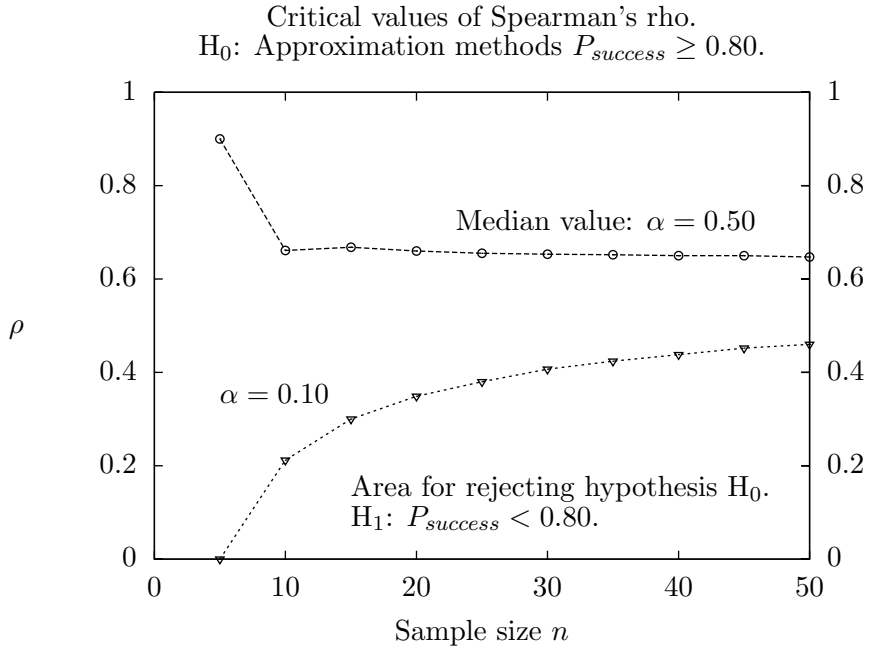

Figure 12: Critical values of Spearman's rho considering $P_{\text{success}} = 0.80$ and significance levels $\alpha = 0.50$ and $\alpha = 0.10$.

Several full length simulation using both the approximate and the detailed method are needed to quantify the success rate of the approximate method.

The purpose of the approximate method is to define n small *time windows*

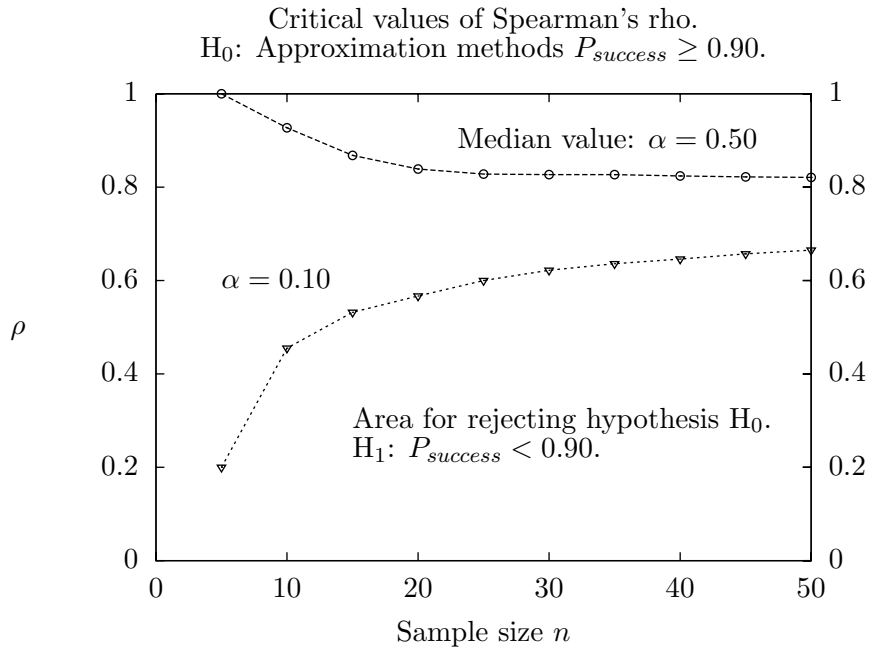

Figure 13: Critical values of Spearman's rho considering $P_{\text{success}} = 0.90$ and significance levels $\alpha = 0.50$ and $\alpha = 0.10$.

through which we optimistically can see all of the n largest values from the detailed analysis. Let c be the count of those that we actually see. The success ratio, P_{success}, is defined as the expectation value of the product c/n. It is calculated as follows after having studied several (k) cases in full length.

$$P_{\text{success}} = \frac{1}{k} \sum_{i=1}^{k} \frac{c_k}{n} \tag{37}$$

The performance of the simplified method is not only dependent on the identification of critical time instants. The quality of extreme estimates from a small sample must also be compared to the true result obtained from several greater length time series.

Ultimately, the quality of a simplified method can only be measured as the difference between the exact and the simplified extreme value estimate. The size of the difference is conjectured to be in the order of the standard error for the statistical estimator used in the simplified analysis.

This suggests that the sample size n needed to obtain a target precision (standard error) can be investigated in the several initial full length simulations when calibrating the simplified model. This information may be used to suggest investigative actions if the simplified model fails to perform later on.

Tentative procedure:

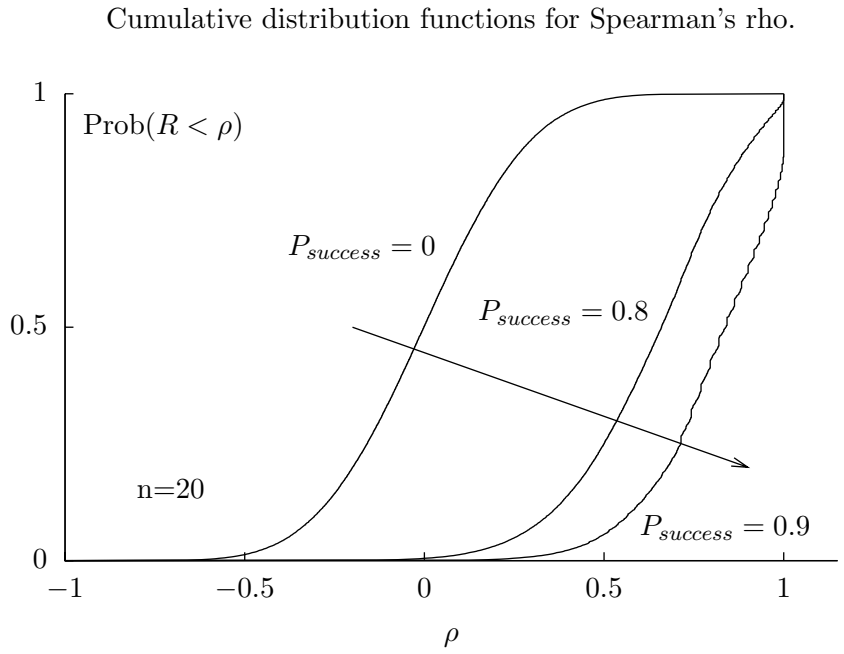

Figure 14: Example cumulative distribution functions for Spearman's rho when considering $P_{\text{success}} = \{0, 0.80, 0.90\}$ and $n = 20$.

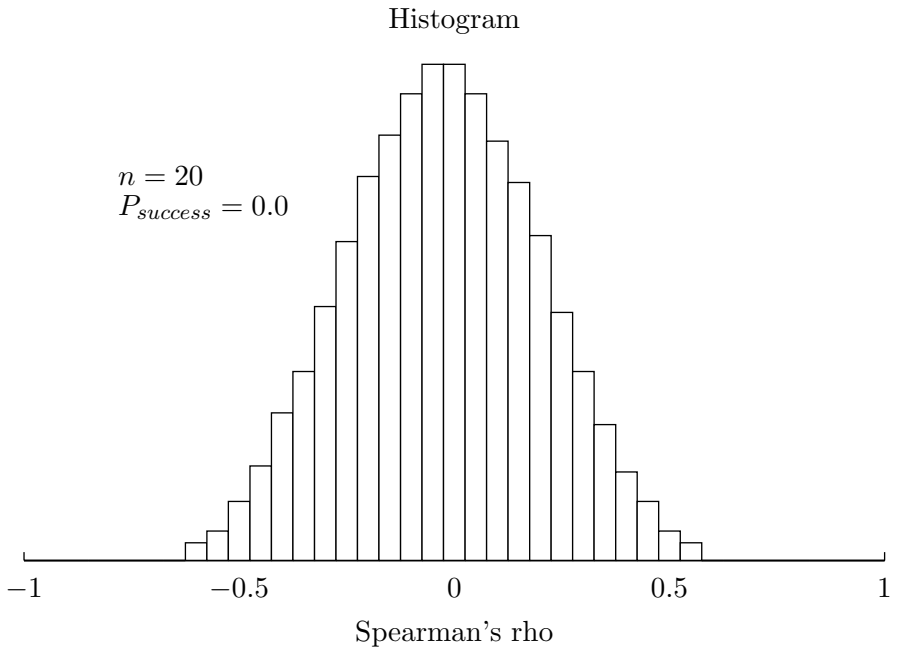

Figure 15: Example histogram from Monte Carlo simulation, $n = 20$, $P_{\text{success}} = 0$.

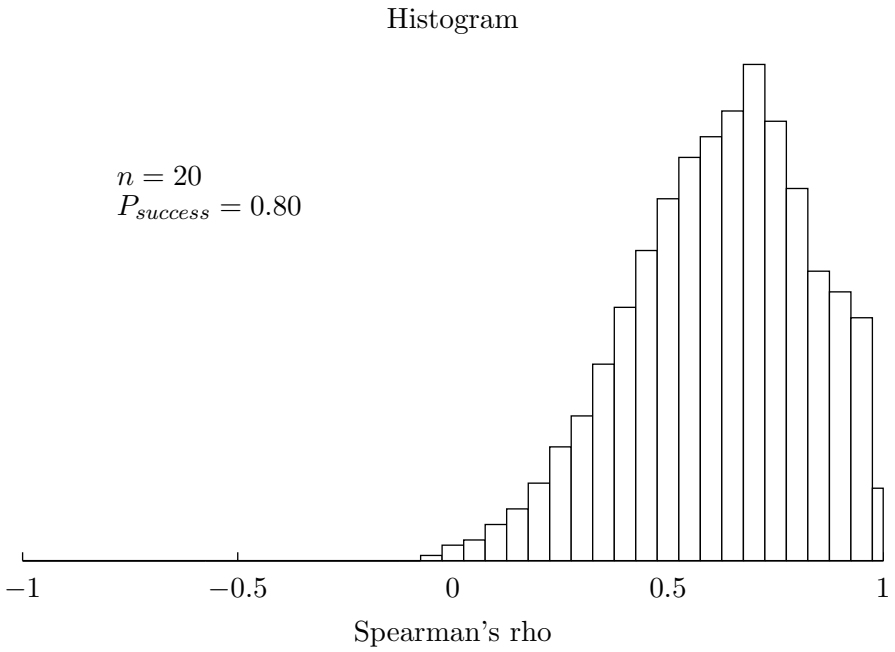

Figure 16: Example histogram from Monte Carlo simulation, $n = 20$, $P_{\text{success}} = 0.80$.

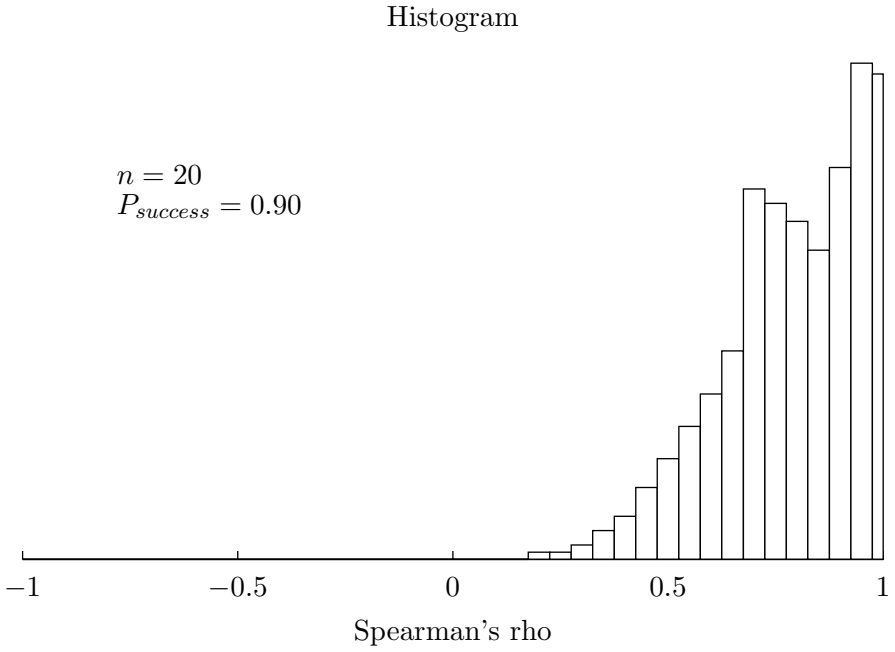

Figure 17: Example histogram from Monte Carlo simulation, $n = 20$, $P_{\text{success}} = 0.90$.

- Use several full length simulations, both detailed and simplified to identify P_{success} as function of n, say 20 per 3 hours.
- Investigate the ratio of extreme values from detailed and simplified method, *exact/approximate*.
- Investigate the *standard error* of the extreme estimates from the simplified method as function of n.
- Determine a sufficient n-value and the associated success ratio: $P_{success}$.

11.4.5 On actions when the hypothesis is rejected.

If the calculated rank correlation r is less than ρ_{critical} from table 17 – the *null*-hypothesis (H_0) is rejected and we must explore the possibility that our approximation method is less accurate then initially assumed. This may happen if the simplified method is used against some new response parameter or if some other new load effect has become significant.

However, it may also happen that the *null*-hypothesis is rejected even if it is true. The probability for this is equal to the selected significance level α.

The simplest investigative procedure is perhaps to do a repeat analysis – a new realization – if the hypothesis test fails. Depending on the chosen significance level α, a second failure to pass the hypothesis test would be a very strong indicator of a significantly changed condition, since the probability of this occurring normally would be small, α^2.

Example: For a selected significance levels $\alpha = 0.10$ – the probability for experiencing a false rejection is 0.1. The probability for experiencing two false rejections in a row is then 0.01.

It should be noted that sea states for which such repeated failures occurs would be natural candidates for calibration of a new simplified model. The simplified method would therefore be gradually improving as we are learning more about the system.

11.4.6 An application example

The relation between axial forced motion at the top end of catenaries was investigated by Passano and Larsen in their 2006 paper: *Efficient analysis of catenary risers*, reference [22].

They claim that there is a strong correlation between the bending moments and the effective tension in the bottom region.

Furthermore, they claim that the correlation between the axial velocity and the effective tension value is excellent. The correlation between the axial velocity and bending moment values is described as good.

They provide a table containing axial displacements and velocity of the catenary riser at the top: X and $\dot{X}$. The associated minimum effective tension (T) and

bending moment (M) for the small time interval surrounding the instant of extreme minimum velocity $\dot{X}$ are also provided.

Their table is reproduced here in entirety for completeness, see table 18. Neither the *time* instant nor the sequence numbers (seq.no) is of any interest for us. The rest is exactly what is needed to exercise the previously described hypotheses check regarding the relation between: velocity and effective tension; velocity and bending moment.

t (-)	time	$\dot{X}$	seq. no (-)	X	seq.no.	T	seq.no.	M)
(-)	(s)	(m/s)	(-)	(m)	(-)	(kN)	(-)	(kNm)
1	76	-2.35	5	-5.36	1	-210	1	1133.0
2	2910	-2.31	21	-4.17	2	-189	6	988.5
3	245.2	-2.27	6	-5.29	3	-172	2	1053.7
4	2666	-2.25	7	-5.22	4	-169	3	1034.2
5	1126	-2.24	41	-3.68	5	-167	12	922.0
6	3234	-2.09	4	-5.40	6	-126	5	1004.4
7	3374	-2.08	2	-5.57	7	-123	4	1005.9
8	2860	-2.07	1	-5.59	8	-113	7	984.2
9	59.2	-2.04	10	-4.94	10	-104	10	946.7
10	1112	-2.04	3	-5.55	11	-103	9	957.4

Table 18: The ten largest axial velocity minima and the corresponding response maxima/minima, 16.5 m sea state, 1800 m water depth.

Our first observation from table 18 is that 9 out of the 10 smallest tension values (T) are found in the same intervals as the 10 smallest velocities. The same finding is made for the bending moment (M) From this limited evidence, we conjecture that the success ratio for the approximate method is 90%. This implies $P_{\text{success}} = 0.90$.

The hypothesis are as follows:

- H_0: The success rate of using the negative axial velocity to identify critical time intervals for effective tension (compression) and extreme bending moment near the bottom is equal to or better than 90%.
- H_1: The success rate of this method is lower.

We believe in the H_0-hypothesis. Our task now is to check if our belief is unreasonable based on the evidence at hand. The procedure described in section 11.4.3 tells us that we must calculate the ranked order correlation, r. The rank values for the raw data are first established, while maintaining the association, see table 19.

The rank correlation coefficient $r_{\dot{X},T}$ is calculated between the velocity and the effective tension, and $r_{\dot{X},M}$ between velocity and bending moment. The results are as follows:

- Effective tension: $r_{\dot{X},T} = 1$.

t	$\dot{X}$(m/s)	T (kN)	M (kNm)	rank($\dot{X}$)	rank(T)	rank(M)
1	-2.35	-210	1133	1	1	1
2	-2.31	-189	988.5	2	2	6
3	-2.27	-172	1053.7	3	3	2
4	-2.25	-169	1034.2	4	4	3
5	-2.24	-167	922.0	5	5	10
6	-2.09	-126	1004.4	6	6	5
7	-2.08	-123	1005.9	7	7	4
8	-2.07	-113	984.2	8	8	7
9	-2.04	-104	946.7	9	9	9
10	-2.04	-103	957.4	10	10	8

Table 19: Raw data values and assigned ranks.

- Bending moment: $r_{\dot{X},M} = 0.648$

Critical rho-value: In table 17, for $n = 10$, $P_{\text{success}} = 0.90$ and selected significance level $\alpha = 0.10$ – we find $\rho_{critical} = 0.455$.

Conclusion: Since the rank correlation coefficients for both effective tension and bending moment are greater than the critical value we do not reject the *null*-hypothesis – our belief.

11.5 Further development needed for use with interval extremes

A rank value x_t must be assigned to the simplified result X_t in the Monte Carlo simulation. According to section 11.4.1, the rank value of X_t is exactly equal to that of Y_t in case of successful identification of the critical time window. For a failure in identifying the critical time window, the rank of X_t is determined based on the definition that $X_t < \min[Y_1, Y_2, \ldots, Y_n]$. Hence, the failure instances would be assigned the largest rank numbers – randomly if several failure instances.

However, the above inequality $X_t < \min[Y_1, Y_2, \ldots, Y_n]$ does not hold when using interval extremes as is often used with Gumbel extreme values. The interval length is then more than 50 characteristic wave cycles, typically. All we can say for a failure instance in any such interval number f – is that $X_f < Y_f$ since Y_f is by definition the largest value of this particular interval. Hence, if the Y-values are initially ordered so that $Y_1 > Y_2 > \ldots Y_n$ we can only claim rank(X_f)$\geq f$.

The effect of this would be increased expected correlation even in failure instances. The critical rho-values as obtained by Monte Carlo simulation and given in table 17 are therefore not accurate in such a case. To evaluate this issue, Monte Carlo simulations with a revised rank assignment rule are needed.

The critical rho-values as given in table 17 may nevertheless be of use monitoring the results of an approximation method, since they form a lower bound.

12 Vessel transfer function, RAO

The response amplitude operator, RAO or transfer function, is most often input when performing riser analysis. The purpose of the RAO is to describe the dynamic vessel motion amplitude and the phase relative to the elevation of the incoming unit wave. The RAO is also known as the frequency response function for a linear system, see [21] pp. 53-58. Because of the linearity, response superposition can be done. The RAOs describe only the dynamic surge, sway, heave, roll, pitch and yaw motion of the vessel. The static and second order (low frequency) vessel motion must be determined by some other means.

Without loss of generality, the dynamic surge motion $x(t)$ is used as an example in the following. The total surge motion is obtained as the sum of the mean and dynamic motion $x_{\text{total}}(t) = x_{\text{mean}} + x(t)$. Note also that the wave elevation is taken at the coordinate system origin. Equation 38 shows the reference wave elevation, whereas the resulting dynamic surge motion is given by equation 39.

$$\zeta(t) = \zeta_0 \cos(\omega t) \tag{38}$$

$$\begin{aligned} x(t) &= x_0 \cos(\omega t + \phi_x) \\ &= H_x(\omega)\zeta_0 \cos(\omega t + \phi_x) \end{aligned} \tag{39}$$

The above equations 38 and 39 are more conveniently using expressed as the real part of the complex equations and 40 and 41. The amplitudes, x_0 and ζ_0, may take complex values. This give a compact representation of both the amplitude and the phase. Example for the wave: $\zeta_0 = a_0 + \mathrm{i}b_0$ defines the wave amplitude as $|\zeta_0| = \sqrt{a^2 + b^2}$, and the phase as $\phi_\zeta = \text{atan2}(b_0/a_0)$. The wave elevation is the real part of equation 40, this equals $\zeta(t) = |\zeta_0| \cos(\omega t + \phi_\zeta)$.

$$\zeta(t) = \zeta_0 e^{\mathrm{i}\omega t} \tag{40}$$

$$\begin{aligned} x(t) &= x_0 e^{\mathrm{i}\omega t} \\ &= H_x(w)\zeta_0 e^{\mathrm{i}\omega t} \end{aligned} \tag{41}$$

12.1 Quality assurance

The transfer function, $H_x(\omega)$ is usually received as tabulated values covering the relevant wave directions and wave periods. These tables cover the vessel motion degrees of freedom: surge, sway, heave, roll, pitch and yaw. The forced top-end motion of the riser caused by combinations of these is likely to be a dominant load for the riser system. Hence it is necessary to interpret and convert the given RAO correctly.

The given data must be checked and converted to the format required by the applicable riser analysis program, in this case Riflex prior to use. This implies

putting the data into the required file structure, assuring the proper normalization of the RAO amplitudes, checking that the correct wave direction convention is used and finally – making sure that the RAO phase angle convention is as expected. For this reason, some basic knowledge of what to expect for RAOs for a floating vessel is required.

Appendix 7A of the Riflex theory manual (2008) [13] contains a useful and general note by Ivar J. Fylling, Marintek on this issue: "Motion characteristics of floating vessel. Motions transfer function specification, diagnostics and transformation."

The motivation is quoted:

> A lot of trouble has been caused by erroneous interpretation of transfer functions and erroneous transformations. In many cases a simple checking of asymptotic phase angles can be useful in verifying the actual interpretation. The present note is an effort to describe the asymptotic phase angles, the different coordinate systems that are often used, and to show a recipe for transformation of phase angles.

The vessel transfer function, $H_x(\omega)$ describes the steady-state harmonic vessel motion caused by a unit amplitude (ζ_0) sinusoidal wave with a fixed frequency (and fixed direction). The frequency of the resulting harmonic vessel motion is the same as that of the wave because of linearity. The unit of the amplitude ratio may therefore be (feet/feet) for a translation (surge, sway, heave) and ($^\circ$/feet) for a rotation.

Considering floating vessels it is for practical reasons beneficial to normalize the RAO values such that the amplitude ratios are dimensionless. The physically relevant wave parameters determines the normalizing scales. For translations, the wave amplitude (length unit) is the obvious choice, e.g. X_0/ζ_0. Likewise, the wave slope amplitude measured in radians is used to normalize the rotational vessel motion, also measured in radians, $\theta_x/(\zeta_0 k)$. The wave slope amplitude is found from studying $\mathrm{d}\zeta(t)/\mathrm{d}x$ where $\zeta(t) = \zeta_0 \cos(\omega t + kx)$ and k is the wave number, $k = 2\pi/\lambda$. Faltinsen (1990) gives an overview of relations for Airy wave theory [9].

The RAO normalization required by Riflex is dimensionless as described above. The referred note by Ivar J. Fylling derives the asymptotic phase angle, $\lim_{\omega\to 0}\phi$, for a stick-like vessel with a coordinate system xyz associated with the longitudinal, transverse and vertical directions. See table 20 for the asymptotic RAO phase angles when using the Riflex programme.

Limiting ourselves to a symmetric stick-like vessel and wave directions parallel to the vessel coordinate system axis 0°, 90°, 180° and 270° we may also make a claim regarding the expected asymptotic amplitude ratio. This is claimed to be unity (1) $\lim_{\omega\to 0}|H(\omega)| = 1$ for vessel motions triggered by the chosen wave direction. Example: For a long wave in direction 0°, the asymptotic amplitude ratio $H = 1$ is expected for the surge-, heave- and pitch-motion. The sway-, roll- and yaw-motion should be zero because of the assumed symmetry.

Wave direction in 2nd quadrant		Wave direction in 1st quadrant	
ϕ_x	$= +90°$	ϕ_x	$= -90°$
ϕ_y	$= -90°$	ϕ_y	$= -90°$
ϕ_z	$= 0°$	ϕ_z	$= 0°$
ϕ_{xx}	$= -90°$	ϕ_{xx}	$= -90°$
ϕ_{yy}	$= -90°$	ϕ_{yy}	$= +90°$
ϕ_{zz}	$= 0°$	ϕ_{zz}	$= +180°$
Wave direction in 3rd quadrant		**Wave direction in 4th quadrant**	
ϕ_x	$= +90°$	ϕ_x	$= -90°$
ϕ_y	$= +90°$	ϕ_y	$= +90°$
ϕ_z	$= 0°$	ϕ_z	$= 0°$
ϕ_{xx}	$= +90°$	ϕ_{xx}	$= +90°$
ϕ_{yy}	$= -90°$	ϕ_{yy}	$= +90°$
ϕ_{zz}	$= +180°$	ϕ_{zz}	$= 0°$

Table 20: Asymptotic RAO phase angles for long wave per Riflex convention for different wave propagation directions. The associated asymptotic RAO amplitude value is unity (1) for relevant motions when wave is parallel to either x- or y-axis.

12.2 Check of applicable RAO files

Two sets of vessel RAOs have been received for the ship shaped FPSO. The length of the close to box-shaped FPSO is about 300 m and the width is about 55 m. The draft of the FPSO is between 7 and 13 m dependent on the loading condition. The two RAO sets are for the ballast and full draft of the ship shaped FPSO, see table 21.

Condition	Draft (m)	Distance of CoG above water line (m)	x_{cog} (m)	y_{cog} (m)	z_{cog} (m)
Ballast	8.0	8.733	0	0	16.733
Full	12.8	2.150	0	0	14.950

Table 21: Vessel RAOs, vessel draft and location of RAO specification point, here CoG. Vessel coordinate system origin is at keel level in the center of the FPSO.

The RAOs have been received in files already in the format required by Riflex. They are nevertheless checked considering the expectations of table 20. For both RAO sets the amplitude ratios and phase angles for the longest wave, highest periode, compares well with the asymptotic results. All wave directions have been checked: $0°, 15°, 30°, \ldots, 360°$. The RAOs for surge, sway and heave are illustrated on figures 20, 21 and 22. The RAOs for roll, pitch and yaw are illustrated on figures 23, 24 and 25 respectively. Table 22 contains the check result for wave direction 90° (beam sea). The vessel surge, pitch and yaw

motions are insignificant for this wave direction, as expected.

DOF	Amplitude (-)	Phase (°)	Asymptotic phase (°)	Finding
sway	0.963	-90.06°	-90°	OK
heave	1.001	0°	0°	OK
roll	1.070	-98.539°	-90°	OK

Table 22: Vessel RAO check, 90° wave direction (beam sea) and 30.1 s wave period.

12.3 Transformation of the vessel RAO

The vessel transfer function defines the harmonic motion of any point on the rigid vessel body using a specified coordinate system, xyz. The vessel motion for the origo of this coordinate system is described by the complex RAO-values, one value for each of the six degrees of freedoms: surge $H_x(\omega)$, sway $H_y(\omega)$, heave $H_z(\omega)$, roll $H_{xx}(\omega)$, pitch $H_{yy}(\omega)$ and yaw $H_{zz}(\omega)$. The frequency dependency will be dropped for brevity in the following.

Let $\mathbf{H} = [H_x\ H_y\ H_z\ H_{xx}\ H_{yy}\ H_{zz}]^T$ be the complex RAO value for a given frequency ω that in general depends on the wave direction. By denoting the RAOs for translations as $\mathbf{H_1} = [H_x\ H_y\ H_z]^T$ and those for rotations as $\mathbf{H_2} = [H_{xx}\ H_{yy}\ H_{zz}]^T$ we can write $\mathbf{H} = [\mathbf{H_1}\ \mathbf{H_2}]^T$.

The motion of a fixed point $\mathbf{r_p} = [x_p\ y_p\ z_p]$ on the vessel can be written as $\mathbf{s}(t) = [\mathbf{s_1}(t)\ \mathbf{s_2}(t)]^T$ where $\mathbf{s_1}(t) = [x(t)\ y(t)\ z(t)]^T$ is the translational motion and $\mathbf{s_2}(t) = [\theta_x(t)\ \theta_y(t)\ \theta_z(t)]^T$ is the rotational motion, see Faltinsen (1990) pp. 41 [9]. The motion $\mathbf{s}(t)$ of an arbitrary point can be calculated as shown by equation 42. Note the linearity, that the rotation is independent of the point position and that the real part corresponds to the physical motion.

$$\begin{bmatrix} x(t) \\ y(t) \\ z(t) \\ \theta_x(t) \\ \theta_y(t) \\ \theta_z(t) \end{bmatrix} = \begin{bmatrix} \mathbf{s_1}(t) \\ \mathbf{s_2}(t) \end{bmatrix} = \begin{bmatrix} \mathbf{H_1} + \mathbf{H_2} \times \mathbf{r_p} \\ \mathbf{H_2} \end{bmatrix} \zeta_0 e^{\mathrm{i}\omega t} \tag{42}$$

12.3.1 RAO for point $\mathbf{r_p}$ – using coordinate system xyz

The RAO, $\mathbf{H'} = [\mathbf{H'_1}\ \mathbf{H'_2}]^T$, for a different point $\mathbf{r_p}$ on the vessel is given by equation 43 when using the same coordinate system xyz. This is the time invariant part preceding $\zeta_0 e^{\mathrm{i}\omega t}$ of equation 42.

$$\mathbf{H'} = \begin{bmatrix} \mathbf{H'_1} \\ \mathbf{H'_2} \end{bmatrix} = \begin{bmatrix} \mathbf{H_1} + \mathbf{H_2} \times \mathbf{r_p} \\ \mathbf{H_2} \end{bmatrix} \tag{43}$$

12.3.2 RAO for motion in specified direction

The RAO for the motion in a specified direction may be interesting. The direction is represented by a unit directional vector, $\mathbf{n} = [n_x \ n_y \ n_z]$. Use equation 44 if the translational motion parallel to the unit vector $\mathbf{n}$ is desired and equation 45 if the RAO for the rotation about the unit vector $\mathbf{n}$ is wanted.

$$\mathbf{H_1'} = \mathbf{n} \cdot (\mathbf{H_1} + \mathbf{H_2} \times \mathbf{r_p}) \tag{44}$$

$$\mathbf{H_2'} = \mathbf{n} \cdot \mathbf{H_2} \tag{45}$$

12.3.3 RAO for origin – using rotated coordinate system $x'y'z'$

Consider now a completely different coordinate system ($x'y'z'$) where the axis directions are changed according to a constant 3×3 transformation matrix $\mathbf{T}$ with real entries. Note that each row of the transformation matrix can be interpreted as the unit vector of a skewed axis direction per previous section.

The transformation matrix satisfies $\mathbf{T}^{-1}\mathbf{T} = \mathbf{T}^T\mathbf{T} = \mathbf{I}$ because it is orthonormal. The transformed RAO $\mathbf{H''} = [\mathbf{H_1''} \ \mathbf{H_2''}]^T$ is given by equation 46.

$$\mathbf{H''} = \begin{bmatrix} \mathbf{H_1''} \\ \mathbf{H_2''} \end{bmatrix} = \begin{bmatrix} \mathbf{TH_1} \\ \mathbf{TH_2} \end{bmatrix} = \begin{bmatrix} \mathbf{T} & \mathbf{0} \\ \mathbf{0} & \mathbf{T} \end{bmatrix} \begin{bmatrix} \mathbf{H_1} \\ \mathbf{H_2} \end{bmatrix} \tag{46}$$

12.3.4 An interesting result

Let us review the motion $\mathbf{s'}(t) = [\mathbf{s_1'}(t) \ \mathbf{s_2'}(t)]^T$ at a fixed point $\mathbf{r_p} = [x_p \ y_p \ z_p]$ on the vessel in the changed coordinate system $x'y'z'$. Note that $\mathbf{r_p'} = \mathbf{Tr_p}$.

First, the harmonic translational ($\mathbf{s_1'}$) and rotational ($\mathbf{s_2'}$) point motion is obtained by the transformation $\mathbf{T}$ on the motion resulting from using RAOs for the xyz-system. See equation 42, the result is given by equation 47.

$$\begin{bmatrix} \mathbf{s_1'}(t) \\ \mathbf{s_2'}(t) \end{bmatrix} = \begin{bmatrix} \mathbf{Ts_1}(t) \\ \mathbf{Ts_2}(t) \end{bmatrix} = \begin{bmatrix} \mathbf{TH_1} + \mathbf{T}(\mathbf{H_2} \times \mathbf{r_p}) \\ \mathbf{TH_2} \end{bmatrix} \zeta_0 e^{\mathrm{i}\omega t} \tag{47}$$

Second, the same harmonic motion is obtained by using the RAOs for the rotated $x'y'z'$-system. This give equation 48, note that $\mathbf{H_1''} = \mathbf{TH_1}$, $\mathbf{H_2''} = \mathbf{TH_2}$ and $\mathbf{r_p'} = \mathbf{Tr_p}$.

$$\begin{bmatrix} \mathbf{s_1'}(t) \\ \mathbf{s_2'}(t) \end{bmatrix} = \begin{bmatrix} \mathbf{H_1''} + \mathbf{H_2''} \times \mathbf{r_p'} \\ \mathbf{H_2''} \end{bmatrix} \zeta_0 e^{\mathrm{i}\omega t} = \begin{bmatrix} \mathbf{TH_1} + \mathbf{TH_2} \times \mathbf{Tr_p} \\ \mathbf{TH_2} \end{bmatrix} \zeta_0 e^{\mathrm{i}\omega t} \tag{48}$$

The cross product term of equations 47 and 48 must be equal.

Hence, $\mathbf{T}(\mathbf{H_2} \times \mathbf{r_p}) \equiv (\mathbf{TH_2}) \times (\mathbf{Tr_p})$.

This means that the vector cross product is rotationally invariant similar to the vector dot product. However, unlike the vector dot product $(\vec{a} \cdot \vec{b})$ which is rotationally invariant for any n-dimensional vector space – the vector cross product $(\vec{a} \times \vec{b})$ is rotationally invariant only for the 3-dimensional vector space according to George B. Arfken and Hans J. Weber in "Mathematical methods for physicist" (1995) pp. 10, 16 and 22 [5]. It is exactly this property that proves that the vector cross product is indeed a proper vector.

12.3.5 Vessel induced motion at the hang-off point

It is reasonable to expect that the dynamic vessel motion at the umbilical hang-off point is a significant cause to the varying loads in the umbilical system. This is in particular so considering vessel rotations which will cause bending in the top bend stiffener. This will happen if the even if the umbilical in itself is standing perfectly still. If the umbilical is also moving due to e.g. wave action, this will increase the total bending variation in the top end.

However, bending is only part of the picture – the associated tension is likewise interesting. Passano (1994) [24] pp. 109 and Passano and Larsen (2006) [22] have demonstrated that the axial velocity of the umbilical at the top is a dominant cause for tension dynamics. They have demonstrated that the time instants for tension maxima and minima in the lower end near the seabed are well predicted from the top end axial velocity extremes.

The above means that the transfer function for the top end axial motion (in fixed initial tangential direction) is well worth studying if the concern is tension dynamics near the seabed. Likewise, the RAO for the vessel angles are interesting since they are closely associated with the bending at the top end.

The RAO for the umbilical hang-off point has been obtained by transformation of the vessel RAO, see section 12.3. These are presented in figure 18 for wave direction 90 ° and figure 19 for wave direction 270 °. The right-handed and Cartesian coordinate system at the top end is given by the umbilical angle with the vertical and the umbilical heading (azimuth direction). The top end coordinate system is set-up such that the x'-axis is in the umbilical tangent direction (positive upwards), The y'-axis is perpendicular to the nominal umbilical configuration plane such that the nominal umbilical configuration plane is entirely in the x'z'-plane. This choice of coordinate system means that the bend stiffener flange is in the y'z'-plane, the x'-axis is perpendicular to the bend stiffener flange, see section 7.3.

The top end motion transfer functions show a significant difference in the axial motion and velocity for wave periods in the range 10-15 s. Wave direction 270 ° is causing the greatest axial motion for a given sea state, a particular Hs-/Tp-combination. It should be observed that the rotational angle is independent of the wave direction. This is as expected since both are beam sea directions inducing roll only. In this case it is natural to choose the angular component parallel to the vessel X-axis for study. Note that even if many different angular

projections exists, all the interesting ones are contained within the plane of the bend stiffener flange – since these are associated with bending.

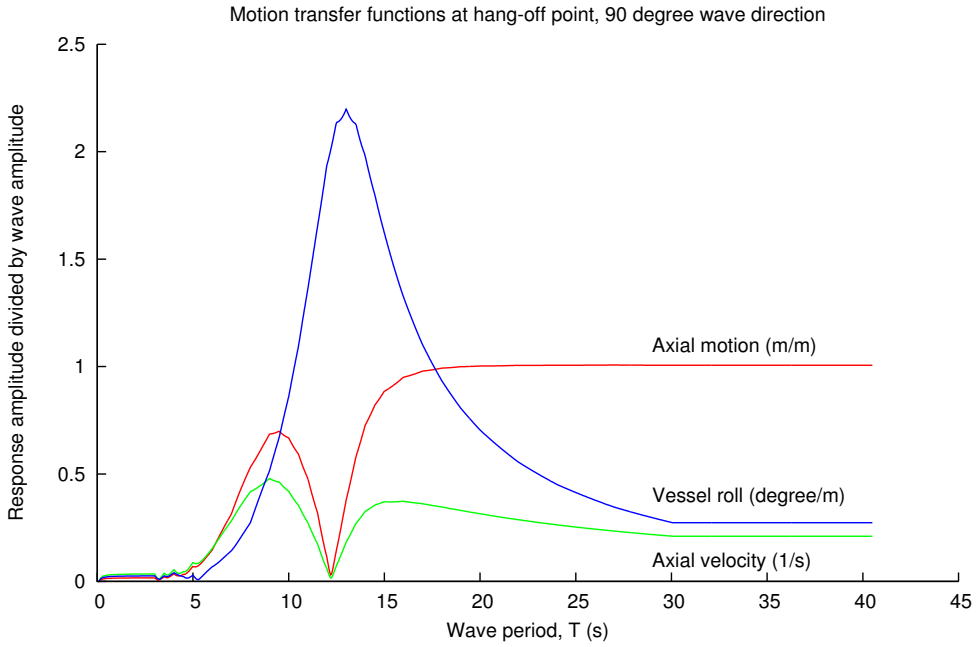

Figure 18: Motion RAOs for the umbilical hang-off point, wave direction 90 °.

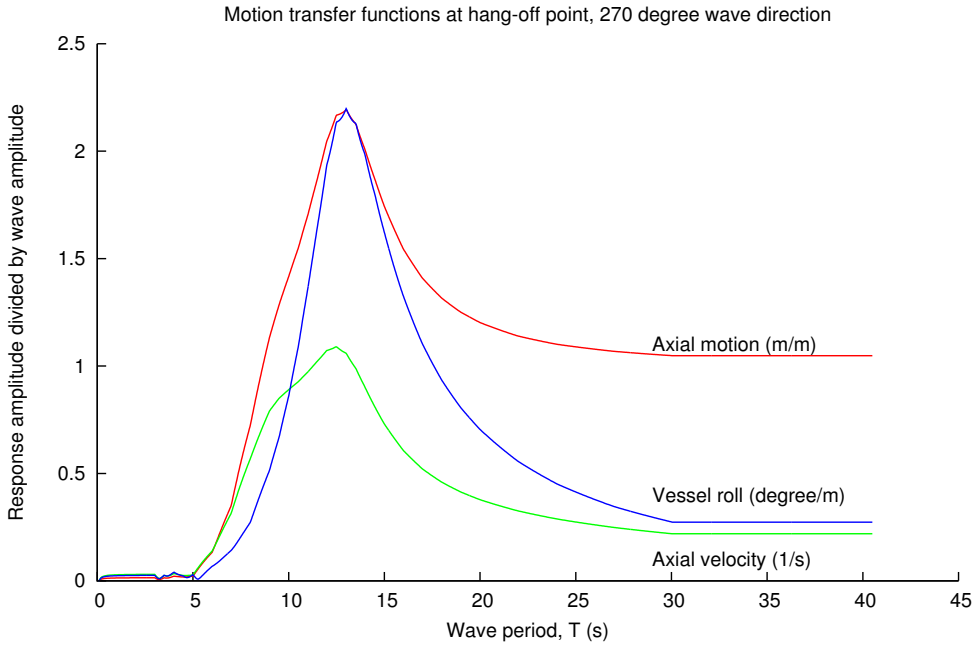

Figure 19: Motion RAOs for the umbilical hang-off point, wave direction 270 °.

12.4 How to calculate the motion from the RAO

The transfer function, $H(\omega)$, has its use in the dynamic analysis of linear systems. It is particularly well suited to describe the stationary dynamic response caused by a stationary and stochastic Gaussian sea state which is assumed Gaussian. The response is then also Gaussian because of the linearity, Larsen, "TMR 4180, Marin dynamikk" (2007) [11].

The dynamic excitation is in this case caused by the superposition of a great number of linear regular waves (Airy wave theory) with different amplitudes A_j and frequencies ω_j where $j = 1 \dots N$. The following description is taken from Faltinsen (1990) pp. 37 [9] with additional information from Newland (2005) [21]. The accumulated wave elevation is then given by:

$$\zeta(t) = \sum_{j=1}^{N} A_j \cos(\omega_j t - k_j x + \epsilon_j) \tag{49}$$

Similar to Faltinsen, the A_j, ω_j, k_j and ϵ_j are respectively the wave amplitude, circular frequency, wave number and the fixed random phase angle from a uniform distribution between 0 and 2π. The variance from each sinusoidal wave with amplitude A_j equals $A_j^2/2$. It is this value which is specified by the wave spectrum $S_\zeta(\omega)$.

$$\frac{1}{2}A_j^2 = S_\zeta(\omega)\Delta\omega \tag{50}$$

The mean value of wave elevation $\zeta(t)$ is zero and the total variance of $\zeta(t)$ is given by sum over all contributing sinusoidal waves: $\sigma_\zeta^2 = \sum_{j=1}^{N} A_j^2/2 = \int_0^\infty S_\zeta(\omega)\,\mathrm{d}\omega$. Recalling that the associated response amplitude is given by $x_{oj} = H_x(\omega_j)\zeta_{0j}$, the contributing variance for each sinusoidal response with the same frequency w_j is known as $x_{0j}^2/2$. Likewise, the response spectrum is also known:

$$S_x(\omega) = |H_x(\omega)|^2 S_\zeta(\omega) \tag{51}$$

Two particularly significant parameters can be extracted from the 1st and 2nd moments of this response spectrum. Namely the response variance σ_x^2 and the zero up-crossing period T_z.

$$\sigma_x^2 = \int_0^\infty |H_x(\omega)|^2 S_\zeta(\omega)\,\mathrm{d}\omega \tag{52}$$

The spectrum of $x(t)$ is given by 51. To obtain the zero up-crossing period it is necessary to consider the response spectrum of the derived process $\mathrm{d}x(t)/\mathrm{d}t = \dot{x}(t)$ – or to be specific, the variance of $\dot{x}(t)$. Since the spectrum for a derived process is $S_{\dot{x}}(\omega) = \omega^2 S_x(\omega)$:

$$\sigma_{\dot{x}}^2 = \int_0^\infty \omega^2 |H_x(\omega)|^2 S_\zeta(\omega)\,\mathrm{d}\omega \tag{53}$$

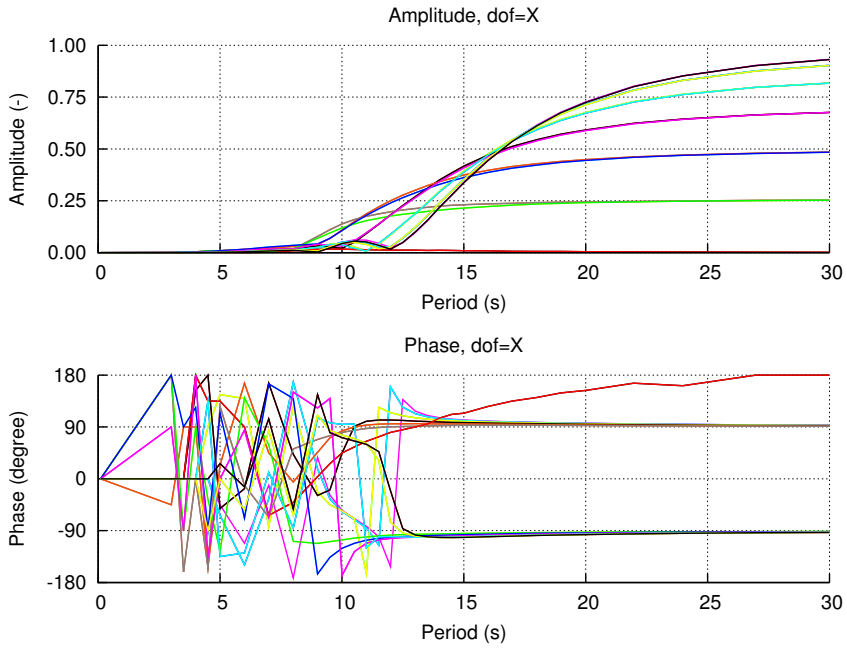

Figure 20: Surge RAO for ballast condition.

The zero up-crossing period is then calculated as Faltinsen (1990) pp. 25 [9], Newland (2005) pp. 89:

$$T_z = 2\pi \frac{\sigma_x}{\sigma_{\dot{x}}} \tag{54}$$

Finally, once we know the mean response and the standard deviation as well as the zero up-crossing period (and the zero up-crossing frequency $\nu_0^+ = 1/T_z$) – we can calculate the characteristic extreme value for a storm duration of typically 3 hours (10800 seconds) by using the Rayleigh distribution. This give: $x_{max} = x_{mean} + \sigma_x \sqrt{2 \ln(10800./Tz)}$.

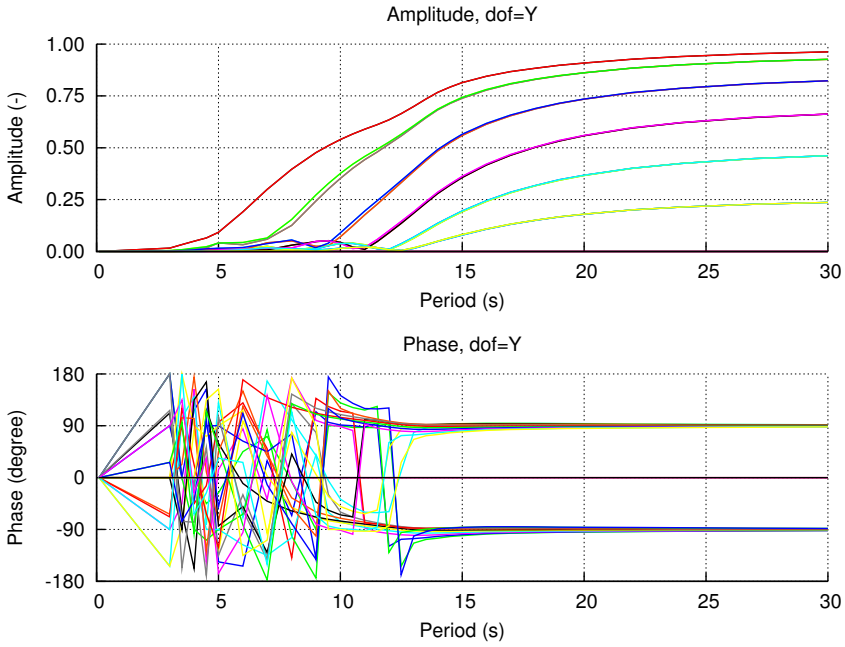

Figure 21: Sway RAO for ballast condition.

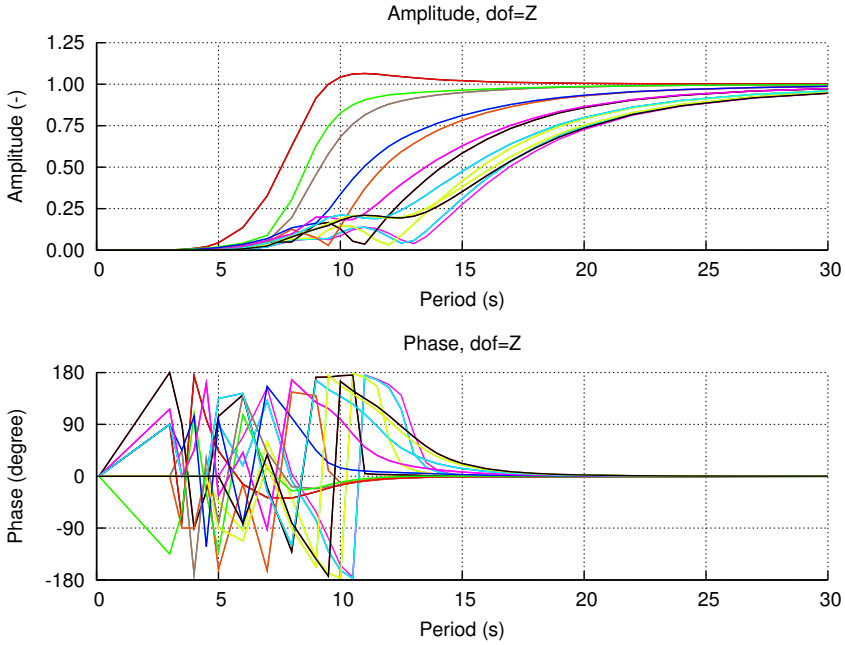

Figure 22: Heave RAO for ballast condition.

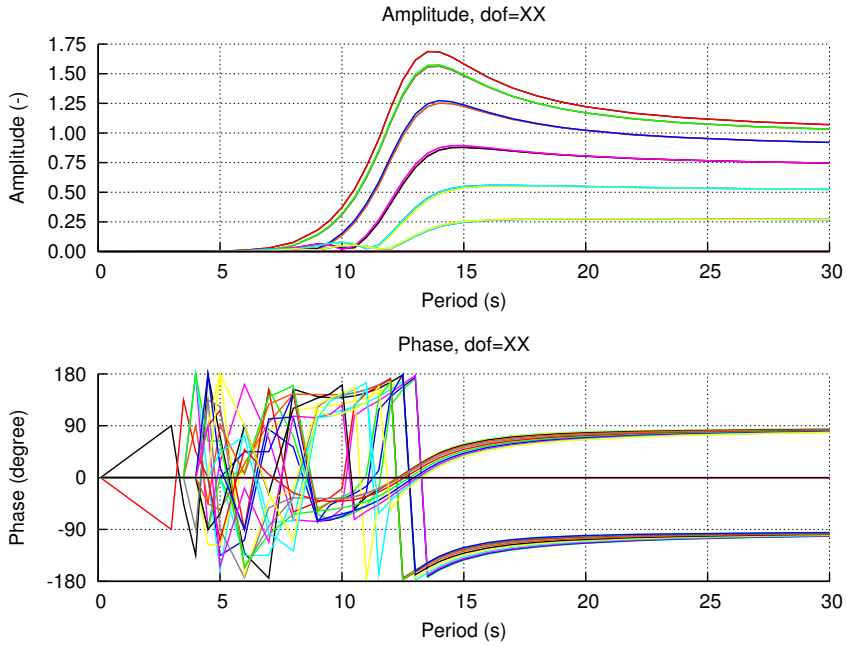

Figure 23: Roll RAO for ballast condition.

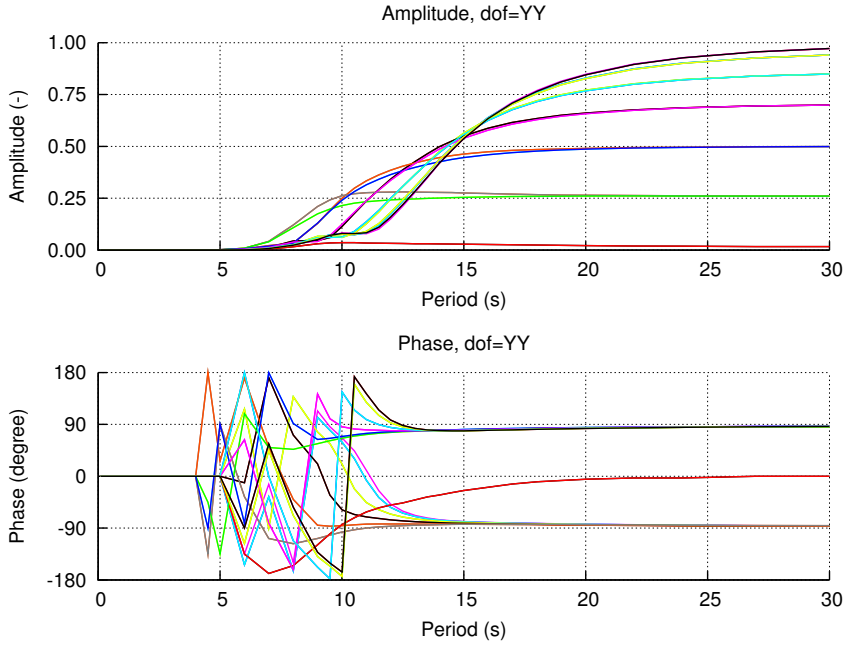

Figure 24: Pitch RAO for ballast condition.

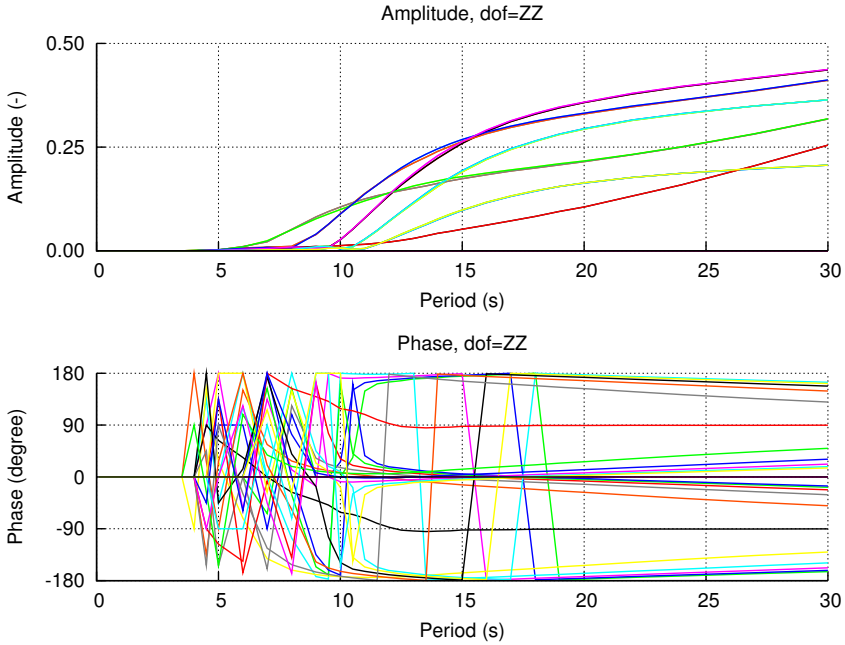

Figure 25: Yaw RAO for ballast condition.

13 Long term 100-year response

The purpose of this section is to calculate long term 100-year response values directly from all the sea states of the wave scatter diagram, table 13. The response values studied are wave, top end motions and selected umbilical response parameters.

The simplified method as described in section 9 is used.

13.1 Reasons for inspecting the vessel induced motions

Inspection of the transfer functions for umbilical axial motion at the hang-off position reveals that the umbilical axial motion is significantly affected by the direction of the wave, see figures 18 and 19. Wave direction 270 ° causes much more axial motion and velocity than wave direction 90 °. Hence, we should expect comparatively less accelerations and therefore also less dynamic tension in the umbilical for the 90° wave propagation direction.

Figures 18 and 19 describe also the transfer function for the roll angle of the vessel. The rotation of the vessel is similar for both directions 90° 270° as it should be since both are beam sea directions are inducing vessel roll only. The roll motion is interesting since even if the umbilical is hypothetically unaffected by the direct wave action, the vessel rotation would cause bending in the bend stiffener.

For these reasons, the long term extreme vessel motion at the top end point is interesting. The long term response is established by performing frequency domain analysis considering the entire scatter diagram, see table 13. It should be noted that the same scatter diagram is used for both vessel beam sea directions, 90° and 270°. The long term wave elevation is obtained in the same manner for comparison purpose.

The main objectives are:

- Verify that wave direction 270° is indeed the most critical as indicated by the motion transfer functions at the hang-off point.
- Determine the long term response values for subsequent comparison with contour curve results. Of particular interest is the non-exceedance probability α for the extreme determined from sea states along the contour curve. S. Haver et al, reference XYZ, suggests that the contour curve extremes should be associated with an α-value of 0.90 to be consistent with long term extreme results.
- For subsequent comparison with estimates of umbilical long term responses, prepare information to see which of the wave elevation or vessel response parameters that is better correlated with the umbilical response.

Subsequently, long term estimates of umbilical response quantities will be investigated using obtained standard deviations and mean level up-crossing frequencies from linear time domain analysis for all the sea states of the wave scatter

diagram. The simulation time is 1 hour (3600 s) for each sea state. These linear time domain analysis are performed using constant system stiffness, damping and mass matrices. Note that the external loads are non-linear similar to those of a full non-linear time domain analysis.

The method for the long term analysis is presented in section 9.

13.2 Top motion, long term 100-year response

The vessel induced motions at the top end of the umbilical has been calculated using frequency domain methods by use of given vessel transfer functions. The responses have been calculated from the response spectrum, see section 12.4.

The following response quantities have been considered: the motion in the static axial direction of the umbilical (7 ° with the vertical) (X), the axial velocity ($\dot{X}$) in the same direction and also the component of the vessel induced angle parallel with the ship's longitudinal axis – the vessel roll angle (θ_y).

The transfer functions for X and θ_y have been obtained from the provided vessel RAOs through transformation, see section 12.3. The transfer function for $\dot{X}$ is obtained from that of X by $H_{\dot{X}}(\omega) = \mathrm{i}\omega H_X(\omega)$.

The long term results are given in table 23 for wave directions 90° and 270°. As indicated by the transfer functions for X, $\dot{X}$ and θ_y, see section 12.3.5 and figures 18 and 19, the vessel angle is similar for the two directions and the axial motion is significantly more severe for wave directions 270°. Note that a 270 ° wave direction means that the waves moves from the umbilical top end towards the bottom end when seen from above.)

Wave direction		90°	270°
Wave elevation, ζ	(m)	8.122	8.122
Axial motion, X	(m)	4.837	13.580
Axial velocity, $\dot{X}$	(m/s)	2.491	6.889
Vessel angle, θ'_y	(°)	12.328	12.328

Table 23: Long term dynamic maximum values.

Table 24 give the contribution for the 8 largest contributors to the long term extreme value of wave elevation, ζ. This table shows that the most contributing sea state to the long term extremes is the sea state with the largest wave height. Note that all the sea states in the wave scatter diagram are included in the analysis even if not shown here..

It is readily observed in table 24 that the sea state with the largest wave height contributes the most for all response quantities: ζ, X, $\dot{X}$ and θ'_y. Limiting ourselves to the three largest contributors a period dependency may also be suspected. This is perhaps most easily seen in table 25 where only the contributions ranks are given, the largest contributor is assigned a rank value of 1, the second largest a rank value of 2 and so on.

Sea state			Contribution to the long term extreme			
Hs (m)	Tp (s)	γ	ζ	X	$\dot{X}$	θ'_y
6.25	13.50	1.783	0.939878	0.990461	0.958859	0.992288
5.75	11.50	1.929	0.047263	0.001368	0.030354	0.000108
5.25	13.50	1.783	0.004947	0.005835	0.005447	0.005935
5.25	10.50	2.017	0.002132	0.000000	0.000064	0.000000
5.25	11.50	1.929	0.001941	0.000029	0.001197	0.000001
5.25	12.50	1.852	0.001783	0.000765	0.003284	0.000436
5.25	14.50	1.722	0.001535	0.001329	0.000331	0.001063
4.75	12.50	1.852	0.000152	0.000057	0.000335	0.000029

Table 24: Sea state contribution to the long term extreme of top motion, wave direction 270°.

Sea state			Contribution rank			
Hs (m)	Tp (s)	γ (-)	ζ	X	$\dot{X}$	θ_y
6.25	13.50	1.783	1	1	1	1
5.75	11.50	1.929	2	3	2	5
5.25	13.50	1.783	3	2	3	2
5.25	10.50	2.017	4	15	9	20
5.25	11.50	1.929	5	9	5	10
5.25	12.50	1.852	6	5	4	4
5.25	14.50	1.722	7	4	7	3
4.75	12.50	1.852	8	7	6	8

Table 25: Ranked sea state contribution to the long term extreme of top motion, wave direction 270°.

As for the contributors to the long term extreme wave elevation ζ, table 25 seems to indicate that the wave height is more important than the wave period. It is the ranks greater than 8 for the other parameters that indicates this. This means that the sea states important for the wave elevation are not so important for the induced top end motions.

The duration associated with the long term extreme are given in table for wave direction 270°. It is seen that the required duration to realize the characteristic largest value in a simulation is about 2000 hours. This means that detailed time domain simulation using a sea state part of the given wave scatter diagram is not practical. The reason for this is probably that the given scatter diagram is *observed*, not analytically extended.

As to the efficiency of the wave elevation in predicting the sea state contribution to the long term maximum, figures 26 and 27 illustrates this for wave directions 90° and 270° respectively. Based on these figures it appears as if the wave elevation is not so strongly correlated to the top end motion.

Sea state			Duration for long term extreme			
Hs (m)	Tp (s)	γ (-)	ζ	X	$\dot{X}$	θ'_y
6.25	13.50	1.783	2122	2014	2080	2010
5.75	11.50	1.929	2.11E4	7.289E5	3.286E4	9.208E6
5.25	13.50	1.783	6.048E5	5.127E5	5.493E5	5.041E5
5.25	10.50	2.017	4.678E5	3.394E10	1.561E7	1.438E15
5.25	11.50	1.929	5.138E5	3.402E7	8.335E5	7.057E8
5.25	12.50	1.852	5.594E5	1.303E6	3.037E5	2.287E6
5.25	14.50	1.722	6.498E5	7.506E5	3.014E6	9.383E5
4.75	12.50	1.852	3.938E7	1.046E8	1.785E7	2.062E8

Table 26: Sea state duration to realize long term extreme (hours) of top motion, wave direction 270°.

Figure 28 contains the data for all the sea states part of the scatter diagram. This figure shows that for any constant wave height, the top end motions are more sensitive to the wave period variation than to the wave elevation ζ. Figure 29 shows that all the top 10 ranks are found in the period band from 10 to 16 seconds.

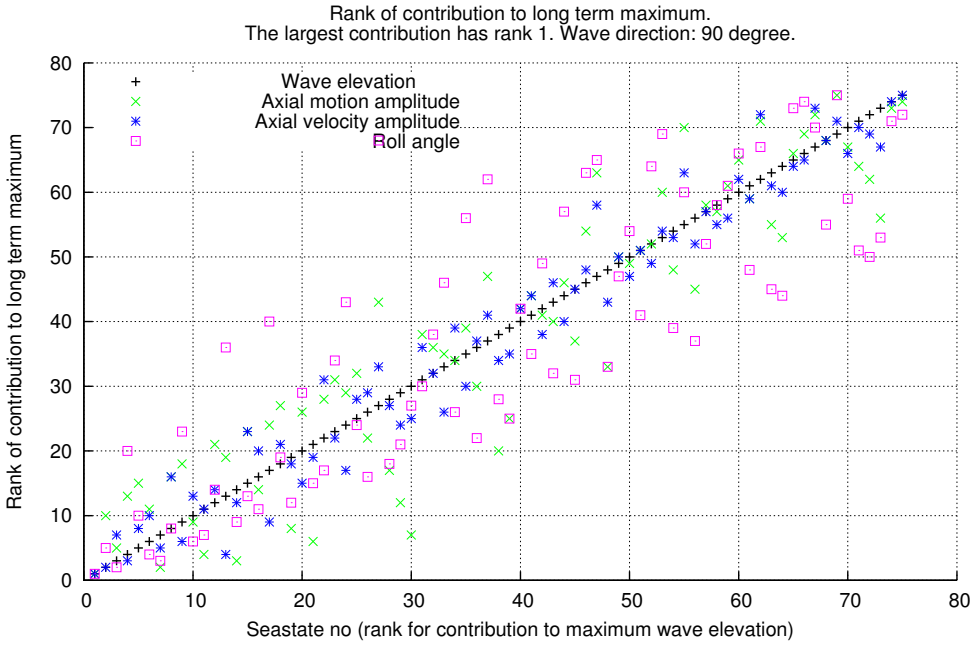

Figure 26: Rank of wave elevation contribution to long term maximum versus rank of vessel induced top end motion contribution, wave direction 90°.

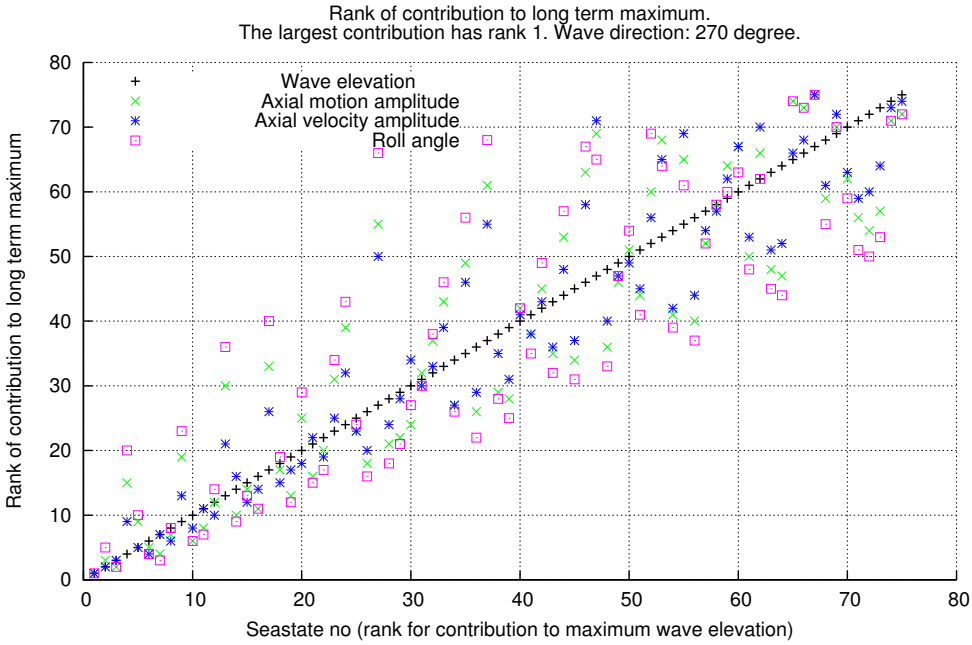

Figure 27: Rank of wave elevation contribution to long term maximum versus rank of vessel induced top end motion contribution, wave direction 270°.

13.3 Umbilical, long term 100-year response

Time domain analysis with constant system matrices have been performed for all sea states in the scatter diagram. From the simulations, each with duration 3600 s, the standard deviation and the up-crossing frequency for selected umbilical response quantities have been obtained.

The studied parameters are:

- T_{BS}, the bend stiffener tension (the umbilical tension immediately below the bend stiffener).
- T_{sag}, the tension in the sag bend of the lazy wave configuration.
- θ_y, component of the bend stiffener angle (the angle between the vessel fixation and the moving umbilical immediately below the bend stiffener tip, see section 7.1 for the calculation method.

The bend stiffener tension and angle are particularly important parameters for the design and verification of bend stiffeners. As to the angle, this is a vector and is expected to be correlated to the vessel rotation since the relative angle between the moving umbilical and the moving vessel may be assumed the sum of two parts, $\theta = \theta' + \theta''$, see section 7:

Part 1: θ', the angle between the moving vessel versus the static direction of the umbilical (top end vector).

Part 2: θ'', the deviation in the umbilical direction from the static direction due to the dynamic loads and the forced top end motion.

Such a description may be beneficial, since the first part may be readily and accurately calculated in advance using RAOs and frequency domain tools. Hence, we would have useful and quick approximation subject to the assumption that part 2 is small in comparison.

Table 27 give the estimated long term umbilical response values, note that these calculated assuming Gaussian response using standard deviations and zero up-crossing frequencies from linear time domain analysis (analysis with constant system matrices).

		Static ± dynamic
Bend stiffener tension, T_{bs}	(kN)	356.377 ± 238.814
Bend stiffener angle, θ_y	(°)	0.034 ± 12.417
Sag tension, T_{sag}	(kN)	45.812 ± 45.768

Table 27: Long term dynamic umbilical response values, 270°wave direction.

Table 28 give the sea state contributions for the eight (8) sea states that contributes most to the wave elevation ζ. The contribution ranking is given in table 29.

The duration associated with the long term extreme are given in table for wave direction 270°. The duration to realize the characteristic largest umbilical response in a time domain simulation is between 2000 and 2600 hours which compares well with the roughly 2050 hours required for the top motion. Again, this means that detailed time domain simulation using a sea state part of the given wave scatter diagram is not practical.

Sea state			Contribution to the long term extreme			
Hs (m)	Tp (s)	γ (-)	ζ	T_{bs}	θ_y	T_{sag}
6.25	13.50	1.783	0.9399	0.7858	0.9942	0.9686
5.75	11.50	1.929	0.04726	0.1937	2.477E-6	0.0308
5.25	13.50	1.783	0.004947	0.002038	0.003855	0.0001052
5.25	10.50	2.017	0.002132	0.004491	3.686E-18	8.634E-6
5.25	11.50	1.929	0.001941	0.008421	1.232E-8	0.0001787
5.25	12.50	1.852	0.001783	0.004631	6.746E-5	0.0002657
5.25	14.50	1.722	0.001535	3.189E-5	0.001749	6.143E-7
4.75	12.50	1.852	0.000152	0.000352	2.259E-6	9.407E-7

Table 28: Sea state contribution to the long term extreme of umbilical response, wave direction 270°.

Sea state			Contribution rank			
Hs (m)	Tp (s)	γ (-)	ζ	T_{bs}	θ_y	T_{sag}
6.25	13.50	1.783	1	1	1	1
5.75	11.50	1.929	2	2	8	2
5.25	13.50	1.783	3	6	2	5
5.25	10.50	2.017	4	5	24	6
5.25	11.50	1.929	5	3	12	4
5.25	12.50	1.852	6	4	4	3
5.25	14.50	1.722	7	10	3	8
4.75	12.50	1.852	8	7	9	7

Table 29: Ranked sea state contribution to the long term extreme of umbilical response, wave direction 270°.

Table 31 provides the response standard deviations and zero up-crossing frequencies for It is interesting to observe that θ'_y and θ_y in the above are very close to each other. The only difference is that for the latter – the dynamic umbilical motion is accounted for whereas it is taken as fixed in the former. It is noted that this analysis is performed without current and that larger deviation may be seen in a case with current.

Sea state			Duration for long term extreme			
Hs (m)	Tp (s)	γ (-)	ζ	T_{bs}	θ_y	T_{sag}
6.25	13.50	1.783	2122	2538	2006	2059
5.75	11.50	1.929	2.11E4	5148	4.027E8	3.238E4
5.25	13.50	1.783	6.048E5	1.468E6	7.762E5	2.843E7
5.25	10.50	2.017	4.678E5	2.22E5	2.706e+20	1.155E8
5.25	11.50	1.929	5.138E5	1.184E5	8.092E10	5.58E6
5.25	12.50	1.852	5.594E5	2.154E5	1.478E7	3.753E6
5.25	14.50	1.722	6.498E5	3.127E7	5.703E5	1.624E9
4.75	12.50	1.852	3.938E7	1.7E7	2.649E9	6.361E9

Table 30: Sea state duration to realize long term extreme of umbilical response (hours), wave direction 270°.

	90°wave direction		270°wave direction	
Response	σ	ν_0^+	σ	ν_0^+
ζ	1.560	0.1001	1.560	0.1001
X	0.932	0.0818	2.635	0.0805
$\dot{X}$	0.478	0.0942	1.332	0.0851
θ'_y	2.396	0.0778	2.396	0.0778
T_{bs}			45.741	0.0909
T_{sag}			8.835	0.0905
θ_y			2.414	0.0772

Table 31: Response standard deviations (σ) and zero up-crossing frequency (ν_0^+)for the most severe sea state in the scatter diagram, Hs=6.25 m, Tp=13.5 s and γ=1.783.

13.4 Example calculation of 100-year extreme value and contribution

The axial top end velocity, $\dot{X}$, is studied. This response parameter is in the static direction of the umbilical at the upper end. From table 31 for the most severe sea state in the scatter diagram – the standard deviation is 1.332 m/s and the zero up-crossing frequency is 0.0851 1/s. The storm duration is 2080 hours per table 13.3, i.e. $T = 2080 \cdot 3600 = 7488000$ seconds.

The desired extreme value is the characteristic largest value which has an up-crossing frequency equal to once per the storm duration, $\nu = 1/T$. The extreme value may therefore be calculated using the up-crossing relation for a Gaussian stochastic process 30, $nu = \nu_0 \exp(-1/2(x/\sigma)^2)$. This give the maximum velocity: $\dot{X}_{\max} = \sigma\sqrt{2\ln(\nu_0 T)} = 1.332\sqrt{2\ln(0.08517488000)} = 6.887$ m/s. When accounting for round off effects, this is equal to the long term maximum value found in table 23, 6.889 m/s.

This sea state, Hs=6.25 m and Tp=13.5 s, has a probability of $P = 2/879$ per the wave scatter diagram, see table 13. The contribution to the maximum value is calculated as follows: $c = \nu_0 T_{100\text{year}} \exp(-1/2(\dot{X}_{\max}/\sigma)^2)P$ The contribution becomes $c = 0.0851 \cdot (100365.25243600) \exp(-1/2(6.887/1.332)^2)2/879 = 0.957$ which is equal to the value reported in table 24 (0.959) when accounting for the effect of round off.

13.5 Summary and evaluation of the long term 100-year response calculation

The long term extremes have been calculated for selected top end motions and selected umbilical response parameters. All sea states part of the scatter diagram have been considered for the top end motions. In this case the wave direction is either 90°wave direction or 270°which both are vessel beam sea directions.

Table 32 show that the long term response is significantly larger for the 270°direction. The 270°wave direction have therefore been chosen for dynamic time domain analysis of the umbilical system. All the load cases part of the scatter diagram are simulated for 1 hour using constant system matrices (linear analysis). Gaussian response distribution is assumed in the long term response estimation.

It is of interest to see how well the umbilical response contributions are correlated with the contribution ranks for the wave elevation ζ. Figure 30 demonstrates that not all sea states contributing most to the long term extreme wave elevation are interesting for the umbilical response. This finding is similar to that considering umbilical top motion, see figures 26 and 27.

It is expected that the top end motions are well correlated with the umbilical response, in special the top axial velocity is expected to be well correlated with the umbilical tension. Based on figure 31 this appear indeed to be the case for both top tension and the sag tension. In a similar manner, it is suspected that the vessel roll angle, here θ'_y, is well correlated with the bend stiffener

Wave direction		90°	270°
Wave elevation, ζ	(m)	8.122	8.122
Axial motion, X	(m)	4.837	13.580
Axial velocity, $\dot{X}$	(m/s)	2.491	6.889
Vessel angle, θ'_y	(°)	12.328	12.328
			Static ± dynamic
Bend stiffener tension, T_{bs}	(kN)		356.377 ± 238.814
Sag tension, T_{sag}	(kN)		45.812 ± 45.768
Bend stiffener angle, θ_y	(°)		0.034 ± 12.417

Table 32: Summary of long term extreme estimates.

angle. This suspicion appears to be verified by figure 32. It should be noted that all response calculations have been based on the assumption of a Gaussian response. This should be acceptable for the top end motions, but may not be accurate for the umbilical response in the most severe sea states.

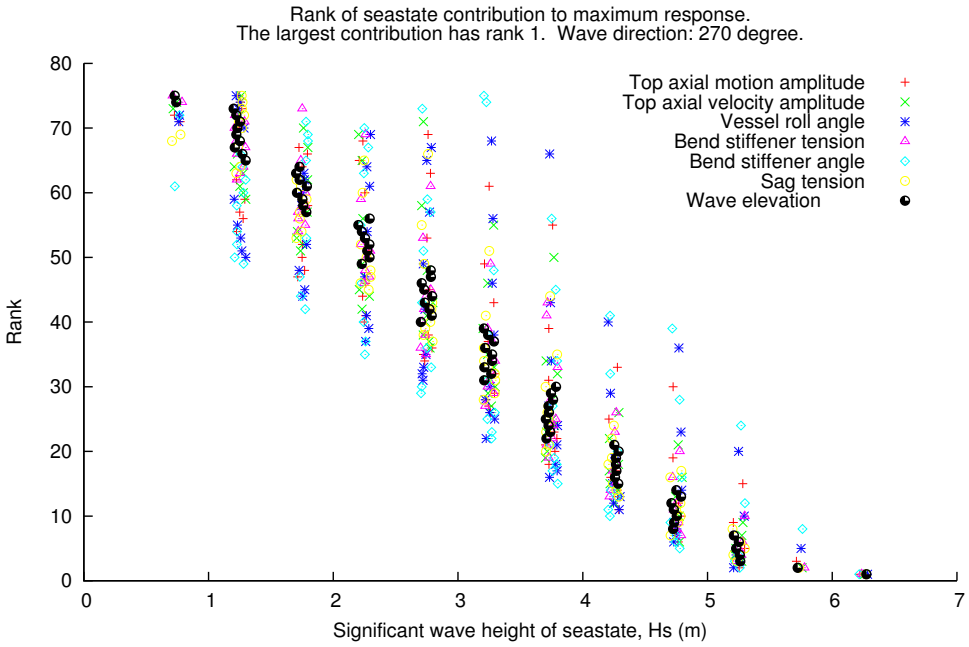

Figure 28: The importance of wave height considering long term response. The scatter for same wave height indicates the sensitivity to wave period. The applied wave heights are 0.75, 1.25, ..., 5.75 and 6.25 m in the analysis. Their horizontal plotting position is slightly distorted for legibility.

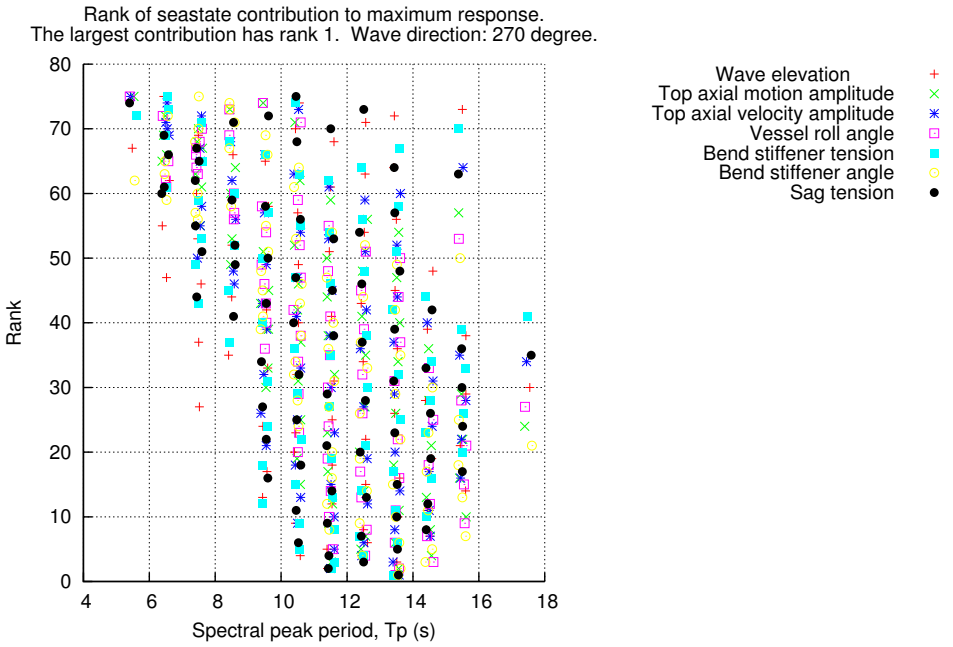

Figure 29: The importance of spectral peak period considering long term response.

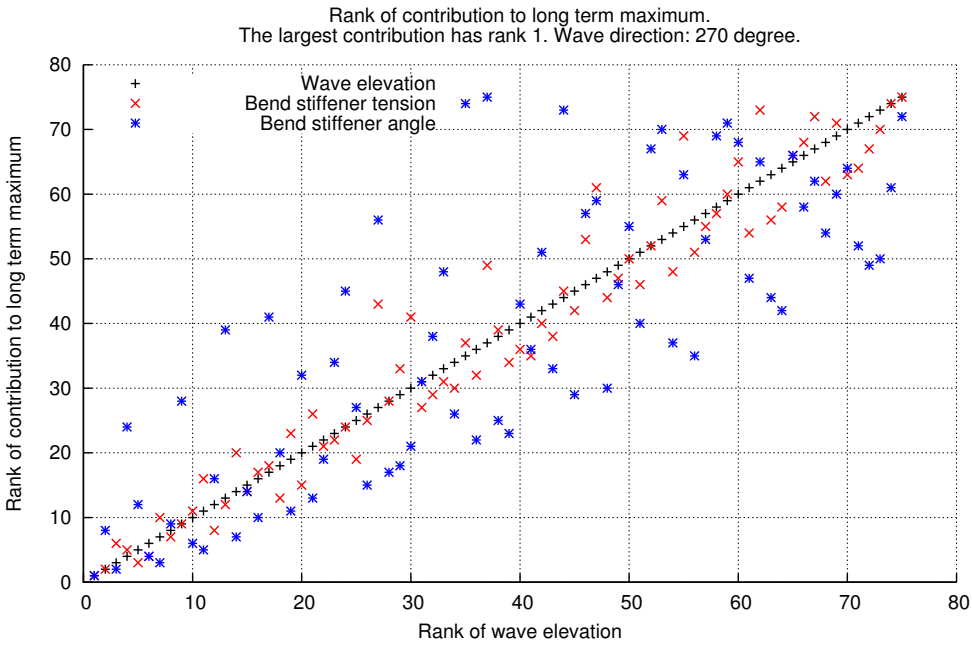

Figure 30: Rank correlation between contribution for long term wave elevation and bend stiffener tension and angle.

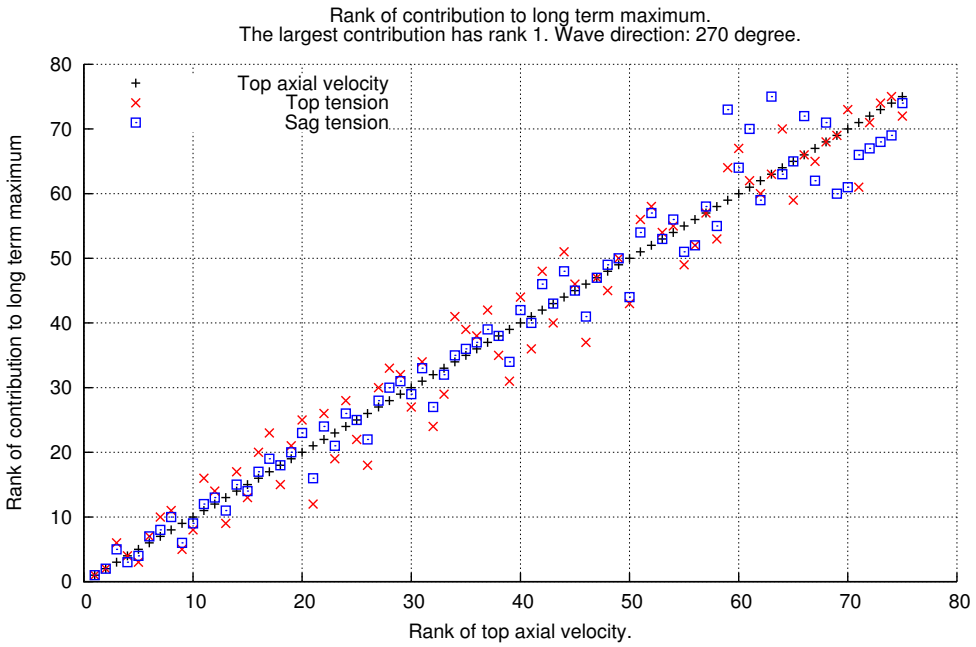

Figure 31: Rank correlation between contribution for long term top axial velocity and tension in bend stiffener and sag.

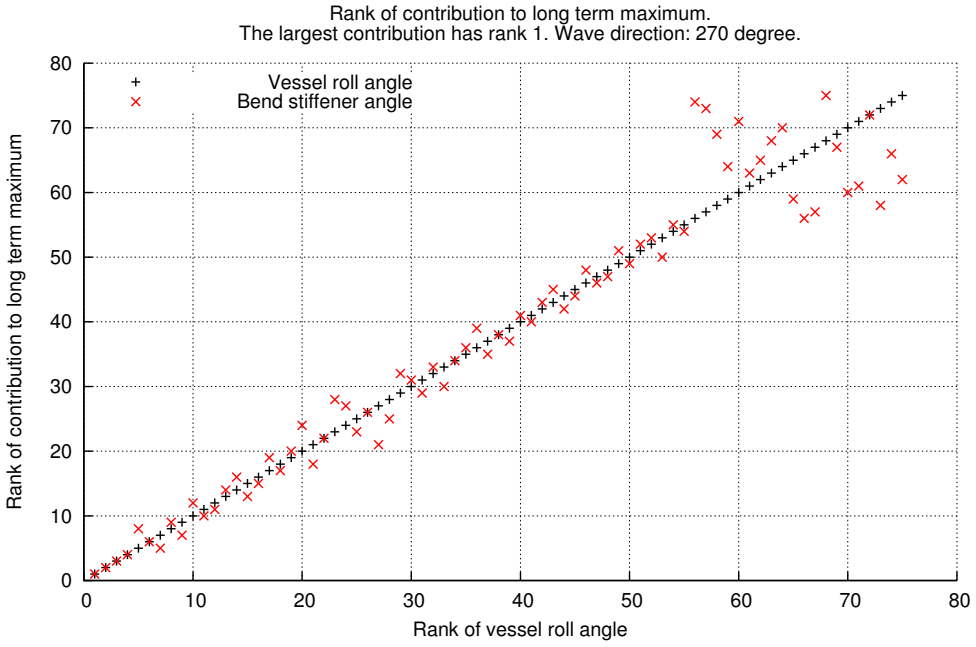

Figure 32: Rank correlation between contribution for vessel roll angle and bend stiffener angle.

14 Extreme response for 100-year contour curve sea states

The extremes response obtained when using sea states from the 100-year contour curve is often taken as an approximation to the 100-year long term response which was studied in 13. This is a convenient approximation since proper evaluation of the long term extreme is considerably more demanding than evaluation of some few sea states along the 100-year contour curve.

The purpose of this section is to evaluate the accuracy of the contour curve approach. The procedure is to determine the maximum response for the specified storm duration, 3 hours, for several sea states on the contour curve. The largest response value thereby obtained is then compared to the long term response value as given in table 32.

It is obvious that the largest value in any sea state will depend on a precise definition of the extreme value, the non-exceedance probability α as mentioned in section 10.2. An α-value of 0.90 will typically be an adequate value when using 100-year contour curves according to Sverre Haver (2007) [1]. If $\alpha = 0.90$ is correct, the extreme value from the 100-year contour curves, table 12, should closely match the corresponding 100-year long term value.

It is clear that the correct α-value is initially unknown and probably different for various response quantities. Hence, it is of interest to learn the correct α-values for the umbilical system studied here. To this end, the 100-year long term response values are given in table 32 are useful.

These long term results will be compared to the 100-year contour curve results based on different values of the α-parameter. The α-value that causes a match between contour curve results and long term results will also be determined.

For consistency the contour curve estimates are prepared using method similar to those used when determining the long term extreme value. Hence, the response is assumed Gaussian and it is sufficient to know the response standard deviation and the up-crossing frequency for the static response level.

14.1 Results, α-values for 100-year contour curve

The long term results and the α-value that brings correspondence between the long term result and the contour curve result are given in table 33.

Response statistics for the different response parameters are given in table 34 for the axial motion X and the axial velocity $\dot{X}$, table 35 for top angles, the vessel angle θ'_y and the bend stiffener angle θ_y (projections) and table 36 for the tension in the bend stiffener and sag region, T_{bs} and T_{sag}.

Example, calculating the expected maximum $\dot{X}_e$ for wave direction 270°: The 3 hour dynamic extreme value of $\dot{X}$ comes in addition to the average which is 0 m/s. For this example, the sea state given by Hs=7.70 m, Tp=14.5 s is chosen. Furthermore, it is chosen calculate the expected maximum axial velocity $\dot{X}_e$ for this storm duration, $T = 10800$ seconds. According to section

10.2 and table 14, the expected largest has an exceedance probability of 57.04%. Since the response is assumed Gaussian, either equation 31 or 32 can be used.

Here, the zero up-crossing frequency ν_0^+=0.0829 1/s and the number of zero-up-crossings is $N = \nu_0^+ T$=895.32, the standard deviation is σ=1.573 m/s and the non-exceedance probability is $F_P(\dot{X}_e)$=0.5704 for a storm duration of 3 hours, see table 34. Equation 31 give $\dot{X}_e = \sigma\sqrt{2\ln(N) - 2\ln[-\ln(F_p(\dot{X}_e))]}$=6.041 m/s whereas equation 32 give $\dot{X}_e = \sigma[\sqrt{2\ln(N)} + 0.57722/\sqrt{2\ln(N)}] = 6.046$ m/s which is the same for all practical purposes.

Wave direction	90°	270°	Note
Wave elevation, ζ (m)	0.842	0.842	See figure 33, same weather.
Axial motion, X (m)	0.022	0.893	See figures 34 and 35.
Axial velocity, $\dot{X}$ (m/s)	0.656	0.927	See figures 36 and 37.
Vessel angle, θ'_y (°)	0.904	0.904	See figure 38, symmetry.
Bend stiffener tension, T_{bs} (kN)		0.893	See figure 39.
Sag tension, T_{sag} (kN)		0.657	See figure 40.
Bend stiffener angle, θ_y (°)		0.801	See figure 41.

Table 33: Non-exceedance probability, α-value for 100-year contour curve results.

Sea state			X (m)		$\dot{X}$ (m/s)	
Hs (m)	Tp (s)	γ (-)	σ	ν_0^+ (1/s)	σ	$\nu_0^+(1/s)$
7.15	12.50	1.852	2.940	0.0839	1.547	0.0880
7.30	13.00	1.816	3.057	0.0821	1.575	0.0864
7.45	13.50	1.783	3.141	0.0805	1.588	0.0851
7.58	14.00	1.752	3.191	0.0791	1.586	0.0839
7.70	14.50	1.722	3.217	0.0779	1.573	0.0829
7.79	15.00	1.693	3.219	0.0767	1.551	0.0820
7.84	15.50	1.666	3.199	0.0756	1.520	0.0812
7.78	16.00	1.640	3.131	0.0746	1.467	0.0805
7.63	16.50	1.616	3.028	0.0736	1.400	0.0797
7.40	17.00	1.592	2.896	0.0726	1.321	0.0791
7.12	17.50	1.570	2.747	0.0717	1.237	0.0784
6.82	18.00	1.548	2.595	0.0707	1.153	0.0777

Table 34: Contour curve response statistics. Standard deviations (σ) and zero up-crossing frequencies (ν_0^+) for X and $\dot{X}$, wave direction 270°.

Sea state			θ'_y (°)		θ_y (°)	
Hs (m)	Tp (s)	γ (-)	σ	ν_0^+ (1/s)	σ	$\nu_0^+(1/s)$
7.15	12.50	1.852	2.634	0.0805	2.585	0.0792
7.30	13.00	1.816	2.768	0.0791	2.773	0.0782
7.45	13.50	1.783	2.856	0.0778	2.914	0.0772
7.58	14.00	1.752	2.897	0.0767	3.003	0.0759
7.70	14.50	1.722	2.906	0.0758	3.053	0.0752
7.79	15.00	1.693	2.886	0.0750	3.067	0.0744
7.84	15.50	1.666	2.842	0.0743	3.047	0.0737
7.78	16.00	1.640	2.754	0.0737		
7.63	16.50	1.616	2.636	0.0732		
7.40	17.00	1.592	2.493	0.0727		
7.12	17.50	1.570	2.338	0.0722		
6.82	18.00	1.548	2.182	0.0718		

Table 35: Contour curve response statistics. Standard deviations (σ) and zero up-crossing frequencies (ν_0^+) for θ'_y and θ_y, wave direction 270°.

Sea state			T_{bs} (kN)		T_{sag} (kN)	
Hs (m)	Tp (s)	γ (-)	σ	ν_0^+ (1/s)	σ	$\nu_0^+(1/s)$
7.15	12.50	1.852	55.841	0.0936	11.373	0.0935
7.30	13.00	1.816	56.014	0.0925	11.578	0.0916
7.45	13.50	1.783	55.725	0.0910	11.625	0.0904
7.58	14.00	1.752	54.935	0.0899	11.514	0.0893
7.70	14.50	1.722	53.873	0.0888	11.309	0.0891
7.79	15.00	1.693	52.513	0.0884	11.009	0.0876
7.84	15.50	1.666	50.872	0.0878	10.616	0.0871

Table 36: Contour curve response statistics. Standard deviations (σ) and zero up-crossing frequencies (ν_0^+) for T_{bs} and T_{sag}, wave direction 270°.

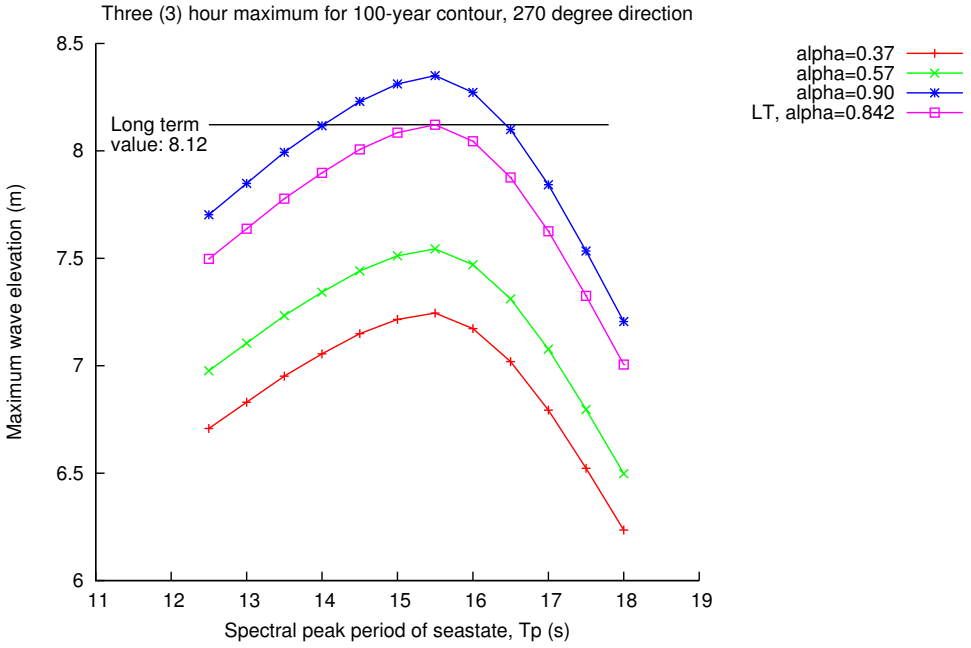

Figure 33: Maximum wave elevation ζ along 100-year wave contour curve. Effect of different α-values.Associated long term maximum and α: ζ=8.12 m, $\alpha = 0.842$.

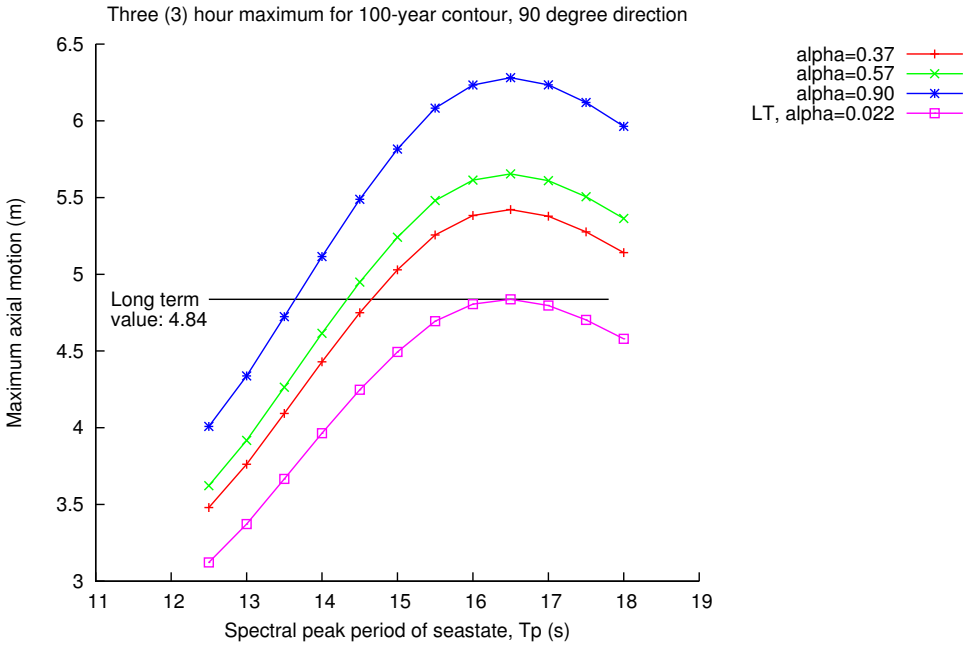

Figure 34: Maximum axial motion X along 100-year wave contour curve, 90° wave direction. Effect of different α-values. Associated long term maximum and α: X=4.84 m, $\alpha = 0.022$.

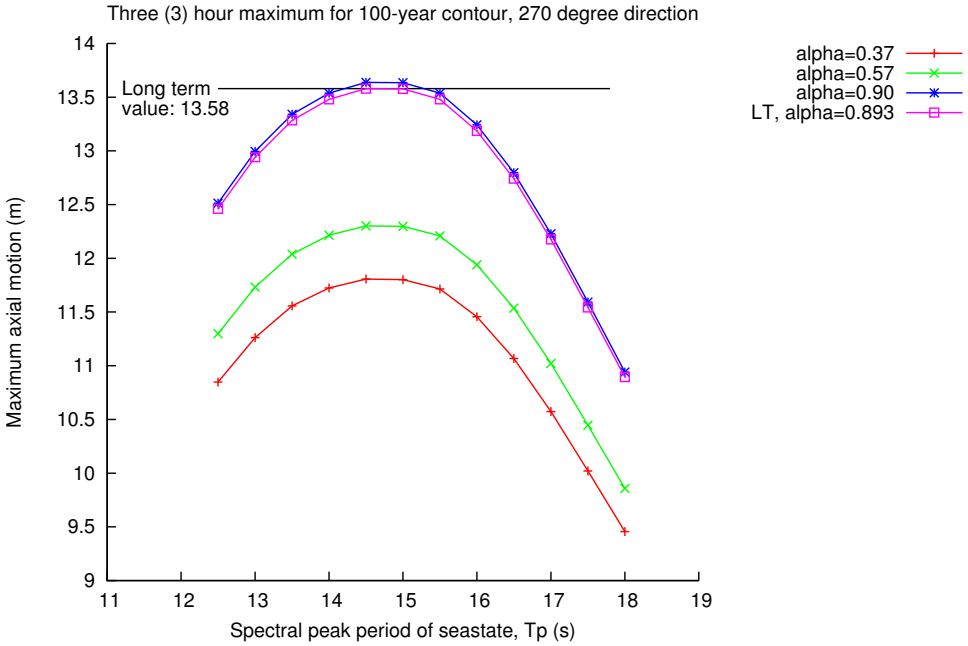

Figure 35: Maximum axial motion X along 100-year wave contour curve, 270° wave direction. Effect of different α-values. Associated long term maximum and α: X=13.58 m, $\alpha = 0.893$.

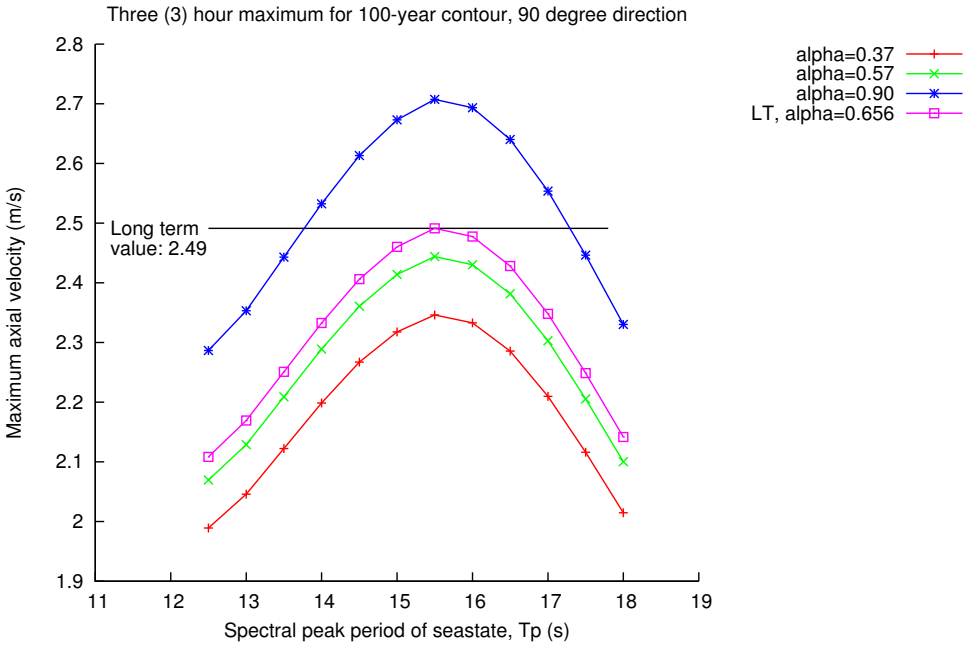

Figure 36: Maximum axial velocity $\dot{X}$ along 100-year wave contour curve, 90° wave direction. Effect of different α-values. Associated long term maximum and α: $\dot{X}$=2.49 m/s, $\alpha = 0.656$.

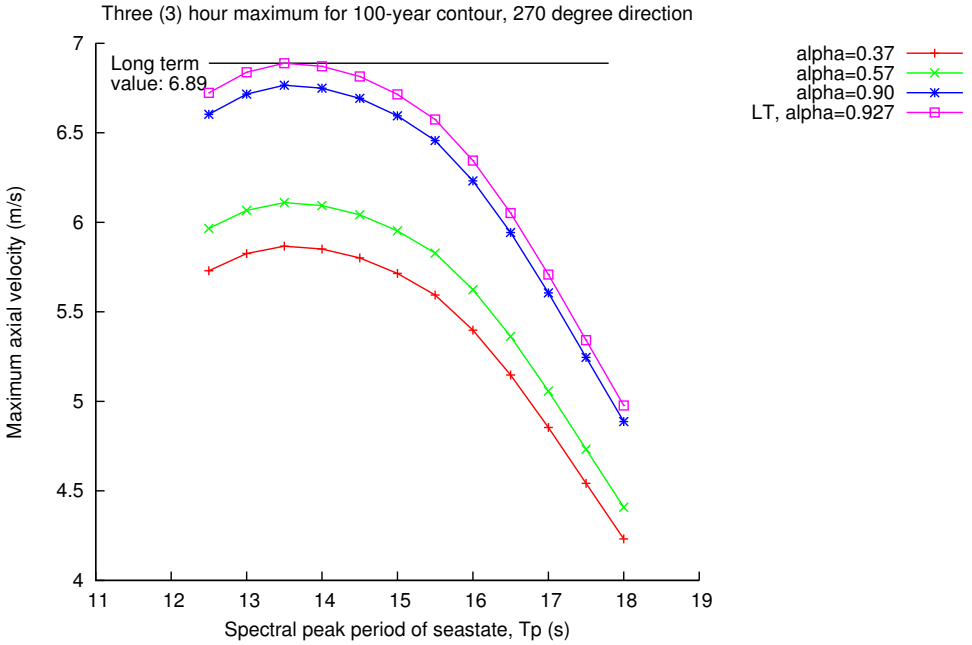

Figure 37: Maximum axial velocity $\dot{X}$ along 100-year wave contour curve, 270° wave direction. Effect of different α-values. Associated long term maximum and α: $\dot{X}$=6.89 m/s, $\alpha = 0.927$.

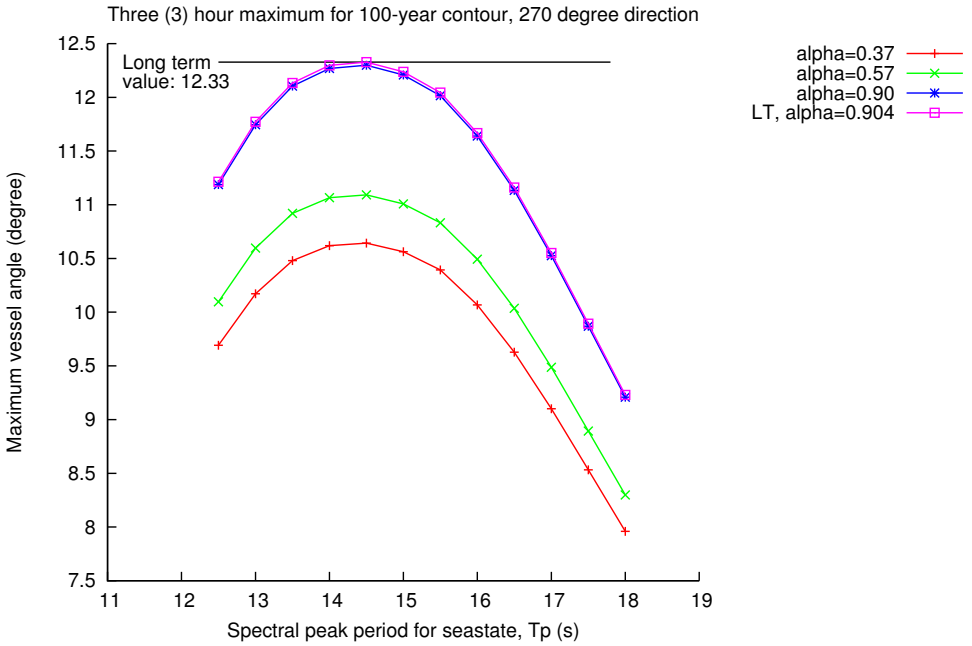

Figure 38: Maximum vessel angle θ'_y (projection) along 100-year wave contour curve, 270° wave direction. Effect of different α-values. Associated long term maximum and α: θ'_y=12.33°, $\alpha = 0.904$.

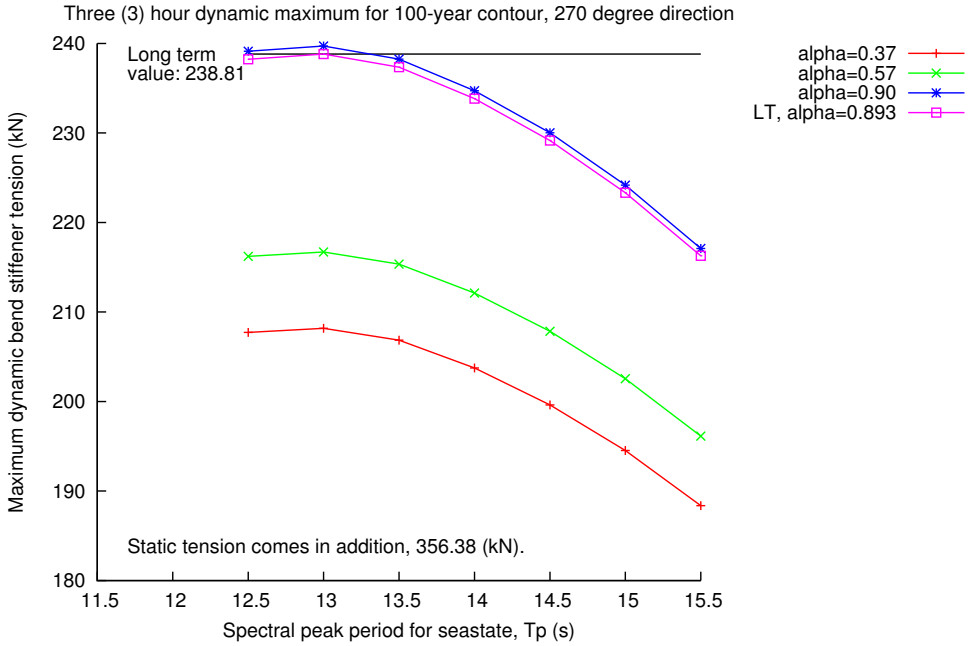

Figure 39: Maximum dynamic bend stiffener tension T_{bs} along 100-year wave contour curve, 270° wave direction. Effect of different α-values. Associated long term maximum and α: T_{bs}=238.81 kN, $\alpha = 0.893$.

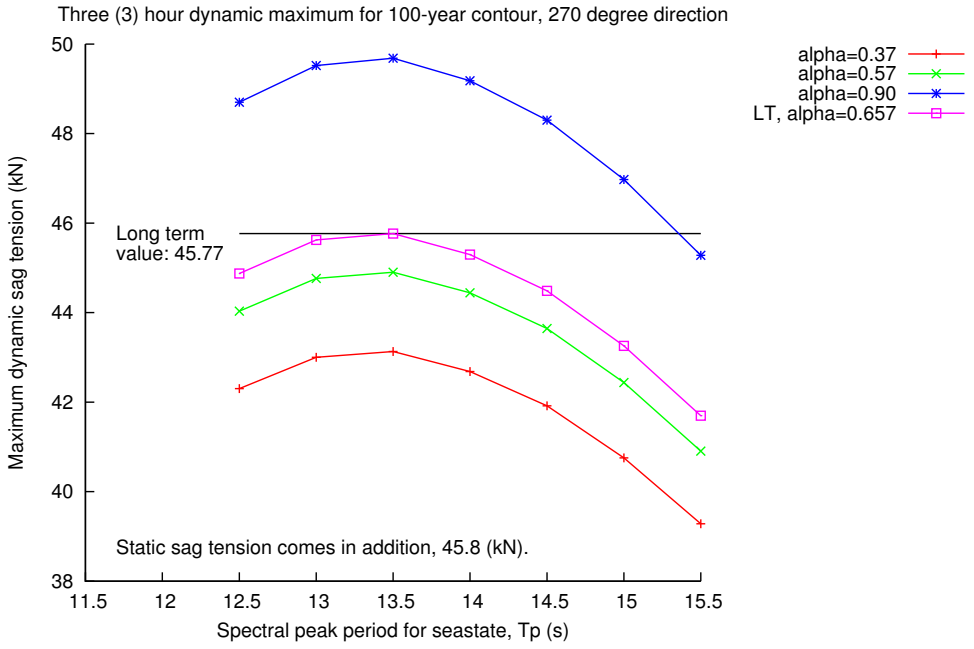

Figure 40: Maximum dynamic sag tension T_{sag} along 100-year wave contour curve, 270° wave direction. Effect of different α-values. Associated long term maximum and α: T_{sag}=45.77 kN, $\alpha = 0.657$.

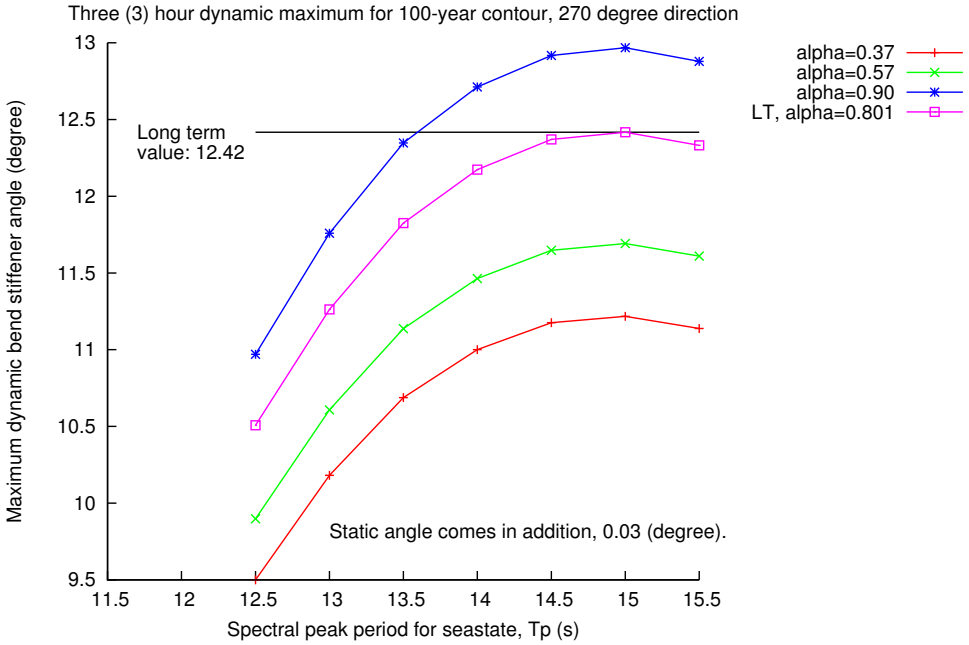

Figure 41: Maximum dynamic bend stiffener angle θ_y (projection) along 100-year wave contour curve, 270° wave direction. Effect of different α-values. Associated long term maximum and α: θ_y=14.42°, $\alpha = 0.801$.

15 Non-linear analysis of a selected sea state

One sea state part of the 100-year contour, table 12, have been selected for further study through non-linear analysis using 3 hour simulations. The choice of the sea state is based on the bend stiffener angle and the axial velocity at the top end. Details about the time domain simulation method is given in section 5.1.

The bend stiffener angle is significant for the bend stiffener design whereas the axial velocity is interesting because the extreme values may predict time instants where compression occurs in the lower sag area of the lazy wave configuration.

Figures 36 and 37 show that wave direction 270° give significantly more axial velocity than direction 90°. Therefore, wave direction 270 ° is selected.

The axial velocity is largest for spectral peak period, Tp=13.5 s according to figure 37 for 270° wave direction. Figure 41 show that the bend stiffener angle is largest for spectral peak period 15.0 s. A sea state with an intermediate spectral peak period is therefore chosen: Hs=7.70 m, Tp=14.5 s and γ=1.722 per table 34.

The simplified methods of interest are those were simplified methods are identifying interesting time windows (hopefully) for subsequent evaluation through more detailed analysis.

To facilitate this investigation, the selected sea state is simulated ten (10) times, each time with a different seed number to generate ten (10) unique wave time series with length three (3) hours .

For each of the unique ten (10) wave time series, a pair of dynamic time domain simulation analysis are performed. The first of this pair is done using constant system stiffness and mass matrices, this is hereafter called a linear time domain analysis. The second of this pair is a full non-linear time domain analysis. This pair of analysis results may then also be used to investigate how well the linear analysis results are in predicting the instances of interesting time windows in a full non-linear analysis.

15.1 The expected extreme value for a 3 hour storm

The objective of the extreme value statistics is determination of the expected extreme for a three hour storm. This is obtained by choosing non-exceedance probability α=0.5704 in the extreme value estimation according to section 10.2 and table 14. This is done to allow comparison with observed maximum and minimum values from the simulation which is slightly longer than three (3) hours, actually 3 hour and 140 seconds.

For the bend stiffener tension T_{bs}, see table 37 – the skewness is close to zero as expected for a Gaussian response whereas the kurtosis is slightly larger (3.3) than the expected value for a Gaussian response, 3.0. Hence, the tension signal may be characterized as non-linear. The average of the Gumbel minimum and maximum bend stiffener tension from the time series are 106.4 and 601.3

Case	Bend stiffener tension, T_{bs} (kN)					Expected Gumbel extreme	
	Average	Std.	Skew.	Kurt.	Tz (s)	Minimum	Maximum
lw-32700405	356.3	54.92	-0.04	3.28	11.04	111.8	591.3
lw-32700415	356.4	55.69	-0.03	3.24	11.17	91.0	577.3
lw-32700425	356.4	54.34	-0.04	3.15	11.11	125.9	594.2
lw-32700435	356.4	54.13	-0.03	2.97	11.07	134.7	571.4
lw-32700445	356.4	55.10	-0.06	3.55	11.15	77.2	621.3
lw-32700455	356.4	54.79	-0.03	3.30	11.02	105.2	613.3
lw-32700465	356.4	56.16	-0.04	3.39	11.17	92.3	637.5
lw-32700475	356.4	54.26	-0.05	3.13	11.22	114.3	598.6
lw-32700485	356.3	54.35	-0.04	3.26	11.12	118.2	595.6
lw-32700495	356.4	54.14	-0.07	3.40	11.25	93.1	612.6

Table 37: Bend stiffener tension results from non-linear analysis.

kN. This is -4.56 and +4.47 standard deviations from the average value. The corresponding Gaussian extreme would be 3.86 standard deviations from the average, yielding 568 kN as the maximum. Hence, the non-linearity induces larger deviations from the average. Note that the observed ten sample maximum values from the ten 3 hour + 140 s long simulation are in the range 551 to 651 kN with an average value equal to 582 kN and a sample standard deviation of 25.9 kN.

Case	Axial velocity, $\dot{X}$ (m/s)					Expected Gumbel extreme	
	Average	Std.	Skew.	Kurt.	Tz (s)	Minimum	Maximum
lw-32700405	0.00	1.564	0.00	3.12	11.96	-6.46	6.11
lw-32700415	0.00	1.588	0.02	3.04	12.07	-6.73	6.08
lw-32700425	0.00	1.548	0.01	2.94	12.03	-5.88	6.23
lw-32700435	0.00	1.545	0.01	2.84	12.21	-6.01	5.72
lw-32700445	0.00	1.564	0.00	3.22	12.06	-7.40	7.12
lw-32700455	0.00	1.560	0.02	3.06	12.01	-6.34	6.60
lw-32700465	0.00	1.600	0.00	3.13	12.11	-6.85	7.34
lw-32700475	0.00	1.554	0.00	2.94	12.11	-6.57	6.62
lw-32700485	0.00	1.558	0.01	3.02	12.22	-6.11	6.38
lw-32700495	0.00	1.546	-0.01	3.11	12.03	-6.62	6.64

Table 38: Axial velocity ($\dot{X}$) results from non-linear time domain analysis.

For axial velocity $\dot{X}$, see table 38 – the standard deviation from a separately calculated response spectrum is 1.573 m/s which is bracketed by the values from the simulations, 1.545-1.600. The average from the simulations is 1.563 m/s. The zero up-crossing period from the response spectrum is 1/0.0829=12.06 s which is close to the average from the simulations, 12.08 s. The expected mini-

mum and maximum value is ± 6.04 m/s based on a Gaussian assumption. The average of the Gumbel minimum and maximum values from the time series are -6.50 m/s and +6.48 m/s respectively. For a Gaussian response, the skewness and kurtosis should be 0 and 3 respectively. The simulations supports the view that the axial velocity is a Gaussian response, which it should be since the velocity is the time derivative of the axial motion, which is linearly obtained from the Gaussian waves through the vessel RAOs.

Case	Vessel angle θ'_y (°)					Expected Gumbel extreme	
	Average	Std.	Skew.	Kurt.	Tz (s)	Minimum	Maximum
lw-32700405	0.00	2.899	0.00	3.28	13.23	-12.77	12.72
lw-32700415	0.00	2.957	0.00	3.06	13.21	-11.66	11.88
lw-32700425	0.00	2.851	0.00	2.89	13.24	-10.41	11.01
lw-32700435	0.00	2.838	0.00	2.83	13.16	-10.42	10.55
lw-32700445	0.00	2.892	0.00	3.21	13.18	-13.17	13.29
lw-32700455	0.00	2.889	0.00	3.00	13.24	-11.48	11.86
lw-32700465	0.00	2.999	0.00	3.14	13.37	-12.82	13.56
lw-32700475	0.00	2.886	0.00	2.98	13.16	-11.91	12.25
lw-32700485	0.00	2.909	0.00	2.94	13.29	-10.77	10.45
lw-32700495	0.00	2.865	0.00	3.20	13.12	-12.26	12.77

Table 39: Vessel angle θ'_y (projection) results from non-linear time domain analysis.

For the vessel angle projection θ'_y, table 39 – the standard deviation and the zero up-crossing period from a separately calculated response spectrum is 2.906° and 1/0.0758=13.19 s which are both bracketed by the results in table 39, the average standard deviation is 2.898° from the table. The expected minimum and maximum value of θ'_y is ± 11.092° based on a Gaussian assumption. The average of the Gumbel minimum and maximum values from the time series are -11.77° m/s and +12.03° respectively. Again, the time series results seem to confirm that this vessel inclination angle projection is a Gaussian response, which it should be since it is obtained from a linear transformation of the assumed Gaussian waves through the vessel motion transfer function, the vessel RAO.

The bend stiffener angle projection θ_y found in table 40 have an average standard deviation equal to 3.054° which is slightly larger (5%) than the average for the vessel angle projection θ'_y, 2.898°. The average zero up-crossing period for θ_y and θ'_y are 13.59 s and 13.22 s respectively. The average skewness value is -0.14, which means that values less than the average are, in a sense, more likely to occur. The kurtosis value is 3.3 on average. This indicates a non-linear response. Hence, it is expected to see extremes comparatively larger than those associated with a Gaussian assumption. The Gaussian extreme would be ±3.81 standard deviations from the average. The average of the ten Gumbel maximums is +12.11° which is 3.99 standard deviations from the average. The average Gumbel minimum is -14.26° which is 4.65 standard deviations from the

Case	Bend stiffener angle θ_y (°)					Expected Gumbel extreme	
	Average	Std.	Skew.	Kurt.	Tz (s)	Minimum	Maximum
lw-32700405	-0.07	3.054	-0.17	3.68	13.62	-15.94	13.43
lw-32700415	-0.08	3.126	-0.15	3.34	13.57	-14.35	12.00
lw-32700425	-0.07	2.988	-0.12	3.09	13.66	-12.49	11.59
lw-32700435	-0.07	2.968	-0.11	3.03	13.44	-12.16	10.33
lw-32700445	-0.07	3.047	-0.17	3.52	13.61	-16.08	13.08
lw-32700455	-0.07	3.042	-0.13	3.18	13.71	-13.70	11.40
lw-32700465	-0.08	3.192	-0.16	3.43	13.66	-16.14	14.00
lw-32700475	-0.07	3.041	-0.13	3.20	13.46	-14.20	12.14
lw-32700485	-0.07	3.067	-0.12	3.12	13.64	-12.24	10.71
lw-32700495	-0.07	3.017	-0.16	3.59	13.51	-15.33	12.42

Table 40: Bend stiffener angle θ_y (projection) results from non-linear time domain analysis.

average.

The difference between θ_y and θ'_y is that the umbilical moves in the calculation of θ_y. The 5% angle increase and the induced non-linearity is caused by the combined effect of the moving vessel and the wave action on the umbilical.

Case	Utilization, $g = g(T,C) = T/T_0 + \lvert C\rvert/C_0$ (-)					Expected Gumbel extreme	
	Average	Std.	Skew.	Kurt.	Tz (s)	Minimum	Maximum
lw-32700405	0.313	0.0695	1.22	5.56	10.27	0.112	0.798
lw-32700415	0.315	0.0703	1.10	4.77	10.27	0.104	0.751
lw-32700425	0.313	0.0667	0.99	4.46	10.11	0.101	0.689
lw-32700435	0.312	0.0657	0.94	4.32	10.06	0.117	0.696
lw-32700445	0.313	0.0689	1.17	5.59	10.14	0.082	0.836
lw-32700455	0.313	0.0684	1.03	4.45	10.25	0.105	0.745
lw-32700465	0.317	0.0716	1.13	5.04	10.23	0.104	0.797
lw-32700475	0.313	0.0681	1.03	4.59	10.15	0.105	0.764
lw-32700485	0.314	0.0681	1.01	4.47	10.19	0.110	0.717
lw-32700495	0.312	0.0683	1.19	5.55	10.05	0.099	0.768

Table 41: Umbilical utilization, $g(T,C) = T/T_0 + \lvert C\rvert/C_0$ results from non-linear time domain analysis.

Table 41 show a highly non-linear result, $g = g(T,C)$. This is the umbilical utilization norm, $g = g(T,C) = T/T_0 + |C|/C_0$. The simultaneous combination of tension T and absolute curvature $|C|$ is acceptable from a structural point of view if $g(T,C) \leq 1$. The parameters T_0 and C_0 are parameters of a linear segment of the capacity curve. Note that a capacity curve may consist of several such piecewise linear segments that all must be checked. Here, the critical linear

segment have been determined by inspection.

The g-results given in table 41 show that the distribution is highly positively skewed and feature large kurtosis. This is always the case due to the absolute curvature value in the equation. The average expected extreme value is g=0.756 based on the Gumbel extreme value results. Note that the average of the observed ten sample maximum values have been calculated to g=0.734, the sample standard deviation is 0.05. The observed ten maximum values from the ten 3 hour + 140 s long simulations are between 0.673 and 0.850.

Case	Sag tension, T_{sag} (kN)					Expected Gumbel extreme	
	Average	Std.	Skew.	Kurt.	Tz (s)	Minimum	Maximum
lw-32700405	45.9	11.58	0.11	6.50	11.08	-25.3	118.4
lw-32700415	45.9	11.79	0.13	6.13	11.27	-31.2	118.6
lw-32700425	45.9	11.28	0.09	5.86	11.21	-26.4	127.5
lw-32700435	45.9	11.16	0.10	5.32	11.25	-19.4	115.0
lw-32700445	45.9	11.68	0.14	7.58	11.22	-38.6	136.9
lw-32700455	45.9	11.51	0.16	6.27	11.13	-25.9	128.8
lw-32700465	45.9	12.00	0.15	6.62	11.28	-28.6	133.5
lw-32700475	45.9	11.30	0.09	6.02	11.25	-28.2	127.0
lw-32700485	45.9	11.43	0.11	6.02	11.27	-24.3	125.4
lw-32700495	45.9	11.36	0.07	6.89	11.20	-29.7	125.1

Table 42: Sag tension results from non-linear analysis.

The sag tension is also highly non-linear as shown in table 42. The skewness is close to zero as expected for a Gaussian signal. However, the value of the kurtosis (on the average 6.3) is significantly higher than the Gaussian value of 3.0. As expected, this shows in the Gumbel maximum and minimum values. The average of the Gumbel minimum and maximum values is calculated to -27.8 and 125.6 kN respectively. These values deviates from the average value with -6.4 and 6.9 times the standard deviation.

The average Gumbel minimum value of -27.8 kN for 3 hours is bracketed by the range of the realized minimum values, from -32.3 to -8.8 kN for the 10940 s long simulations. The average of the ten observed sample minimum values is -22.0 kN with a sample standard deviation equal to 6.7 kN.

Likewise, the average Gumbel maximum value of 125.6 kN for 3 hours is bracketed by the range of the maximum values from the 10940 s long simulations, from 103.7 to 151.1 kN. The average of the ten observed sample maximum values is +118.1 kN, the sample standard deviation is 12.0 kN.

15.2 On the extreme value estimation method, Gumbel

The Gumbel estimates for maximum (or minimum) extreme values are based on so called interval maxima (or minima). For each analysis case, the full time

series length of 11000 seconds, except the initial 60 seconds, is divided into 20 equal length intervals. For each of these intervals, the occurring maximum (or minimum) values are identified. Hence, 20 sample points associated with an interval length of (11000-60)/20=547 seconds is used to estimate the Gumbel extreme value for 3 hours, 10 800 seconds.

The Gumbel estimate is prepared using the method of maximum likelihood, see Bury (1999) [8] pp. 272. Once the Gumbel location and scale parameters μ and σ respectively have been determined. The following *cdf* equation is used to determine the 3 hour maximum value, Bury (1975) [7] pp. 376:

$$F(x) = \exp\left[-\exp(-\frac{x-(\mu+\sigma\ln(n)}{\sigma})\right] \tag{55}$$

Here n is the number of intervals in 3 hours, n=10800/547=19.744 intervals. This stems from the fact that the extreme values from an initial Gumbel distribution are also Gumbel distributed. Again the left hand value, the non-exceedance probability is taken from table 14 for consistency, here α=0.5704.

Figure 42 illustrates the sample analysis results for the umbilical utilization norm $g = g(T,C) = T/T_0 + |C|/C_0$ for the simulation labeled *lw-32700405*. The underlying time series of g feature a skewness value of 1.22 and a kurtosis value equal to 5.56. The Gumbel analysis tells the expected 3 hour extreme value, g_e=0.786.

Figure 43 presents the empirical level up-crossing frequencies of $g(t)$ from the ten realizations. Also indicated in this figure is the average g-value determined by the Gumbel method. The results seem to compare well as is expected.

Figure 44 provides a graphical way of presenting the statistical 3 hour extremes for load case *lw-32700405*. This figure show that the statistical boundary summarizes the statistical extremes for the bend stiffener tension T_{bs} and also the g-parameter, see tables 37 and 41. Also included in the figure is the corresponding statistical extreme for the maximum curvature in the bend stiffener. Note that this curvature result is not reported elsewhere. The statistical boundary is obtained by the method described by Ottesen and Aarstein (2006) [23].

Figure 45 show the empirical up-crossing frequencies from the ten realizations considering the sag tension. Included in this figure is analytical curves associated with up-crossing frequencies for a linear or quadratic load based on Gaussian input. These analytical results brackets the obtained simulation results. The Gumbel extreme values are also included. Again, the results seem to compare well as is expected.

15.3 Investigating the relation between top axial velocity and sag tension

The scope of this section is to investigate the relation between the top axial velocity and the sag tension. As described by Passano and Larsen (2006) [22] – the time instants for maxima (or minima) of top axial velocity are close to

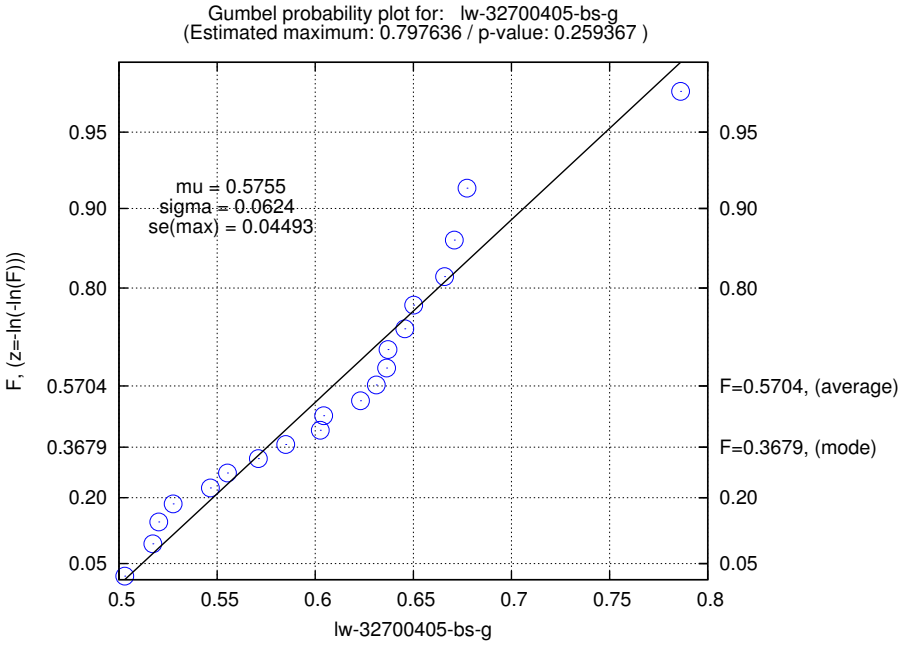

Figure 42: Gumbel probability plot for $g(T, C)$, simulation: *lw-32700405*.

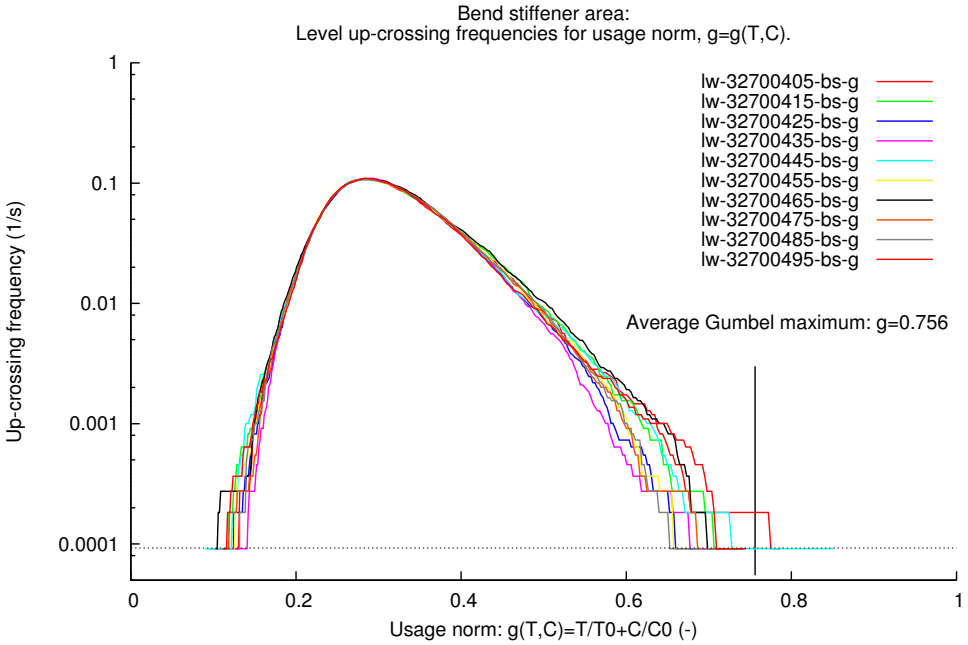

Figure 43: Level up-crossing frequencies for $g(T, C)$, ten realizations.

the time instants for maxima (or minima) of tension in the lower part of the configuration. Their focus was on a catenary configurations and the situation near the seabed mainly. Here, the tension in the sag bend of a lazy wave configuration is investigated.

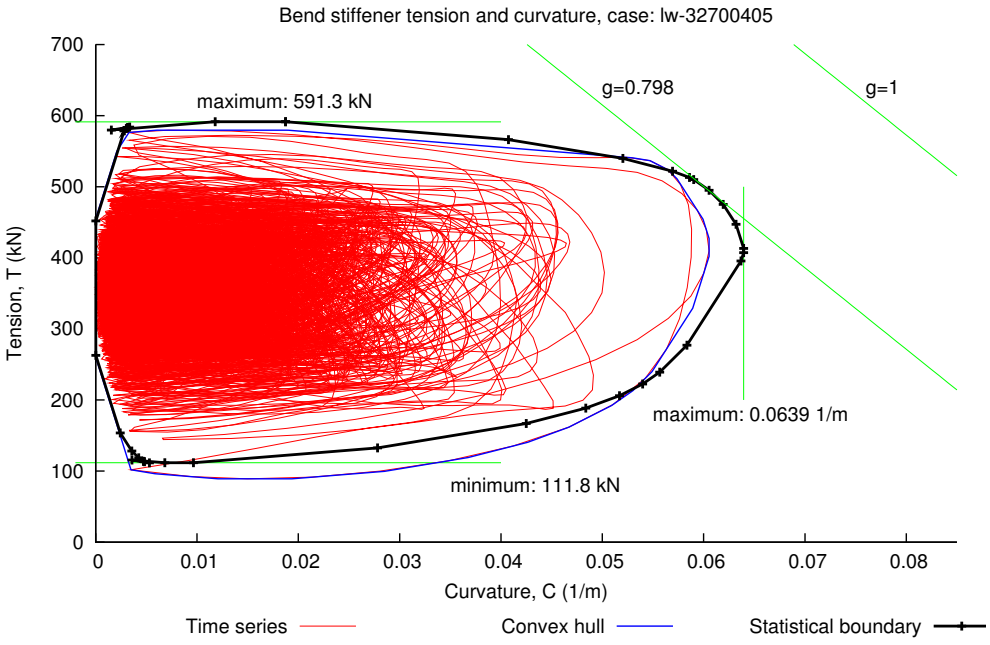

Figure 44: Statistical boundary polygon describing critical tension and curvature combinations for load case *lw-32700405*.

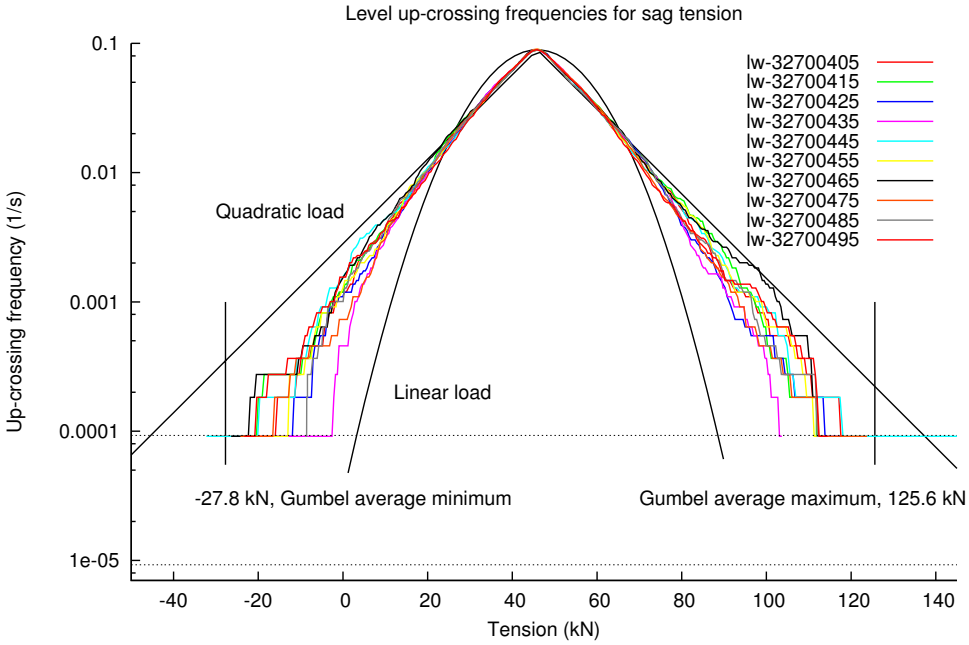

Figure 45: Level up-crossing frequencies for sag tension, ten realizations including analytical results for a linear or quadratic load, $L(\zeta) = A\zeta$ or $Q(\zeta) = B|\zeta|\zeta$, associated with Gaussian input ζ.

Figure 46 demonstrates clearly that there is a quite strong and monotonic trend between the top axial velocity and the sag tension. However, as indicated by the scatter around the central values in particular, this is not a perfect monotonic relation. It is the strength of this relationship that is studied here.

The selected basic tool in this evaluation is the rank order of maxima (or minima), according to the idea presented by Passano (1994) pp. 17 [24]. Hence, we are not interested in the response values as such. Our interest is in the relative size of the response values – if the largest of the velocity maxima is correlated with the largest of the tension maxima or if the second largest is associated with the second largest maxima and so on. The following three questions are attempted answered:

- How good is the correlation between the axial velocity and the sag tension?
- When do the tension maxima (or minima) occur relative to the axial velocity maxima (or minima)?
- How many of the n largest velocity maxima are associated with the n largest tension maxima? Is this a constant fraction, and is it possibly time dependent?

The ranks are assigned as follows considering either maxima- or minima-values: Rank 1 is assigned to the value that deviates most from the average, rank 2 is assigned to the value that deviates second most and so on. There would be perfect correlation between the axial velocity and the sag tension if corresponding ranks where similar and clustered on the line $y = x$, rank($\dot{X}$)=rank(F_x). However, the term *corresponding* must be defined, this means that for each maximum of axial velocity occurring at time t_i, a time window around this instant $-T_z/4+t_i \leq t \leq T_z/2+t_i$, is searched for the largest sag tension maxima. The procedure is similar for the axial velocity minima, except that the time window is then searched for the smallest tension minima.

15.3.1 Using all maxima and minima in the time series

Figure 47 illustrates the corresponding maxima ranks for axial acceleration $\ddot{X}$ versus sag tension F_x when all the maximas of acceleration and sag tension are considered. All figures referred to, contain the information from in excess of 30 hours of non-linear time domain simulations unless otherwise stated. Figure 47 demonstrates that a large acceleration value is a very poor indicator of a large sag tension value. Figure 48 show that the associated tension peak occurs about 3 seconds after the acceleration peak value for the largest accelerations and tensions. The findings are similar for the minimas regarding axial acceleration and sag tension. Hence, we abandon the acceleration and consider instead the integrated value of the axial acceleration, the axial velocity $\dot{X}$.

Figures 49 and 50 demonstrates that the axial velocity maxima are much better suited to predict the time instances of large sag tension maximas. Figure 51

show that the extreme tension value comes come just before the extreme axial velocity value, about 0.5 second.

The results for the axial velocity minima and the correspond sag tension minima are similar. Again, the extreme tension value come just before the extreme velocity value, see figures 52, 53 and 54.

However, as can be seen by comparing the results for the 30 largest maxima and minima values, see figures 50 and 53 – the rank correlation is less for the minima values than for the maxima values.

Now, if we study a list of associated rank pairs, example: [(1,2), (2,3) (3,4), (4,1), (5,9), ...] – where each pair (r_x, r_y) is made by the rank values of associated X and Y maxima (or minima), so that $(r_x, r_y) = (\text{rank}(X), \text{rank}(Y))$. Then we may for the n first pairs study the count of r_y-values that are maximum n. Given many such lists we may speculate if the fraction P=count/n is a constant on the average for any given n? If so, this may be a probability. It is conjectured that this fraction is a proper probability. Example: Choosing n=5 in the above example list give a count of 4, since 4 of the 5 first r_y-values satisfy $r_y \leq n$. Hence, the probability is claimed to be, Prob=4/5=0.8.

Figures 55 and 56 illustrates this probability for maximas and minimas respectively. If we select n=10, the maxima data on figure 55 suggest that we can expect to observe minimum 0.9×10=9 of the 10 largest sag tension maximas, for n=100 we should expect to observe minimum 90 of the 100 largest. For the minima, see figure 56 – if we select n=10, the minima data suggest that we can expect to observe minimum 0.8×10=8 of the 10 most extreme sag tension minima. For n=100, on the average we can expect to observe about 90 of the most extreme sag tension minima.

Tables 43 and 44 give some sample data for one of the one of the ten realizations. These tables provides further demonstration of the ranking procedure and the method used to calculated the mentioned probability. An interesting finding in these tables is that the extreme maxima and minima values appears to be clustered. In a small time window with length about 3 wave periods starting at about 7600 seconds we find not only the maximas ranked number 1, 2 and 7 but also the minimas ranked 1 and 2, see figure 57 for the time series around time 7600 seconds. Other parts of the realized time series have been inspected, it appears as if the extremes are indeed clustered as shown on the figure 57. It is mentioned that the more narrow the response spectrum is, the greater group length is expected (number of consecutive high responses). It is also mentioned that the method used to generate the wave time series from a wave spectrum may affect the group length. As discussed by Tucker el al (1984) [27], for a finite number of Fourier amplitudes the statistics of wave groups and the wave group length is affected by the wave generation method. In these simulations, the fast Fourier transform is used, see the Riflex manual (2008) [14]. A finite number of deterministic amplitudes and random phase angles are used, the number of frequencies is 4520 where 564 associated amplitudes have zero value.

The effect of such clustering can be reduced if studying interval maxima instead. The interval should then be long compared to the characteristic wave

period. Such interval extremes are then convenient sample data for extreme value estimation using the Gumbel distribution, Bury (1975) [7].

15.3.2 Using only interval maxima and minima

For each realization the entire time series, 11000-60=10940 seconds, is divided into n intervals, where n-values of 5, 10, 20, 40 and 80 have been considered. The interval length is therefore from 137 to 2189 seconds.

For each interval,the interval extreme of the axial velocity, $\dot{X}$ is established. This is done for both maxima and minima. The associated maxima (or minima) for the sag tension is then searched for in a small time window with length $3/4 \cdot Tz$ around the time instant of the velocity extreme, similar as described in the previous section.

The following information is then established: 1) The rank correlations from these interval pairs of associated velocity and sag tension; 2) The fraction of these sag tension extremes that also are interval extremes, this is conjectured to be a probability. Example: We use 10 intervals and have determined the ten time instants for the axial velocity maxima. Next, we record the time of the ten associated sag tension maximas which occurs almost at the same time as the velocity maximas. Separately,we determine the time instants for the 10 interval extremes of sag tension. We then count how many of the sag tension maximas that occurs at the same time, the count divided by the number of intervals is then the probability.

Figure 58 show the rank correlation between the axial velocity maxima and the associated sag tension maxima when dividing the time series into 20 intervals. Figure 58 show the same for 80 intervals. Based on the figures, the correlation appears to be good. The probability (fraction) of the associated sag tension maximas that are also the correct interval sag tension maximas is on the average about 0.93 according to table 45. The probability appears to be independent on the length of the intervals.

The rank correlation between the sag tension minima and the axial velocity minima is shown in figures 60 and 61 for number of intervals equal to 20 and 80 respectively. Also, here the correlation is good – but perhaps slightly less than for the maxima. The probability (fraction) of the associated sag tension minimas that are also the correct interval sag tension minimas is on the average about 0.88 according to table 46. Again, this probability is independent of the interval length.

Finally, the rank order correlation – Spearman's rho has been calculated for the interval results, see table 47 for the maxima and table 48 for the minima.

15.3.3 Summary

The axial velocity maxima (or minima) comes about 0.5 second after the corresponding sag tension maxima (or minima) for extreme values. There appear

to be good rank correlation between both maxima values and minima values. The rank correlation seem to be slightly better for maxima values.

The time series show tendency of grouping of large responses. For this reason the ranking of interval maxima and minima was also studied. The number of intervals in the time series was between 5 and 80. Again, the rank correlation seem to be slightly better for the maxima than for the minima.

The interval results was used to investigate the P_{success} as described in the section dealing with Spearman's rho, 11. A basic assumption of that section seem to be confirmed since the probability P_{success} for identifying a critical time window appears time independent. For the interval maxima $P_{\text{success}} = 0.93$ while $P_{\text{success}} = 0.88$ for the interval minima. The observed rank correlation values was also reported for the interval cases studied.

rank($\dot{X}$) (-)	rank(F_x) (-)	Prob. (-)	$\dot{X}$ (m/s)	F_x (kN	time($\dot{X}$) (s)	time(F_x) (s)	Δt (s)
1	2	0.000	5.85	117.20	7612.75	7612.75	0.00
2	1	1.000	5.85	118.32	7626.00	7625.75	-0.25
3	4	0.667	5.44	109.43	1099.00	1098.75	-0.25
4	3	1.000	5.43	110.54	8846.00	8845.75	-0.25
5	5	1.000	5.37	108.25	7722.50	7722.50	0.00
6	6	1.000	5.25	105.63	8215.00	8214.75	-0.25
7	7	1.000	5.00	100.57	7600.50	7600.25	-0.25
8	9	0.875	5.00	99.68	5205.00	5204.75	-0.25
9	8	1.000	4.95	100.43	5148.25	5148.00	-0.25
10	11	0.900	4.85	97.47	5705.75	5705.75	0.00
20	20	0.950	4.36	88.91	6264.25	6264.00	-0.25
30	27	0.967	4.14	86.97	10761.50	10761.00	-0.50
40	41	0.950	3.95	82.35	2110.75	2110.50	-0.25
50	49	0.940	3.84	81.34	1135.75	1135.25	-0.50
60	61	0.933	3.73	79.36	7853.25	7853.00	-0.25
70	81	0.943	3.61	76.92	7814.75	7814.25	-0.50
80	76	0.963	3.55	77.52	841.25	841.00	-0.25
90	93	0.967	3.40	74.66	6541.75	6541.50	-0.25
100	90	0.950	3.31	75.12	1048.50	1048.25	-0.25
200	227	0.960	2.70	64.34	9109.75	9109.00	-0.75
300	308	0.960	2.31	61.55	1436.00	1435.50	-0.50

Table 43: Associated maxima of axial velocity and sag tension, some sample data from case *lw-32700405*.

rank($\dot{X}$) (-)	rank(F_x) (-)	Prob. (-)	$\dot{X}$ (m/s)	F_x (kN	time($\dot{X}$) (s)	time(F_x) (s)	Δt (s)
1	1	1.000	-6.60	-30.93	7606.50	7606.00	-0.50
2	2	1.000	-5.82	-15.55	7619.50	7619.00	-0.50
3	3	1.000	-5.40	-10.96	6757.75	6757.25	-0.50
4	5	0.750	-5.30	-7.70	5198.50	5197.75	-0.75
5	4	1.000	-5.20	-10.16	4729.75	4729.25	-0.50
6	8	0.833	-5.07	-3.56	7716.25	7715.75	-0.50
7	7	0.857	-5.00	-4.45	2272.25	2271.75	-0.50
8	6	1.000	-4.99	-4.49	8840.50	8840.00	-0.50
9	10	0.889	-4.93	-1.95	5142.50	5142.00	-0.50
10	9	1.000	-4.83	-3.42	8813.75	8813.25	-0.50
20	15	0.950	-4.38	1.38	6689.50	6689.00	-0.50
30	25	0.967	-4.16	4.69	9816.75	9816.25	-0.50
40	37	0.950	-3.94	9.78	8378.00	8377.25	-0.75
50	51	0.880	-3.81	12.01	4518.00	4517.50	-0.50
60	57	0.950	-3.71	12.49	4949.00	4948.50	-0.50
70	66	0.900	-3.54	14.32	4629.75	4629.25	-0.50
80	63	0.963	-3.48	13.41	66.00	65.50	-0.50
90	93	0.956	-3.36	18.34	2742.25	2741.50	-0.75
100	111	0.930	-3.25	20.13	6493.50	6493.25	-0.25
200	182	0.950	-2.75	24.42	10996.50	10995.75	-0.75
300	269	0.950	-2.32	28.16	7240.75	7240.00	-0.75

Table 44: Associated minima of axial velocity and sag tension, some sample data from case *lw-32700405*.

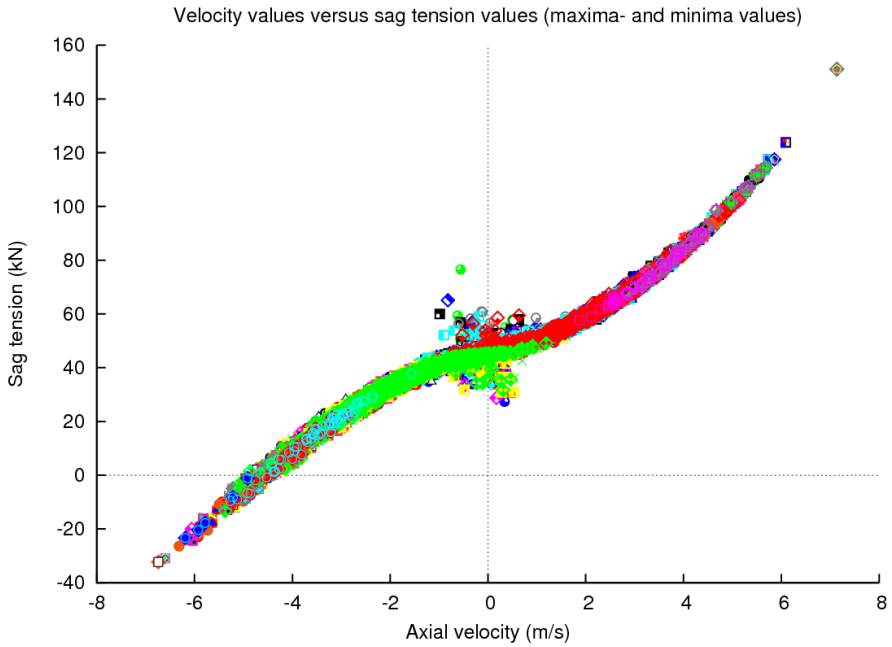

Figure 46: Velocity in static axial direction versus associated values of sag tension maxima and minima.

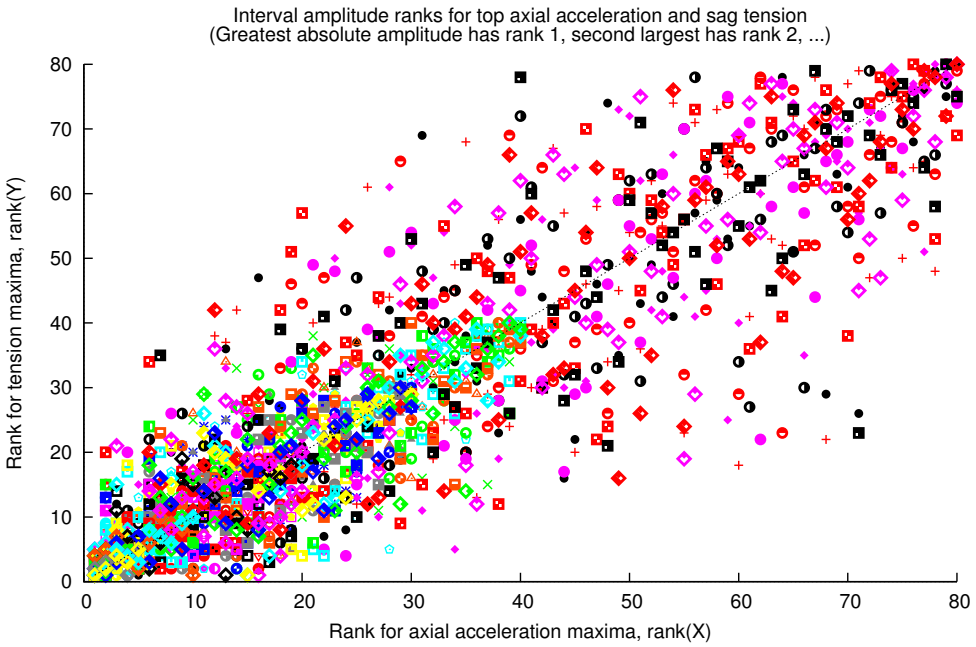

Figure 47: Rank of axial acceleration maxima versus rank of sag tension maxima.

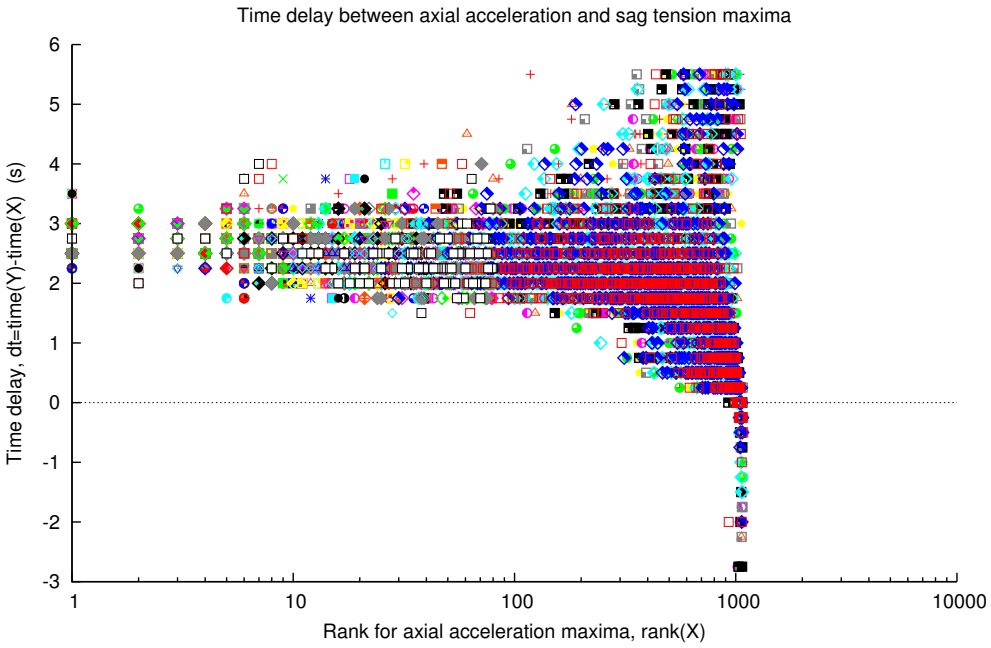

Figure 48: Time delay between axial acceleration maxima and sag tension maxima.

$r_y \leq n$.

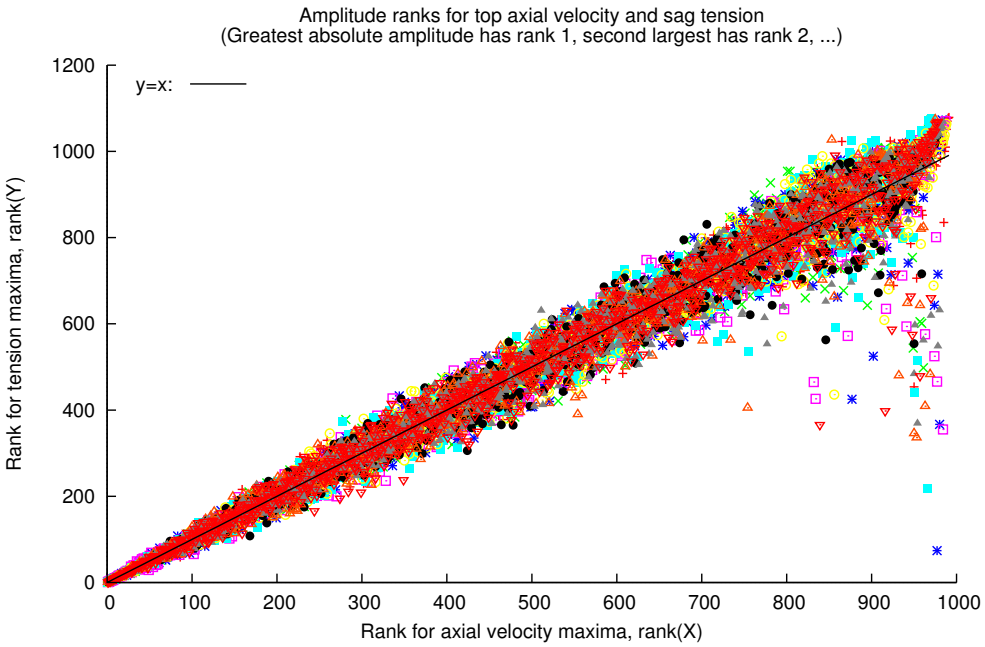

Figure 49: Rank of axial velocity maxima versus rank of sag tension maxima, all velocity maxima.

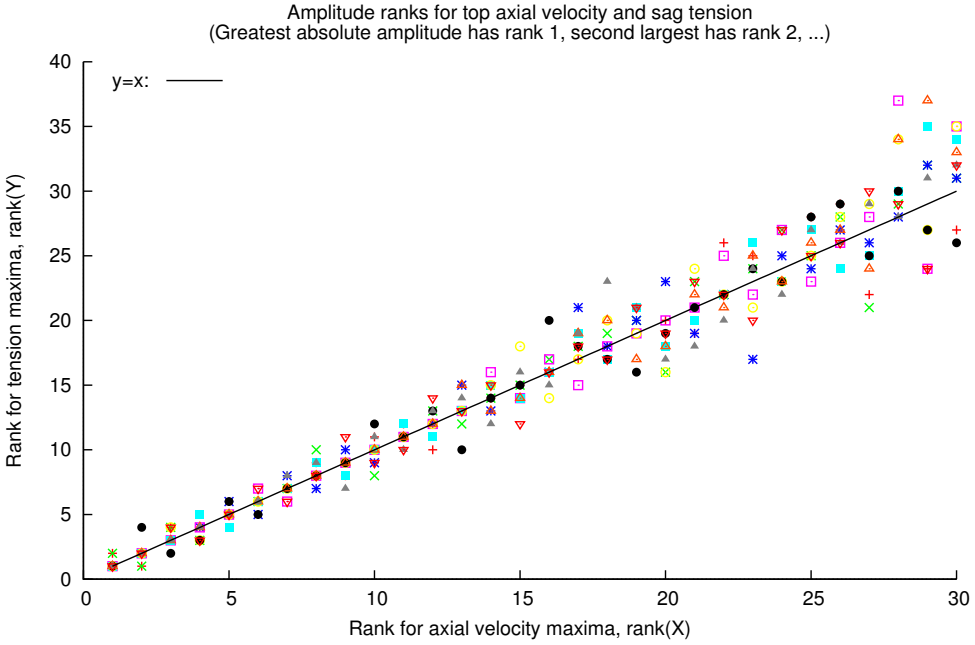

Figure 50: Rank of axial velocity maxima versus rank of sag tension maxima, the 30 most extreme velocity maxima.

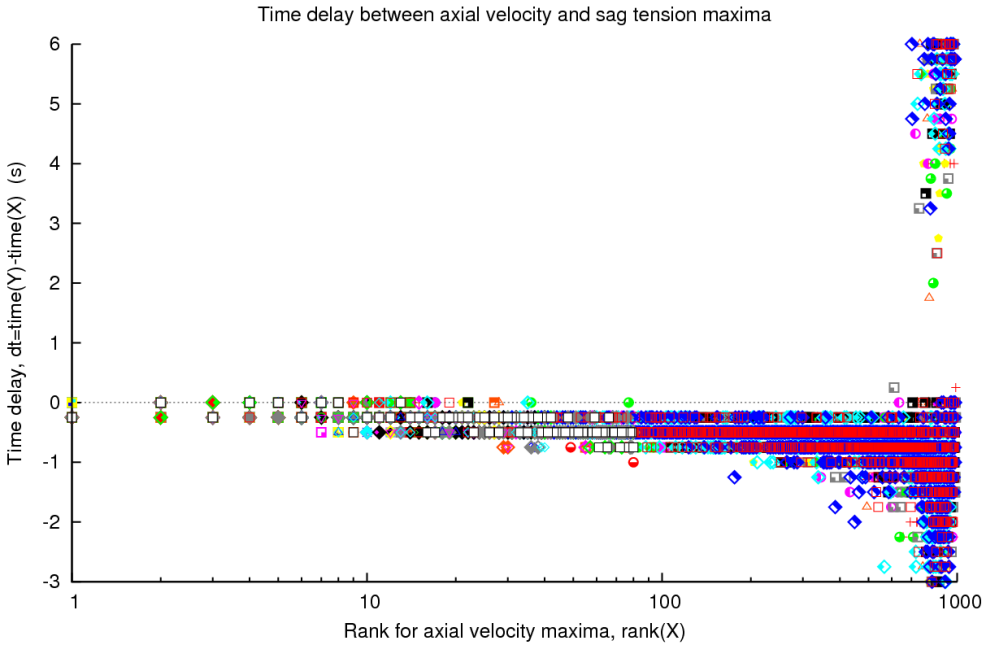

Figure 51: Time delay between axial velocity maxima and sag tension maxima.

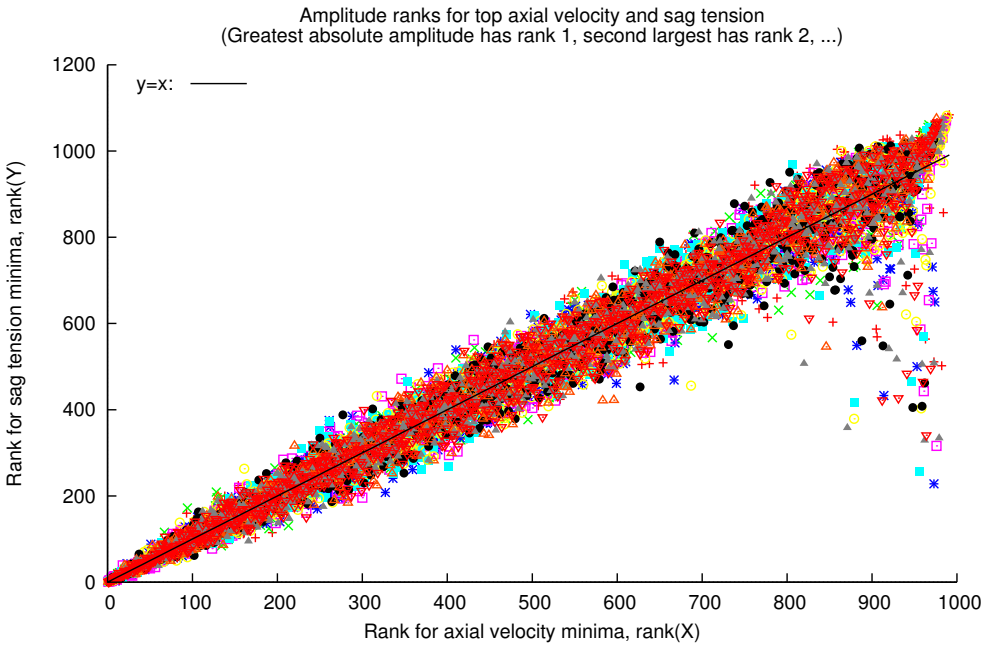

Figure 52: Rank of axial velocity minima versus rank of sag tension minima, all velocity minima.

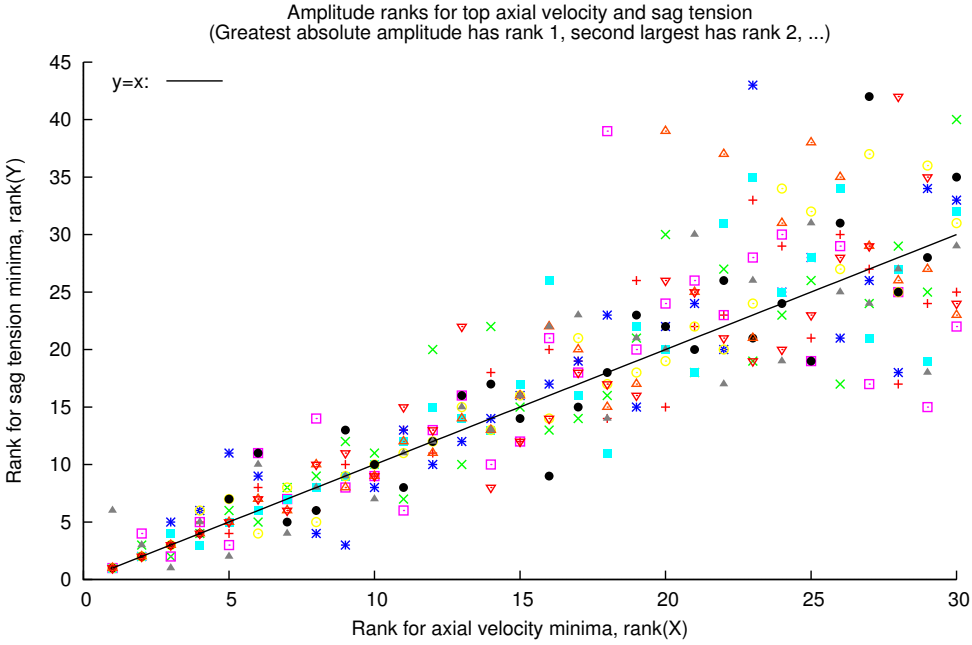

Figure 53: Rank of axial velocity minima versus rank of sag tension minima, the 30 most extreme velocity minima.

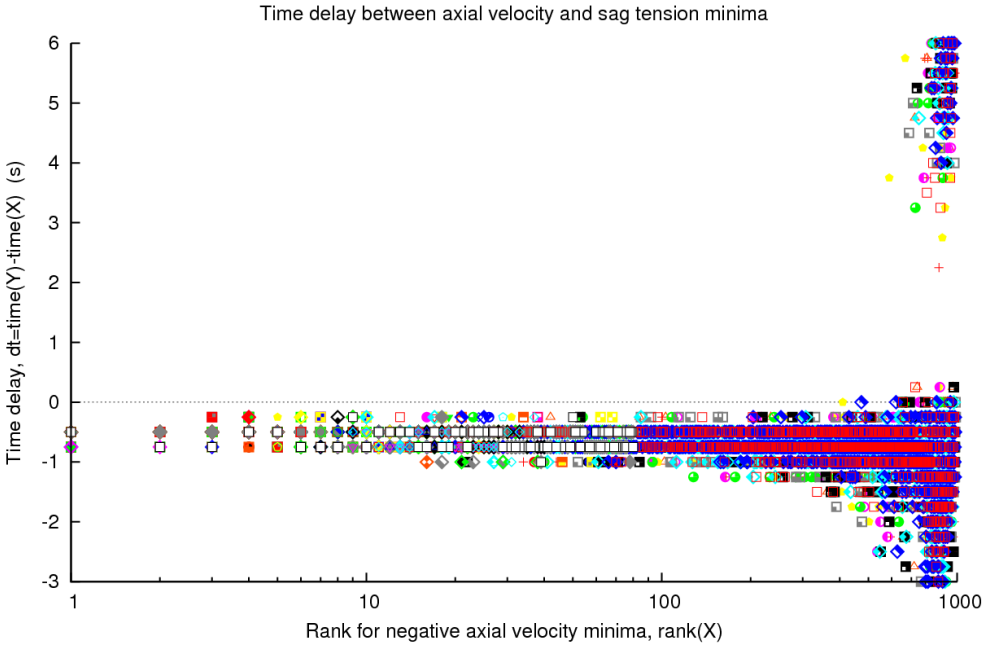

Figure 54: Time delay between axial velocity minima and sag tension minima.

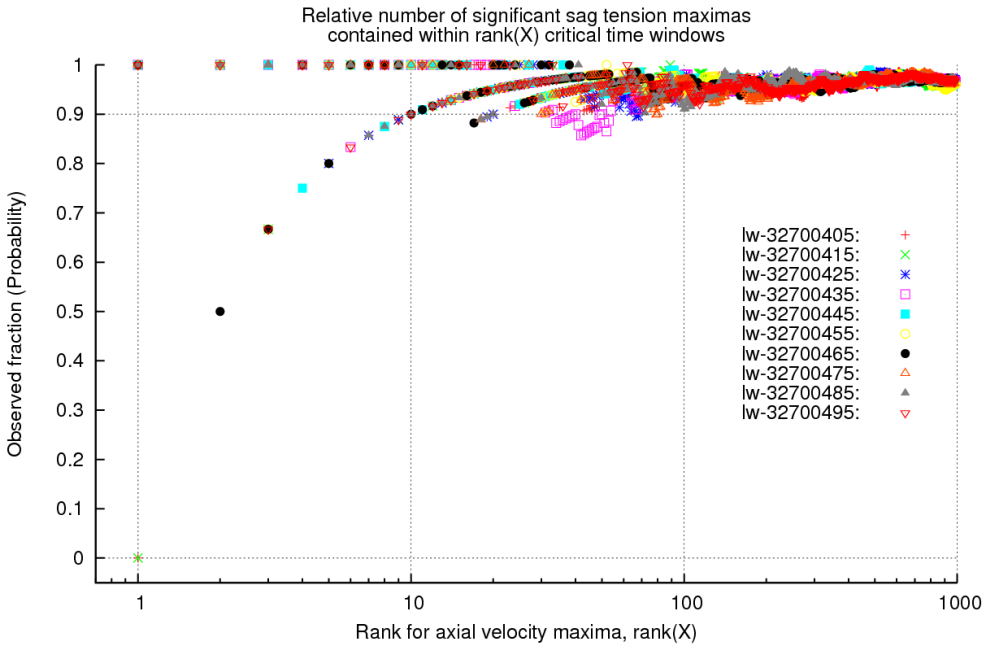

Figure 55: Fraction of pairs (r_x, r_y) satisfying $r_x \leq n$ and $r_y \leq n$ plotted against n on first axis. Plot is for axial velocity maxima and sag tension maxima.

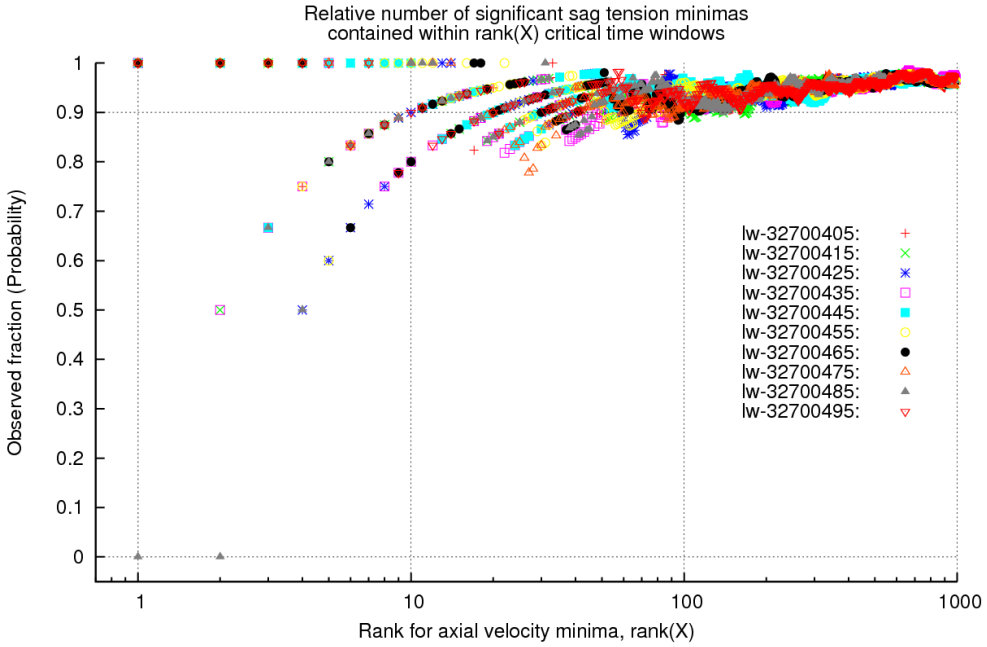

Figure 56: Fraction of pairs (r_x, r_y) satisfying $r_x \leq n$ and $r_y \leq n$ plotted against n on first axis. Plot is for axial velocity minima and sag tension minima.

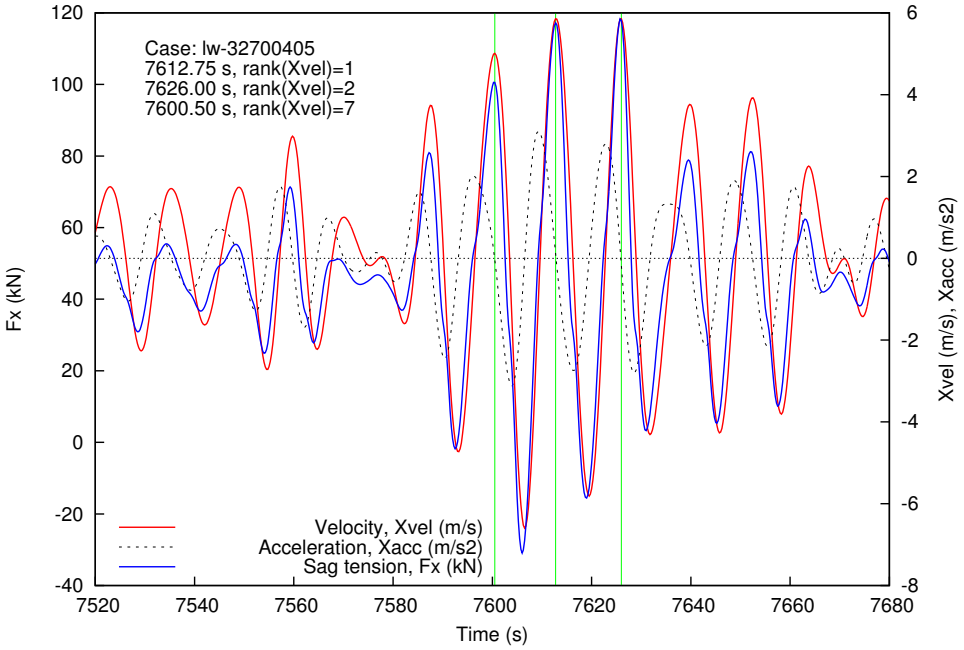

Figure 57: Group of large extremes in time series around time 7600 seconds, load case *lw-32700405*.

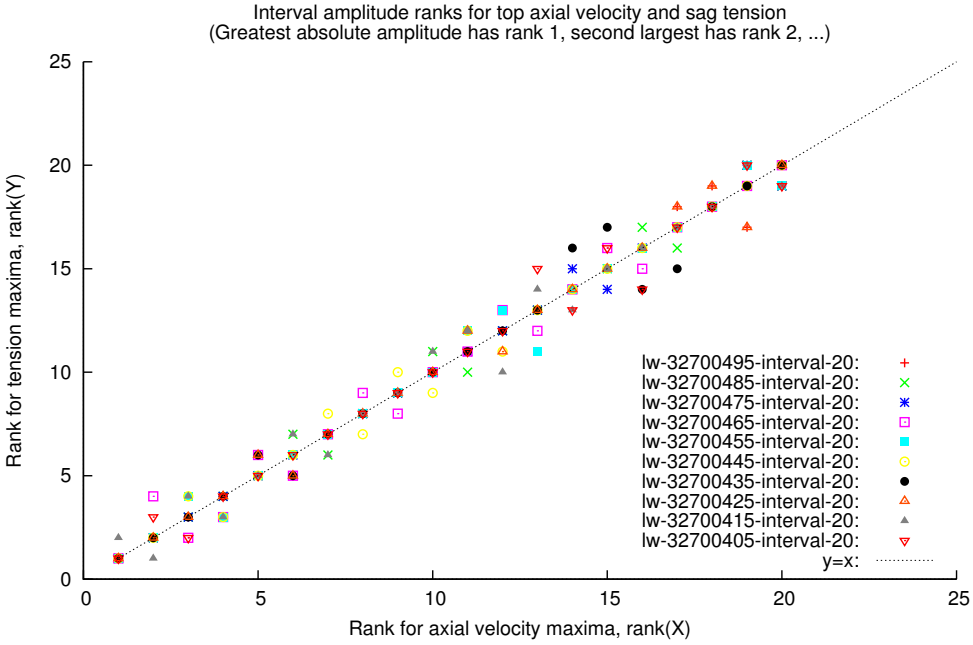

Figure 58: Rank of axial velocity maxima versus rank of sag tension maxima, 20 intervals.

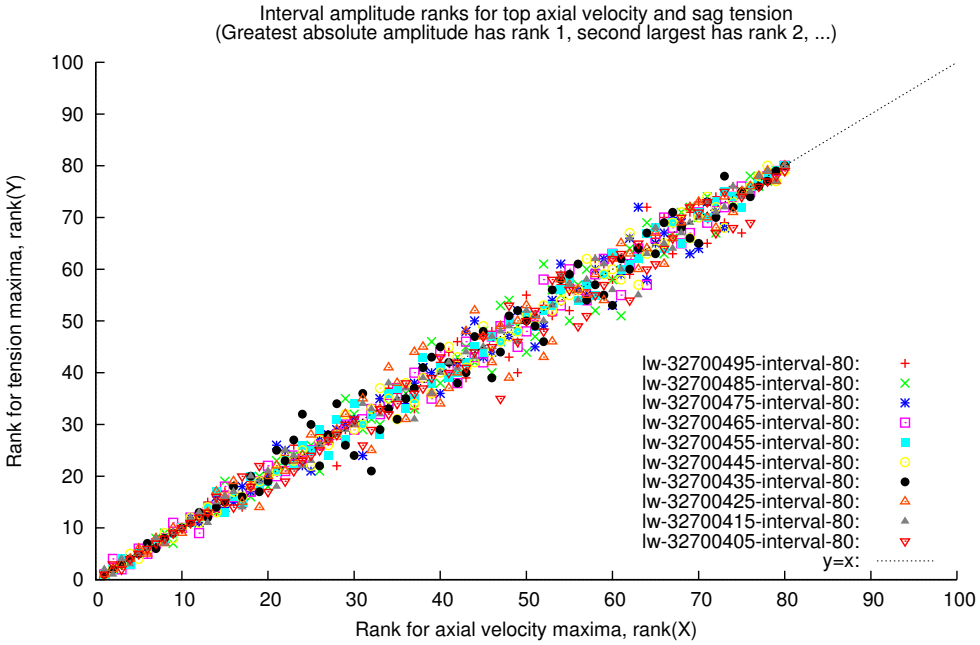

Figure 59: Rank of axial velocity maxima versus rank of sag tension maxima, 80 intervals.

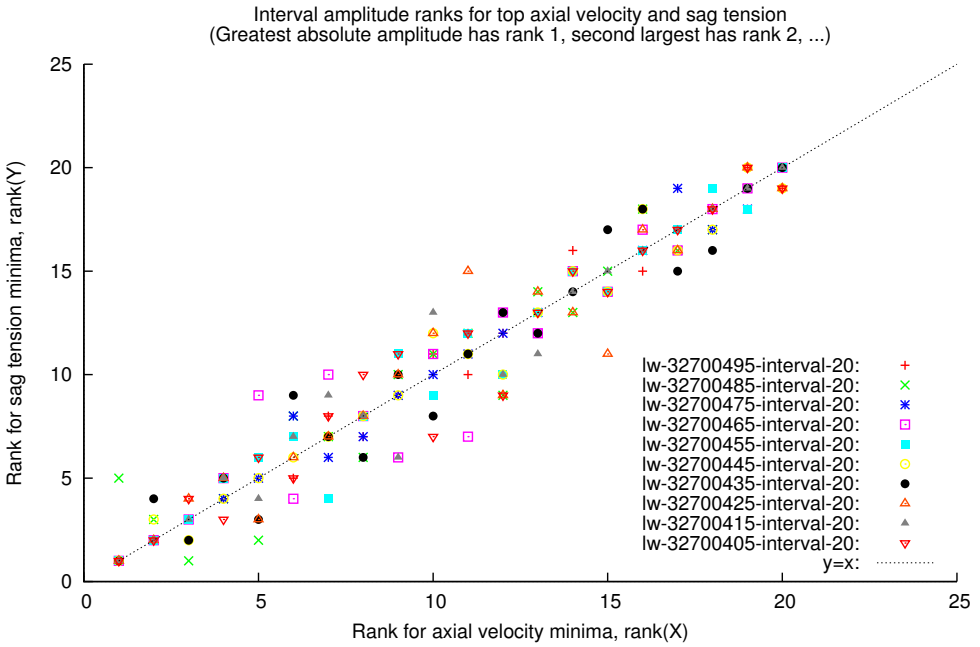

Figure 60: Rank of axial velocity minima versus rank of sag tension minima, 20 intervals.

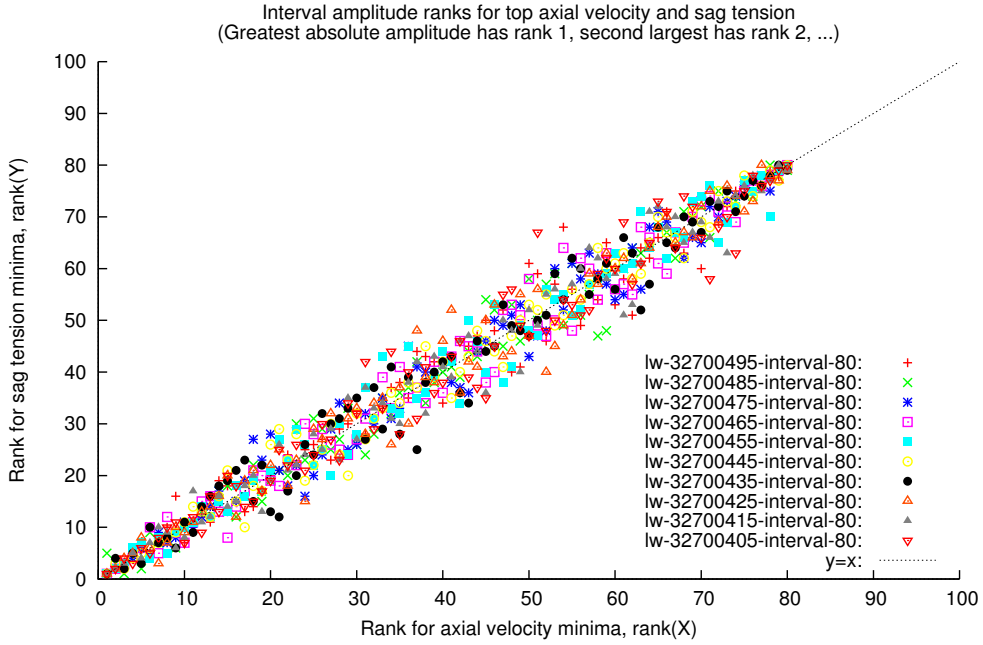

Figure 61: Rank of axial velocity minima versus rank of sag tension minima, 80 intervals.

	Number of intervals				
Simulation	5	10	20	40	80
lw-32700405	0.600	0.800	0.850	0.850	0.911
lw-32700415	1.000	1.000	1.000	1.000	0.975
lw-32700425	1.000	0.900	0.800	0.950	0.912
lw-32700435	1.000	0.800	0.900	0.850	0.875
lw-32700445	1.000	1.000	1.000	0.925	0.963
lw-32700455	0.800	0.900	0.950	0.950	0.938
lw-32700465	1.000	0.900	0.950	0.950	0.938
lw-32700475	1.000	1.000	1.000	0.950	0.938
lw-32700485	1.000	1.000	0.850	0.950	0.925
lw-32700495	0.800	0.800	0.900	0.925	0.887
Interval length (s)	2188.8	1094.0	547.0	273.5	136.8
Average, P	0.920	0.910	0.920	0.930	0.926

Table 45: Probability, P, for maxima identification, from interval results.

	Number of intervals				
Simulation	5	10	20	40	80
lw-32700405	0.800	0.800	0.900	0.875	0.863
lw-32700415	0.600	0.700	0.800	0.775	0.875
lw-32700425	0.600	0.800	0.950	0.925	0.912
lw-32700435	1.000	0.900	0.800	0.800	0.875
lw-32700445	1.000	0.900	0.900	0.925	0.863
lw-32700455	1.000	0.800	0.850	0.825	0.863
lw-32700465	0.800	0.900	0.900	0.850	0.925
lw-32700475	1.000	1.000	1.000	0.950	0.887
lw-32700485	1.000	1.000	1.000	0.925	0.887
lw-32700495	1.000	1.000	1.000	0.950	0.850
Interval length (s)	2188.8	1094.0	547.0	273.5	136.8
Average, P	0.880	0.880	0.910	0.880	0.880

Table 46: Probability, P, for minima identification, from interval results.

	Number of intervals				
Simulation	5	10	20	40	80
lw-32700405	0.900	0.976	0.989	0.991	0.992
lw-32700415	0.800	0.976	0.988	0.995	0.996
lw-32700425	1.000	1.000	0.992	0.987	0.990
lw-32700435	1.000	0.988	0.986	0.986	0.990
lw-32700445	0.900	0.988	0.994	0.998	0.996
lw-32700455	1.000	0.988	0.992	0.997	0.997
lw-32700465	1.000	0.976	0.989	0.997	0.996
lw-32700475	1.000	1.000	0.997	0.994	0.992
lw-32700485	1.000	0.988	0.994	0.990	0.991
lw-32700495	1.000	1.000	0.994	0.992	0.993
Interval length (s)	2188.8	1094.0	547.0	273.5	136.8
Minimum	0.800	0.976	0.986	0.986	0.990

Table 47: Rank order correlation for interval maxima, Spearman's rho.

	Number of intervals				
Simulation	5	10	20	40	80
lw-32700405	0.900	0.952	0.973	0.982	0.979
lw-32700415	0.900	0.964	0.974	0.988	0.987
lw-32700425	1.000	0.964	0.956	0.983	0.985
lw-32700435	0.900	0.903	0.965	0.982	0.985
lw-32700445	0.900	0.988	0.985	0.982	0.991
lw-32700455	1.000	0.976	0.980	0.991	0.986
lw-32700465	0.700	0.891	0.953	0.980	0.987
lw-32700475	1.000	1.000	0.989	0.986	0.987
lw-32700485	-0.500	0.758	0.956	0.980	0.987
lw-32700495	1.000	0.988	0.989	0.983	0.983
Interval length (s)	2188.8	1094.0	547.0	273.5	136.8
Minimum	-0.500	0.758	0.953	0.980	0.979

Table 48: Rank order correlation for interval minima, Spearman's rho.

16 Concluding remarks

Long term extremes have been calculated considering the entire wave scatter diagram based on the assumption of Gaussian response. It has been inspected which of the top end parameters that are better correlated with the umbilical response. Instead of the wave elevation – the top axial velocity is a better indicator for the most important sea states considering umbilical tension. Likewise, the vessel angle is a better indicator for the most important sea states considering umbilical top angle. This is as expected.

These long term 100-year extreme estimates are then compared to the results obtained from the 100-year contour curve sea states. The non-exceedance quantile α needed to realize the long term 100-year extreme by the contour curve approach has also been determined. It appears that $\alpha = 0.90$ is an adequate value, see table 33 from section 14.1. That table is reproduced here as table 49:

Wave direction	90°	270°	Note
Wave elevation, ζ (m)	0.842	0.842	See figure 33, same weather.
Axial motion, X (m)	0.022	0.893	See figures 34 and 35.
Axial velocity, $\dot{X}$ (m/s)	0.656	0.927	See figures 36 and 37.
Vessel angle, θ'_y (°)	0.904	0.904	See figure 38, symmetry.
Bend stiffener tension, T_{bs} (kN)		0.893	See figure 39.
Sag tension, T_{sag} (kN)		0.657	See figure 40.
Bend stiffener angle, θ_y (°)		0.801	See figure 41.

Table 49: Non-exceedance probability, α-value for 100-year contour curve results.

The investigation of a particular extreme sea state in section 15 gave the opportunity to exercise extreme value estimation and also to establish empirical level up-crossing frequencies and to compare these results with the obtained estimates from using the Gumbel approach, see section 15 and figures 42, 43, 44 and 45.

The overall finding from investigating the relation between the axial velocity and the sag tension in section 15.3 – is repeated from section 15.3.3:

The axial velocity maxima (or minima) comes about 0.5 second after the corresponding sag tension maxima (or minima) for extreme values. There appear to be good rank correlation between both maxima values and minima values. The rank correlation seem to be slightly better for maxima values.

The time series show tendency of grouping of large responses. For this reason the ranking of interval maxima and minima was also studied. The number of intervals in the time series was between 5 and 80. Again, the rank correlation seem to be slightly better for the maxima than for the minima.

The interval results was used to investigate the P_{success} as described in the section dealing with Spearman's rho, 11. For the interval maxima $P_{\text{success}} = 0.93$ while $P_{\text{success}} = 0.88$ for the interval minima. A basic assumption of that section

seem to be confirmed since the probability P_{success} for identifying a critical time window appears time independent. Hence, statistics on Spearman's rho may be suitable for on-line monitoring of an approximative method whose basic principle is identification of critical time windows.

17 Further work

A natural extension of the simplified method using the top end axial velocity as an indicator for interesting events near the seabed – is to investigate if the top end vessel angle can used in a similar manner regarding the bend stiffener angle and curvature at the top.

However, a more encompassing approach would be use of linearized time domain analysis to identify interesting time windows for further refined analysis.

A hypothesis test regarding Spearman's rho have been suggested. This is suitable for on-line monitoring of an approximative method that identifies critical time windows. Further development of this statistics is necessary in case of using interval extremes. This is discussed in section 11.5. The character of the parameter called P_{success} is somewhat unclear. It is uncertain if it is time independent as suggested by the data in this study.

References

[1] *A discussion of long term response versus mean maximum response of the selected design sea state*, volume OMAE2007-29552, 2007.

[2] *Estimating extreme response of drag dominated offshore structures from simulated time series of structural response*, volume OMAE2007-29119, 2007.

[3] Metocean data, Jubarte field development - phase 2. Technical specification I-ET-3010.72-1000-941-PPC-001, Petrobras, Cenpes, April 18. 2005.

[4] 578–580. Adapted from Zar, J. H. (1972). Significance testing of the Spearman rank correlation. Journal of the American Statistical Association. 67. Critical Values of the Spearman Rank Order Correlation Coefficients: The rs Tables. http://www.ace.upm.edu.my/ bas/5950/Spearman

[5] G.B Arfken and H.J. Weber. *Mathematical methods for physicists*. Academic press, 1995.

[6] Pål G. Bergan, Per Kr. Larsen, and Egil Mollestad. *Svingning av konstruksjoner*. Tapir, 1985 edition, November 1981.

[7] Karl V. Bury. *Statistical Models in Applied Science*. Number 0471125903. John Wiley & Sons, 1975.

[8] Karl V. Bury. *Statistical Distributions in Engineering.* Number 0521635063. Cambridge University Press, 1999.

[9] O.M. Faltinsen. *Sea loads on ships and offshore structures.* Cambridge University Press, 1990.

[10] ISOPE. *Extreme response estimation of flexible risers by use of long term statistics*, volume 2, 1992.

[11] Carl M. Larsen. TMR4180, Marin dynamikk, January 2007.

[12] B. Leira, T. Moan, S. Haver, and N. Spidsøe. TMR4235, Stochastic theory of sealoads, August 2005.

[13] Marintek. Riflex theory manual. Manual, Marintek, 2008.

[14] Marintek. Riflex user's manual. Technical report, Marintek, 2008.

[15] George E. Mase. *Continuum mechanics.* McGraw-Hill Inc., 1970.

[16] A. Naess and O. Gaidai. Monte carlo methods for estimating the extreme response of a dynamical system. *Journal of Engineering Mechanics*, pages 628–636, August 2008.

[17] A. Naess, O. Gaidai, and O. Batsevych. Extreme value statistics of combined load effect processes (preprint october 7. 2008). *Elsevier Science*, 2008.

[18] A. Naess, O. Gaidai, and S. Haver. Efficient estimation of extreme response of drag-dominated offshore structures by monte carlo simulation. *Ocean Engineering*, 34:2188–2197, 2007.

[19] Arvid. Naess. On a rational approach to extreme value analysis. *Applied Ocean Research*, 6(3):173–174, 1984.

[20] Arvid. Naess. On the long-term statistics of extremes. *Applied Ocean Research*, 6(4):227–228, 1984.

[21] D. E. Newland. *An Introduction to Random Vibrations, Spectral & Wavelet Analysis.* Number 0486442748. Dover Publications, third edition edition, 2005.

[22] OMAE. *Efficient analysis of a catenary riser*, number 92308, 2006.

[23] OMAE. *The statistical boundary polygon of a two parameter stochastic process*, number 92179, 2006.

[24] Elizabeth Passano. *Efficient analysis of nonlinear slender marine structures.* PhD thesis, Department of Marine Structures, Norwegian Institute of Technology, University of Trondheim, 1994.

[25] Svein Sævik and Janne K.Ø. Gjøsteen. Uflex2d version 2.2.2, User manual. Manual, Marintek, 2010.

[26] Nils Sødahl. *Methods for design and analysis of flexible risers*. PhD thesis, Department of Marine Structures, Norwegian Institute of Technology, University of Trondheim, 1991.

[27] M.J. Tucker, P.G. Challenor, and D.J.T Carter. Numerical simulation of a random sea: a common error and its effect upon wave group statistics. *Applied Ocean Research*, 6:118–122, 1984.

[28] Wikipedia. Dirac delta. http://en.wikipedia.org/wiki/Dirac_delta_function.

[29] Wikipedia. Heaviside step function. http://en.wikipedia.org/wiki/Heaviside_step_function.

[30] Wikipedia. Spearman's rho. http://en.wikipedia.org/wiki/Spearman's_rank_correlation_coefficient.

A Master thesis assignment

NTNU Trondheim
Norwegian University of Science and Technology
Faculty of Engineering Science and Technology
Department of MarineTechnology

M.Sc. thesis 2010

for

Stud.techn. Torfinn Ottesen

Extreme response estimation of umbilical on very deep water

Umbilicals are today in use for several purposes in floating production systems. This class of structures has a complicated cross section, and important non-linear effects have to be accounted for in a global dynamic analysis. Design analysis is hence a challenge both with regard to structural capacity, dynamic analysis and statistics. The purpose of this thesis work is to describe methods for estimation of structural capacity and estimation of lifetime extreme response, and to carry out a case study for an umbilical in a specific application.

The scenario for the case study is an FPSO at water depth 1300 m. An umbilical is arranged between the FPSO and the seabed in a lazy-wave type of configuration. The environment at the field can be characterized as tropical and is typical for Brazil. The FPSO is not able to weathervane. It is secured at the field using a passive mooring system. The mooring lines are attached to the bow and stern of the FPSO. The length of the FPSO is about 300 m, the width of the FPSO is about 55 m. The draft of the FPSO is between 7 and 13 m dependant on the loading condition. The umbilical departs from the FPSO in an azimuth direction that is close to perpendicular to the longitudinal axis of the FPSO. The umbilical is hung-off close to mid-ship, and at the FPSO side.

At the keel level of the FPSO there is a steel tube with a flange at the lower end. A bend stiffener is mounted to this steel flange. The mounting angle of the bend stiffener flange is close to the nominal top angle of the lazy wave configuration. The top angle is the angle with the vertical. The lazy wave configuration has a buoyancy section close to the seabed.

The work should be organized as follows:

1. Literature study. This should cover umbilical technology including capacity versus axial force and bending, methods for dynamic analysis and methods for estimation of long term extreme response.
2. Case study based on the system description above. Extent of this part of the work should be discussed with the supervisor.
3. Evaluation of analysis methods for the actual case, and concluding remarks on the applicability of the selected method for extreme response estimation on this type of structures.

The work may show to be more extensive than anticipated. Some topics may therefore be left out after discussion with the supervisor without any negative influence on the grading.

The candidate should in his report give a personal contribution to the solution of the problem formulated in this text. All assumptions and conclusions must be supported by mathematical models and/or references to physical effects in a logical manner.
The candidate should apply all available sources to find relevant literature and information on the actual problem.

The report should be well organised and give a clear presentation of the work and all conclusions. It is important that the text is well written and that tables and figures are used to support the verbal presentation. The report should be complete, but still as short as possible.

The final report must contain this text, an acknowledgement, summary, main body, conclusions, suggestions for further work, symbol list, references and appendices. All figures, tables and equations must be identified by numbers. References should be given by author and year in the text, and presented alphabetically in the reference list. The report must be submitted in two copies unless otherwise has been agreed with the supervisor.

The supervisor may require that the candidate should give a written plan that describes the progress of the work after having received this text. The plan may contain a table of content for the report and also assumed use of computer resources.

From the report it should be possible to identify the work carried out by the candidate and what has been found in the available literature. It is important to give references to the original source for theories and experimental results.

The report must be signed by the candidate, include this text, appear as a paperback, and - if needed - have a separate enclosure (binder, diskette or CD-ROM) with additional material.

Supervisor at NTNU is professor Carl M. Larsen

Trondheim, February 2010

Carl M. Larsen

Submitted: January 2008
Deadline: June 2008